**THE UNIVERSITY OF TURKISH AERONAUTICAL ASSOCIATION**

**INSTITUTE OF SCIENCE AND TECHNOLOGY**

**NUMERICAL AND EXPERIMENTAL ANALYSIS OF DIRECT ABSORPTION CONCENTRATED SOLAR COLLECTOR USING NANO-FLUID.**

**Master Thesis**

**Mohammed Yaseen Nawaf**

**1403730025**

**Institute of Science and Technology**

**Mechanical and Aeronautical Engineering Department**

**Master Thesis Program**

**July 2017**

**THE UNIVERSITY OF TURKISH AERONAUTICAL ASSOCIATION**

**INSTITUTE OF SCIENCE AND TECHNOLOGY**

# NUMERICAL AND EXPERIMENTAL ANALYSIS OF DIRECT ABSORPTION CONCENTRATED SOLAR COLLECTOR USING NANO-FLUID.

**MASTER THESIS**

**Mohammed Yaseen Nawaf**

**1403730025**

**IN PARTIAL FULFILLMENT OF THE REQUIREMENT FOR THE DEGREE OF MASTER OF SCIENCE IN MECHANICAL AND AERONAUTICAL ENGINEERING**

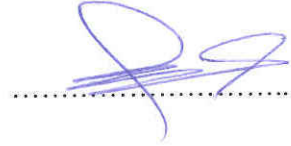**Supervisor: Assist. Prof. Dr. SUDANTHA BALAGE**

**Co. Supervisor: Assist. Prof. Dr. Amar HAMEED**

Türk Hava Kurumu Üniversitesi Fen Bilimleri Enstitüsü'nün 1403730025 numaralı Yüksek Lisans öğrencisi, " Mohammed Yaseen Nawaf " ilgili yönetmeliklerin belirlediği gerekli tüm şartları yerine getirdikten sonra hazırladığı "NUMERICAL AND EXPERIMENTAL ANALYSIS OF DIRECT ABSORPTION CONCENTRATED SOLAR COLLECTOR USING NANO-FLUID" başlıklı tezini, aşağıda imzaları bulunan jüri önünde başarı ile sunmuştur.

**Tez Danışmanı :**   Yrd. Doç. Dr. Sudantha BALAGE
Türk Hava Kurumu Üniversitesi

**Eş Danışmanı :**   Yrd. Doç. Dr. Amar HAMEED
KTO Karatay Üniversitesi

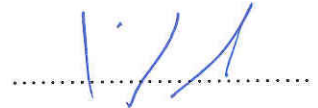**Jüri Üyeleri :**   Yrd. Doç. Dr. Muharrem KUNDURACI
Türk Hava Kurumu Üniversitesi

Yrd. Doç. Dr. Sudantha BALAGE
Türk Hava Kurumu Üniversitesi

Yrd. Doç. Dr. Munir ELFARRA
Ankara Yildirim Beyazit Üniversitesi

**Tez Savunma Tarihi:** 14.07.2017

**THE UNIVERSITY OF TURKISH AERONAUTICAL ASSOCIATION**

**INSTITUTE OF SCIENCE AND TECHNOLOGY**


I hereby declare that all the information in this study I presented as my Master's Thesis, called "Numerical and Experimental Analysis of Direct Absorption Concentrated Solar Collector Using Nano-Fluid" has been presented in accordance with the academic rules and ethical conduct. I also declare and certify on my honor that I have fully cited and referenced all the sources I made use of in this present study.


Date 14/07/2017

**Mohammed Yaseen Nawaf**

# ACKNOWLEDGEMENTS

# TABLE OF CONTENTS

# TABLE OF FIGURE

# LIST OF TABLE

**Abbreviations**

| | |
|---|---|
| **CFD** | **Computational Fluid Dynamics** |
| **DASC** | **Direct Absorption Solar Collector** |
| **PTSC** | **Parabolic Trough Solar Collector** |
| **UDF** | **User Defined Functions** |
| **FVM** | **Finite volume method** |

**Nomenclature**

| | |
|---|---|
| $\varphi$ | Volume fraction of Nano-fluid [%] |
| $\overline{q}$ | Convective heat transfer per unit length [W/ m] |
| $\dot{m}$ | Mass flow rate [kg /s] |
| $A_a$ | Collector's area [m$^2$] |
| $C_P$ | Specific heat capacity [J/(kg K)] |
| $C_R$ | Collector's Concentration ratio [dimensionless] |
| $D_{ci}$ | Inner diameter of receiver copper tube [mm] |
| $D_{co}$ | Outer diameter of receiver copper tube [mm] |
| $D_{gi}$ | Inner diameter of receiver glass tube [mm] |
| $D_{go}$ | Outer diameter of glass tube [mm] |
| $D_{sp}$ | Nanoparticles diameter [nm] |
| $f$ | Optical efficiency [dimensionless] |
| $G$ | Solar radiation [W/m$^2$] |
| $g$ | Gravitational acceleration [m/s$^2$] |
| $h_f$ | Convective heat coefficient inside receiver tube [W/(m$^2$ K)] |
| $I_o(\theta)$ | Incident solar radiation around the cylindrical surface of tube [W/m$^2$] |
| $I_s$ | Scattered radiation [W/m$^2$] |
| $I_t$ | The transmitted radiation intensity [w/m$^2$] |
| $k$ | Thermal conductivity [W/m K] |
| $K_a$ | Absorption coefficient [1/m] |
| $K_e$ | extinction coefficient [1/m] |
| $L$ | Length of collector [m] |
| $Nu$ | Nusselt number [dimensionless] |

X

| | |
|---|---|
| $\varnothing$ | Rim angle [deg] |
| $Pr$ | Prandtl number [dimensionless] |
| $q_s$ | The absorbed heat flux of nano-fluid [W/m$^2$] |
| $q_{loss}$ | Heat flux to ambient [W/ m$^2$] |
| $r$ | Radius |
| $Ra$ | Rayleigh number [dimensionless] |
| Re | Reynolds number [dimensionless] |
| $T_{amb}$ | Ambient temperature [K] |
| $T_{anul}$ | Receiver and glass cover Annuals temperature [K] |
| $T_c$ | Glass cover temperature [K] |
| $T_f$ | Fluid mean temperature [K] |
| $T_i$ | Inlet temperature [K] |
| $T_o$ | Outlet temperature [K] |
| $T_r$ | Receiver temperature [K] |
| $T_{sky}$ | Sky temperature [K] |
| $u$ | Velocity [m /s] |
| $U_L$ | The loss coefficient [W/m$^2$ .°C] |
| $w$ | Width of collector [m] |
| $\theta$ | Circumference arc angle [deg] |
| $\tau_g$ | Transmittance of glass [dimensionless] |
| $\Phi$ | The heat generated (internal heat source) [W/m$^3$] |
| $\alpha$ | Thermal diffusivity [m$^2$/s] |
| $\beta$ | Thermal expansion [1/K] |
| $\varepsilon_c$ | Receiver copper emittance [dimensionless] |
| $\varepsilon_g$ | Glass emittance [dimensionless] |
| $\eta_{th}$ | Thermal efficiency [dimensionless] |
| $\mu$ | Dynamic viscosity [Pa.s] |
| $\rho$ | Density [kg /m$^3$] |
| $\sigma$ | Steven Boltzmann constant [5.6697 x 10$^{-8}$ W/(m$^2$ K$^4$)] |

**Thesis Layout**

This research has been published in the following conferences and journals

- Amar Hasan Hameed, Mohammed Yaseen Nawaf, and S. Balage, "NOVEL CONFIGURATION FOR DIRECT ABSORPTION SOLAR COLLECTOR WITH NONE-CIRCULATED NANOFLUID," *JOURNAL OF THERMAL ENGINEERING , INTERNATIONAL CONFERENCE ON ENERGY AND THERMAL ENGINEERING: ISTANBUL  25-28 April 2017, Yildiz Technical University, Istanbul,  Turkey.*

- AMAR HASAN HAMEED, MOHAMMED YASEEN NAWAF, and SUDANTHA BALAGE, "A NOVEL CONFIGURATION FOR CONCENTRATED SOLAR COLLECTOR WITH NONE-CIRCULATED NANOFLUID," presented at the ISER - 122nd International Conference on Heat Transfer and Fluid Flow (ICHTFF), Dammam, Saudi Arabia, 2017.

# ABSTRACT

## NUMERICAL AND EXPERIMENTAL ANALYSIS OF DIRECT ABSORPTION CONCENTRATED SOLAR COLLECTOR USING NANO-FLUID

Mohammed Yaseen Nawaf

Master, Department of Mechanical engineering

Thesis Supervisor: Assist. Prof. Dr. Sudantha Balage

Co-supervisor: Assist. Prof. Dr. Amar Hameed

July 2017,   91 pages

The parabolic trough solar collector is one of the most efficient and it has been studied widely. Direct absorption solar collector (DASC) is a new technique used recently in harvesting solar energy.  Since this technique is new, the number of research publication are still fewer than that of conventional solar collectors. A novel configuration, for direct absorption solar collector, is been developed. In this study, none-circulated Nano-fluid is used to absorb the solar radiation through a glass wall. The absorbed heat is directly transferred to circulated water flowing inside a copper tube submerged in the Nano-fluid. Numerical models has been developed using ANSYS FLUENT. The numerical model simulate the buoyancy driven flow and the solar radiation absorption of the nanofluid as well as the heat transfer through the walls to the flowing water. The heat absorption of concentrated solar rays reflected by parabolic trough is simulated as a heat source in the energy equation solved in the Nano-fluid region. The efficiency of one meter length of solar receiver unit, with glass-to-copper tube size ratio of ½, increases significantly with flow rate up to 65% at 100 l/h. The numerical results obtained from the simulation are compared with the experimental results. A study of the effect of changing the volumetric flow rate and the inlet fluid temperature on the efficiency of the new configuration is performed.  Also, the effect of the concentration of nanofluid at 0.055% and 0.100% on the efficiency of the new configuration is reported. This study provides a novel concept of a collector tube as well

as a methodology and codes for simulation that can be used in the development and manufacture of solar collectors that works on the principle of direct absorption solar energy.

# ÖZET

## Nano-sıvı kullanarak yoğunlaşmls direk emme yöntemi kolektörünüm sayısal ve deneysel analizi

Mohammed Yaseen Nawaf

Yüksek lisans Tezi, Makine ve Uçak Mühendisliği Bölümü

Tez Danışmanı: Yrd. Doç. Dr. Sudantha Balage

Co. Tez Danışmanı: Yrd. Doç. Dr. Amar Hameed

Temmuz - 2017, 91 sayfa

Parabolik oluk güneş kolektörü, termik verimliliği artırmak için birçok çalışma yürüten güneş kolektörlerinin en etkili tiplerinden biridir.Doğrudan absorpsiyon güneş kolektörü (DASC), son zamanlarda kullanılan yeni birsolartoplama tekniğidir.Bu yeni teknik hakkında yayınlanan pek az araştırma vardır. Doğrudan absorpsiyon güneş kolektörü için yeni bir konfigürasyon geliştirildi.Bu çalışmada, dolaşımda olmayan nano-sıvılar,güneş radyasyonunu bir cam tüp duvarından absorbe eder. Emilen ısı, doğrudan nano-sıvı içine batırılmış bakır boru içinde akan dolaşımdaki suya aktarılır. Sayısal olan bu model, ANSYS FLUENT tarafından akan su için, halkalı nano-sıvı bölgesive iki farklı akan sıvıyı ayıran bakır boru için geliştirildi. Parabolik oluk tarafından yansıtılan yoğunsolar dizinlerinin ısı emilimi, nano-sıvı alanında çözülen enerji denkleminde ısı kaynağı olarak simüle edilir. Ölçü oranı ½ olan ve cam-bakır borudan oluşan bu solar alıcı ünitenin bir metre uzunluğundaki verimliliği 100 l/s'de yüzde 65'e kadar çıkar. Simülasyondan elde edilen sayısal sonuçlar, deney sonuçlarıyla karşılaştırılmıştır.Daha sonra, bu yeni konfigürasyonunvolümetrik akış değişiminin etkisi ve giriş sıvı sıcaklığının verimliliği ve performansı üzerine bir çalışma yapılır.Ayrıca, bu yeni konfigürasyonun0.055% ve0,1% oranında nano-sıvı yoğunluk değişiminin etkisi üzerine bir çalışma yapıldı. Bu yeni çalışma, prensip ve simülasyon

kodu olarak metedolojide doğrudan solar toplama yöntemiyle çalışan benzer güneş kolektörlerinin imalat ve geliştirilmelerine kılavuzluk eder.

**Anahtar kelimler:**Doğrudan absorpsiyon güneş kolektörü, nano-sıvı, yoğun solar kolektörü.

**Chapter one: Introduction**

**1.1 Introduction.**

In the midst of the rapid development in all facilities of life, which in led to increased consumption of fossil fuels in several sectors, including transport and electricity generation, which will lead to the quick depletion of fossil fuels, and increase pollution of the environment due burning fuel. These reasons gave motivation to countries to find a new alternative energy. Solar energy is one of the best types of renewable energy, which can be invested by countries, because of it is clean, free and the easy for obtaining. All of these reasons motivated the researchers to developed solar collector of all kinds, but focus on parabolic trough solar collector is largely due to the domain of power generation. Nanotechnology was introduced in this field of solar harvesting via the new technique called direct absorption solar. This was recently used in the new generation of solar collectors instead of using the conventional method which absorbed solar radiation by the spectral selective coating of the metallic pipe. In the new technique, solar radiation is absorbed by the nanofluid. The nanofluid is a compound produced by mixing nanoparticles with base fluid which flows through a glass tube and then passed into a heat exchanger to convey the absorbed heat into a cold fluid. The addition of nanoparticles to the fluid will improve the thermal properties of the fluid, which will increase the efficiency and performance of the solar collectors.

**1.2 problem statement.**

Solar energy harvesting needs further development to reduce the consumption of fossil fuel due to its cost and its environmental concerns of burning it. Solar collectors got extended interest from researchers, but still, the incident heat of the sun faces multi-stages of thermal resistances to flow before reaching the end user. Direct Absorption Solar Collector (DASC) is a novel technique used recently for the new generation of solar collectors. Instead of using metallic tube painted with special spectral paint to absorb solar irradiation and transfer heat to a fluid inside the tube, flowing nanofluid in a glass tube absorbs solar irradiation directly and transport the absorbed energy as a heat

exchanger for usage. Since, DASC's are frost developed, many researchers studied the performance of these collectors numerically and experimentally and compared it with the conventional solar collectors. Water was found to be the best absorber for solar radiation among four liquids, namely; water; ethylene glycol; propylene glycol and therminol VP-1, which has been tested by Otanicar [1] . However, the above is still a weak absorber, only absorbing 13% of the energy. The presence of nanoparticles promises superior capability for solar irradiation absorption since nanoparticles are generally opaque and may be black. Tyagi [2]observed that for the non-concentrating flat-plate collector the presence of nanoparticles increases the absorption of incident radiation by more than 9 times over that of pure water. The efficiency of Direct Absorption Collector by using nanofluid has been found to be up to 10% higher than that of the flat-plate collector. Nanofluids, even of low-content, has good absorption in direct absorption collector (DAC) compared with the base fluid or compared with coating absorber as has been demonstrated by Luo [3] and the model of Xu [4]. The purpose of this research is to enhance irradiance absorption capacity and efficiency of concentrating parabolic solar collectors by using nanofluid for direct absorption in glass tube compound with copper tube for direct heat exchange.

### 1.3 The importance of research.

A new technology has been developed. This new technology uses a stationary envelop of nanofluid for enhanced absorption of the solar radiation. Above is in contrast to conventional application of nanofluid as the working fluid for the heat exchanger. The present technology removes the need of a heat exchanger and significantly reduce the required volume of nanofluid compared to the conventional.

At direct absorption solar collector (DASC), nanofluid is circulated in a system. Nanofluid absorbs solar irradiation while flowing inside a glass tube. Nanofluid absorbs heat from irradiation, then it transfer the absorbed heat to a cold water through a heat exchanger. Nanofluid in traditional system circulates and transfers heat from the solar collector to heat exchanger. In the heat exchanger, heat is used for heating the domestic water or swimming pool water or any other application required. The use of nanofluid in conventional solar collectors requires a large amount of nanoparticles to prepare

nanofluid because nanofluid will be flowed inside a heat exchanger to conveys the absorbed heat, which in turn will increase the costs.

The present work proposes a novel approach, the new system uses the principle of direct heat exchange between uncirculated nanofluid and circulating water inside collector tube without using a heat exchanger. As a result of the decrease in total thermal resistance, the overall efficiency of the system will increase. In addition, only one circulating pump will be used instead of two and due to the fact that the nanofluid is uncirculated. The amount of nanofluid required is lesser due to the fact nanofluid is uncirculated, this will decrease the costs.

### 1.4 Thesis objective.

The used of new technologies in the field of solar energy has increased the harvesting of solar energy, but despite this increase, there is still a need to increase the efficiency of solar collectors, so we produced a system that enhances irradiance absorption capacity and efficiency of concentrating parabolic solar collectors by using nanofluid for direct absorption in glass tube compound with a copper tube for direct heat exchange. The thermal conductivity of the fluid conveying thermal heat was improved by using nanofluid is reported in the literature. But, still heat exchange needs more improvement by enhancing the fluid thermal conductivity or by improving the configuration to boost heat transfer. The main objective of this research is to increase solar energy harvesting by reduction of thermal resistance in the medium fluid. The new configuration will be discussed for heat transmitting from nanofluid to heating system, two volume fraction of nanofluid 0.055% and 0.1% is used to investigate the effect of concentration nanofluids on the new system. The new model was simulated by ANSYS FLUENT.

**1.5 Organization of the Thesis.**

This thesis contains five main chapters. Where the chapter one contains the introduction of the thesis, which showed the problem statement and the importance of research in addition to the thesis objective.

Chapter two: In this chapter, reviewed the previous studies in the field of use of nanofluid in the harvesting of solar energy theoretically and experimentally and the effect of the addition of nanoparticles on the efficiency and performance of the solar collectors.

Chapter three: This chapter provides an overview of the methodology used in this thesis. The design of the new model presented the equations needed to calculate the energy generated inside the nanofluid and calculate the thermal losses in the solar collector, as well as the experimental calculations of the new model. In addition to the materials used in testing the new model.

Chapter four: Provides numerical and experimental results, including charts, tables, and discussion of all results.

Chapter five: Conclusions and Future work.

**Chapter Two: Literature Review**

The topic of solar energy harnessing in various applications and methods of concentration of solar radiation and different types of solar collectors of the important topics that led researchers and international companies specialized in solar energy to conduct many theoretical and experimental studies in their research on the use of solar energy and investment in many applications that serve the communities. The studies were divided between theoretical and experimental studies, but the experimental studies obtained the largest portion of them, and through the review of these research and studies we find that most of them interested in the statement of the effect of the mass flow rate of fluid and others have studied the effect of placing the glass tube around the receiver tube, while others have studied the effect of performance factors on thermal efficiency and other design and operational determinants that directly affect the performance of thermal complexes of different types, designs, and applications. Theory and process for the performance of the parabolic solar collector. It is necessary to search for similar studies, with a review of the different studies for the purpose of using them or for purposes of comparison with them. In this chapter, we will conduct a study of previous research about the PTSC modeling and used nanofluids in the solar collector and the effect of adding nanoparticles on thermophysical properties of the base fluid.

**2.1 Parabolic trough solar collector applications and modeling.**

There are several methods that can be used to harvest solar energy, but the concentrated solar method is one of the most efficient methods in this field, where solar radiation incident is reflected from the reflector to a small area (receiver) for the purpose of capturing the largest amount of heat. There are various forms of solar collectors in concentrated solar energy such as the Stirling dish, the Frasnel reflections and the parabolic trough solar collector, which is considered the most common and used in the field of renewable energy and a large number of previous studies on this application. The solar collector can be defined as a number of parts that are combined with each other to form a solar collector. The parabolic trough solar collector can be divided into the reflector, where is made of parabolic plate aluminum or stainless steel the function is to reflected the solar radiation into the receiver. The receiver is considered the important

part of the solar collector. Where the heat transfer fluid flows inside it and all thermal calculation are carried out on this part. Would review the previous works of parabolic trough solar collector in followed.

Kalogirou [5] Provide an itemized thermal model showing all the thermal analysis carried out on the heat receiver tube from heat transfer processes as conduction, convection, and radiation. Where studied the conduction in the receiver tube through the metal tube, and the wall of envelope glass. As well as for convection inside the receiver tube, and convection into the annulus between vacuum tube and the receiver tube, and the outer diameter of a vacuum tube with the ambient air, and the radiation from the outer diameter of metal receiver tube and envelope glass surface to sky respectively. The results of thermal efficiency and losses were verified by comparing them with data from Sandia National Laboratories, where the results were very satisfactory.

Al-Ansary and Zeitoun [6] Presented a promising technique for Bridging the gap between the cost and performance for collector tube with a glass envelope that is filled air or evacuated. To do that putting insulating material and heat resistance inside the vacuum area between the absorbent tube and the glass envelope into the receiver tube does not expose to the concentrated solar radiation. Predictable that use of heat insulation material would reduce thermal losses for convection and radiation. The results of simulated showed the losses due to conduction and convection were reducing 25% compared with a tube filled with air when using fiberglass as heat insulation. As the thermal conductivity of insulation materials increases with increasing temperatures, this will reduce the benefit of using thermal insulation in applications worked in high temperature. Accomplished that the proposed model can be an appropriate alternative for low-temperature applications, with receivers that are evacuated or filled with air.

Öztürk et al. [7] studied the effect of the geometry for (PTSC) and solar irradiance incident on the reflector surface. Also calculated the total energy inside receiver tube. Furthermore, the model is analyzed with respect to energy and exergy models for meteorological specification in various months at Isparta. The results showed that the highest value of efficiency according to the law of the first efficiency was in July, where the highest intensity of solar radiation, as well as the second law of efficiency, where the highest percentage in July as well as the proportions 76% and 27%, respectively.

Li and Wang [8] Two types of vacuum tubes were used in the parabolic trough solar collector to calculated the heating efficiency and temperature of two types of fluids, namely water, and nitrogen. The results showed that both vacuum tubes used give the heating efficiency of 70-80%, but when the water mass flow rate is less than 0.0046 kg/s, the water began boiling. As for the nitrogen, the heating efficiency was 40% and the temperature between 320-460 C. A model has been built for simulation. For comparing the experimental results with the model, it is shown that it is compatible with the experimental results and with accuracy 5.2%

Padilla et al. [9] presented detailed calculations of the heat transfer in a parabolic trough solar collector using the finite element method. One-dimensional numerical used to analysis the model. The receiver tube and the vacuum tube were divided into several sectors, then applying the energy and mass balance in each sector, as well as the convective and radiative heat transfer correlations in the calculations. The results were compared with the results of the Sanadia National Lab and other models, the simulation results showed in terms of efficiency and thermal losses that the model presented was better compared with the experimental results.

Lobón et al. [10] introduced CFD methodology for assuming the behaviour of a multi-phase fluid in a PTSC. The results of the simulation showed a dependable close agreement with experimental time series data for the different denomination of transient which included varies in solar radiation, inlet mass flow rate, and outlet steam temperature. Average total error for temperature values less than 6%. Furthermore, the

pressure drop predictions and measurements show a mean squared error ranging from 4% to 12%.

He at el. [11] Examined the affects of various geometrics concentretion ratio and various rim angles on heat flux distribution, Where an analysis was conducted on the concentreting characteristic of the (PTSCs) by the coupled method. The resulted showed the two variable effect the heat flux distributions. Where increase GC, the heat flux distributions become gentle, the angle span of reducing area become larger and the shadow effect of receiver tube become weaker. And when the rim angle rising, the maximum value of heat flux become lower, and the curve moves towards the direction $\varphi = 90°$. But the temperature rising only with GC increasing and the effect of rim angle on heat transfer process could be neglected, when rim angle is larger than 15°. if it is small, such as $\theta = 15°$, lots of rays are reflected by the glass cover, and the temperature rising is much lower.

Cheng at el.[12] introduced a detailed three-dimensional computational model of the complete parabolic trough solar collector (PTC) system and uniform numerical simulations by merged the Finite Volume Method (FVM) and the Monte Carlo Ray-Trace (MCRT) method. The results were compared with experimental data show that the MCRT code was a good agreement, proving that the model and method used feasible and reliable. The fractions of the total thermal loss resulting from radiation increase with increasing inlet temperature of (HTF) and become the majority. The convection heat transfer in the annulus space also influenced and enhanced the radiation heat transfer when there is some remaining gas in the annulus space.

Reddy et al. [13] numerically investigated a thermal analysis of an energy-efficient receiver for solar parabolic trough concentrator, with consideration the performance evaluation of a solar parabolic trough concentrator with various porous receiver geometries. The models are an assumption for a porous energy-efficient receiver for internal heat gain characteristics and heat loss because of natural convection. The Ansys FLUENT software was used to solved the models, by assumed the internal flow and heat transfer analysis based on a RNG k-$\epsilon$ turbulent model, while external heat losses are treated as a laminar natural convection model. The modulation of porous inserts in a

tubular receiver of solar trough concentrator enhanced the heat transfer about 17.5% with a pressure penalty of 2 kPa. The numerical data for internal heat transfer inside the receiver proposed based on the extensive of the Nusselt number.

Tao et al. [14] developed a two-dimensional numerical model for the coupled heat transfer process in parabolic solar collector tube, who includes nature convection, forced convection, heat conduction and fluid–solid conjugate problem. The numerical analytics of effects of Rayleigh number (Ra), tube diameter ratio and thermal conductivity of the tube wall on the heat transfer and fluid flow performance were done. The results show that when Ra is more than 105, the effects of nature convection must be taken into consideration. When increasing of tube diameter ratio, the Nusselt number in the inner tube (Nu1) increases and the Nusselt number in annuli space (Nu2) decreases. And the increase of tube wall thermal conductivity, Nu1 decreases and Nu2 increases. When thermal conductivity is bigger than 200 W/(m K), it would have little effects on Nu and average temperatures. Because of the effect of the nature convection, along the circumferential direction (from top to down), the temperature in the cross-section decreases and the temperature gradient on inner tube surface increases at first.

Daniel et al.[15] numerically investigated a performance of the vacuum shell and compared with the non-evacuated and evacuated tube configurations and its influence under various wind velocities. The evacuated tube with selective coating was the highest between all configurations, as expected. The performs of vacuum shell configuration better than the non-evacuated tube even without a selective coating and is considerably better with a selective coating.

### 2.2 Applications of nanofluids

A nanofluid is a fluid containing nanometer size of solid particles called nanoparticles, these fluids are prepared by dispersed of nanoparticles in a base fluid. The nanoparticles utilized in nanofluids are usually made of metals, carbides, oxides, or carbon nanotubes. General base fluids include water, ethylene glycol, and oil. Nanofluids have new properties that make them salutary in many applications in heat transfer, add nanoparticles to the fluid enhance the thermophysical properties and heat characteristics. Therefore, utilizing nanofluids can improve the output parameters of an application used. Nanofluids can be used in solar energy system to harvesting the solar

energy by increase the amount of solar energy captured. Shown in this review the effect of adding nanoparticles on the thermophysical of the base fluid. As well know the effect of nanofluid on solar systems application.

### 2.2.1 Thermophysical properties enhancements.

In this section display literature the effect of adding nanoparticles on the specific heat capacity, viscosity, and thermal conductivity of the fluid, and it is divided into theoretical studies and experimental work.

### 2.2.1.1 Enhancements properties-Theoretical.

### 2.2.1.1.1 Viscosity.

There are various formulas to estimate the effective viscosity of nanofluids.

Einstein [16] He established the first formula to calculate the effective viscosity value of nanofluid in 1906. The formula assumed that the fluid contains spherical particles and the volume fraction does not exceed the 2%.

Brinkman [17] developed Einstein's equation for used in the intermediate particle concentrations. He has considered that the formula is valid in a concentration ratio not exceeding 4%. This is the most accepted formula among researchers in this field.

Franken and Acrivos [18] developed a mathematical expression to calculate the effective viscosity. Lundgren [19] proposed a new equation as a Taylor series expansion of the volume fraction, it is referred to as the reduction of Einstein's formula.

Nguyen et al.[20] derived the expression of a temperature dependent viscosity for particle volume fractions between 1% to 4%.

### 2.2.1.1.2 Thermal conductivity.

Thermal conductivity is one of the most important characteristics of heat transfer analysis of nanofluid, various models are presented in this review.

Maxwell [21] established the first formula to calculate the thermal conductivity of nanofluid in 1881. The formula assumed that the fluid contains spherical particles and the volume fraction does not exceed the 1%.

Bhattacharya et al. [22] developed a formula for effective thermal conductivity of nanofluids based on Brownian dynamic simulations and used the equilibrium Green-

Kubo method. The formula is a linear combination of particle conductivity and liquid conductivity.

Mehta et al. [23] introduced a theoretical model to predict the thermal conductivity of nanofluids at a low volume fraction of particles. The heat transfer gained from liquid/solid conduction and micro-convection around particles were considered separately using thermal resistance modeling. The diffusion velocities of particles because of Brownian motion were used for the modeling of micro-convection around the nanoparticles.

Yu and Choi [24] studied the effect of the liquid nanolayer formed between the spherical nanoparticles and renewed the Maxwell model. The model was the first to take into account the nanolayer formation.

Xiao et al. [25] presented a model to calculate the effective thermal conductivity of nanofluid, taking into account the effect of Brownian motion and the use of fractal geometry. The theoretical results were consistent with the practical models. The results showed that the effective thermal conductivity increases by increasing the volume fraction. in addition, the results showed that the small nanoparticles achieved greater thermal conductivity than the larger particles.

### 2.2.1.2 Enhancements properties-Experimental.

### 2.2.1.2.1 Viscosity

Chandrasekar et al. [26] experimentally investigated viscosity of Al2O3/H2O nanofluid. The method used to prepare nanofluid was synthesizing Al2O3 nanoparticles by using microwave-assisted chemical precipitation, then dispersing them in distilled. The nominal diameter of particles was 43 nm at different volume concentrations (0.33–5%) at room temperature were used for the investigation. The results showed that the viscosity of nanofluids increases with the nanoparticle volume concentration.

Namburu et al. [27] experimentally investigated viscosity of silicon dioxide (SiO2) nanofluid with different diameters (20, 50 and 100 nm) suspended in a 60:40 (by weight) ethylene glycol and water mixture. The nanofluids prepared with various fraction volume ranging from 0 to 10%. Viscosity experiments were carried out over wide temperature ranges, from −35 till 50°C, to demonstrate their applicability in cold

regions. Non-Newtonian behavior was observed for the particle volume concentrations of these nanofluids at sub-zero temperatures.

Shokrlu and Babadagli [28]carried a different set of experiments to become clear the mechanism of additional viscosity reduction of heavy oil/bitumen using nanosize metal particles during steam injection techniques. The first group, of experiments was an endeavor to study the effect of metal particles on the viscosity of the produced oil at a low temperature below a 100 °C , while the second was aim to study their effect in the presence of aqueous phase at a high temperature of around 300 to simulate the steam stimulation process. Finally, the third set of experiments was aim to study the effect of micro and nano-sized particles on the enhancement of the heat transfer within the oil phase. The results showed that at low temperature the particles reduce the heavy oil viscosity after being mixed with the oil phase and that amount of reduction was a function of the particle concentration.

### 2.2.1.2.2 Thermal conductivity.

Eastman et al. [29] carried out some primary experiments to research the effect of suspending Cu, CuO, and Al2O3 nanoparticles in HE-200 oil and water. The results showed the volume fraction of CuO at 5% when dipped in the water, the thermal conductivity increased 60%.

Xie et al. [30] studied the effect of the particle shape on the enhancement of the effective thermal conductivity. in addition, the authors examined the effect of the base fluid on the enhancement of the effective thermal conductivity and accomplished those base fluids with lower thermal conductivity will lead to a higher thermal conductivity enhancement. It was determined that stretched particles provide better enhancements. For example, a 26 nm spherical and 600 nm cylindrical particles of were dispersed in ethylene glycol at a volume fraction of 3%. The experiment showed that the ratio of thermal conductivity enhancement for the spherical was 1.10 and for cylindrical particles was 1.16.

Li and Peterson [31] experimentally measured the effect of the volume fraction, temperature and particle size on the effective thermal conductivity of CuO and Al2O3

and water based nanofluids. the results showed that the effective thermal conductivity of Al2O3-water nanofluid increased up to three times when the temperature increasing from 27 °C till 34.7 °C.

Colangelo et al.[32] evaluated the possibility of using Al2O3, CuO, Cu and Zn dispersed in water and diathermic oil as a heat transfer fluid in high-temperature solar collectors by measuring their thermal conductivity. The results shown that the thermal conductivity enhancement in diathermic oil was higher than that water for the same nanoparticles, volume fraction and conditions. Furthermore, it was found that the thermal conductivity enhancement is reduced by the increase of the particle size.

Liu et al. [33] dispersed Cu nanoparticles in engine oil, EG, and water and studied the effects on the thermal conductivity. Experimental results showed that for Cu/water nanofluid with a volume fraction of 0.1%, the thermal conductivity is increased by 23.8%.

### 2.2.2 Applications of nanofluids in parabolic trough solar collector.

There are two methods for harvesting solar energy in the parabolic trough solar collector. The first method called the direct absorption, in this method the solar radiation is absorbed by the nanoparticle, which found in the heat transfer fluid (HTF) when the nanofluid is inside a glass tube. The second method called indirect absorption, in this method the solar radiation absorbed by the spectral selective coated, which coated the wall of a metal tube.

### 2.2.2.1 Direct Absorption Solar Collector.

Khullar et al. [34] introduced the new idea of harvesting solar radiant energy via usage of the nanofluid-based concentrating parabolic solar collector (NCPSC). The new model (NCPSC) was modeled mathematically and used finite difference method for solved the energy equation. The results showed that the (NCPSC) model where compared with conventional concentrating parabolic solar collector under the similar condition, has about 5-10% higher efficiency from the conventional collector. Indicated the results of theoretical that the NSPSC has the potential to harness solar radiant energy

13

more efficiently than a conventional parabolic solar collector. Figure 1 shows the difference between the conventional parabolic solar collector and (NCPSC).
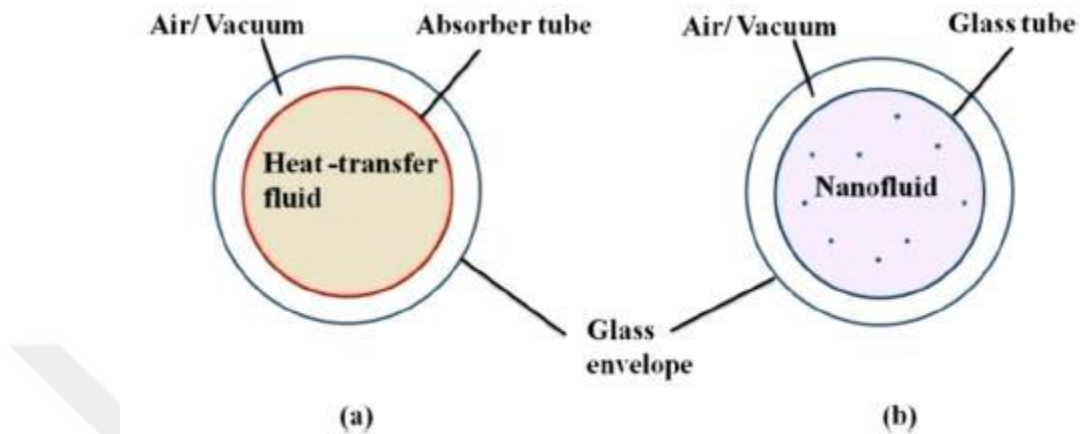


**Figure 2.1**: Difference between conventional collector and NCPSC.
a. conventional parabolic solar collector   b. NCPSC

Xu et al. [4] introduced a theoretical and experimental study of a nanofluid-based direct solar collector (NDASC) of medium temperature type. CuO nanoparticle was used with synthetic oil to be used as a working fluid. The results were evaluated and compared with a conventional indirect solar collector (iASC) model the results showed that the distribution of fluid temperature in (NDASC) was more uniform than the (iASC) figure 2 show that, and the efficiency of (NDASC) was higher than (iASC) when operated below a critical temperature value at 139 °C in theoretical analysis and 128 °C in experiments. Figure 3 shows variations of solar collection efficiencies with tfi for both the NDASC and the IASC.
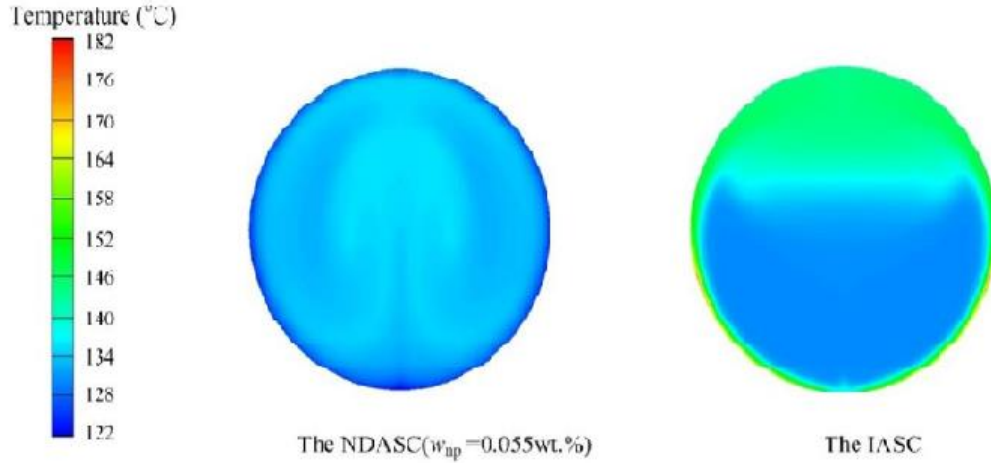
**Figure 2.2**: temperature distribution inside working fluid.
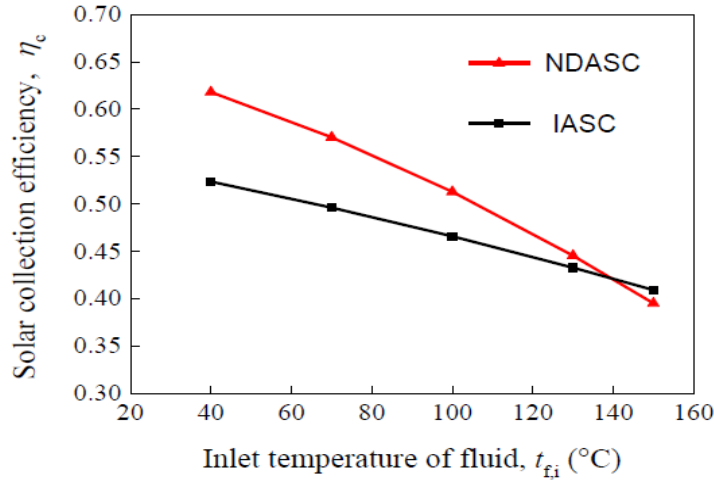


**Figure 2.3**: Variations of solar collection efficiencies with tfi for both the NDASC and the IASC.

Chen et al. [35] presented numerical study on the solar collection characteristics of (NDASC) on a parabolic trough concentrator. The nanofluid prepared with different volume fraction from 0.05% till 0.1% and used as a working fluid. Observed when decreased of the volume fraction of nanofluid the fluid temperature distribution achieved more uniform, also the volume fraction had an influence on the efficiency and the critical temperature. The optimum volume fraction of nanofluid used in (NDASC) was between 0.05% and 0.06%. The internal heat source ($\Phi$) at different positions is used to describe the radiation convey inside the nanofluids. This method was not limited to analyzed the performance of NDASC using specific nanofluids under a given operating

condition but could be used to research different nanofluids and other operating conditions. it could provide direction for the feasibility evaluation of the NDASCs with a concentrator, figure 4 shown the variations of the internal heat source with the optical path and different volume fraction.
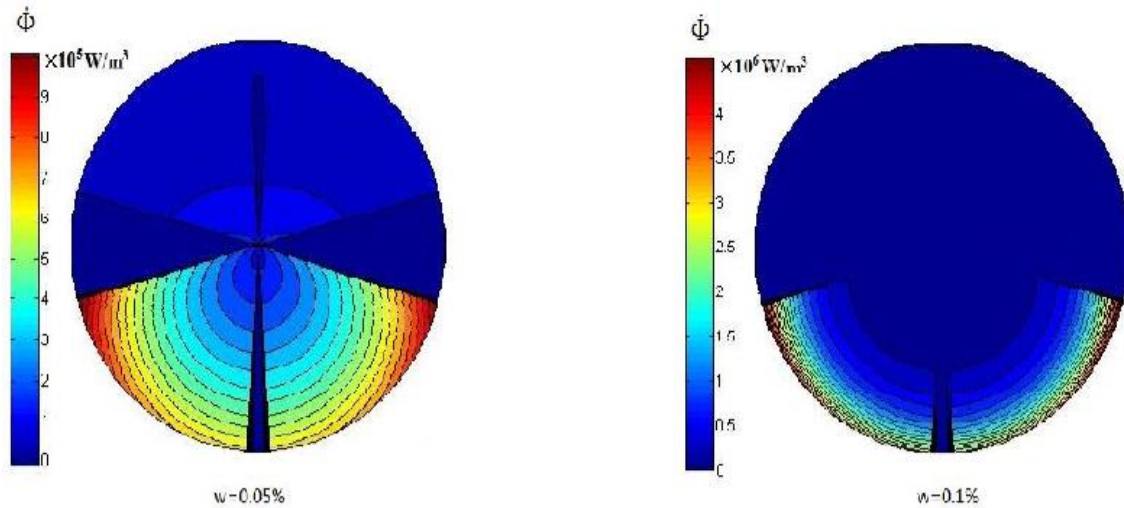


**Figure 2.4**: variations of the internal heat source with the optical path and different volume fraction.

Menbari et al. [36] experimentally investigated the absorption and thermal conductivity of binary nanofluids on direct absorption solar parabolic trough collectors, the binary fluids is a new class of nanofluids included a base fluid and two different nanoparticles may exhibit a behavior different from any of their components. Selected two different nanoparticles, $\gamma$-Al2O3 (with high scattering properties) and CuO (with high absorption properties) to prepare a binary nanofluid. The results showed that solar irradiance is absorbed and converted to a significant amount of sensible heat over the length of the receiver tube, also the thermal efficiency of the system could be enhanced by increasing weight concentration of nanofluid and flow rate. Figure 5 shows the efficiency at different volume fraction and various flow rate.
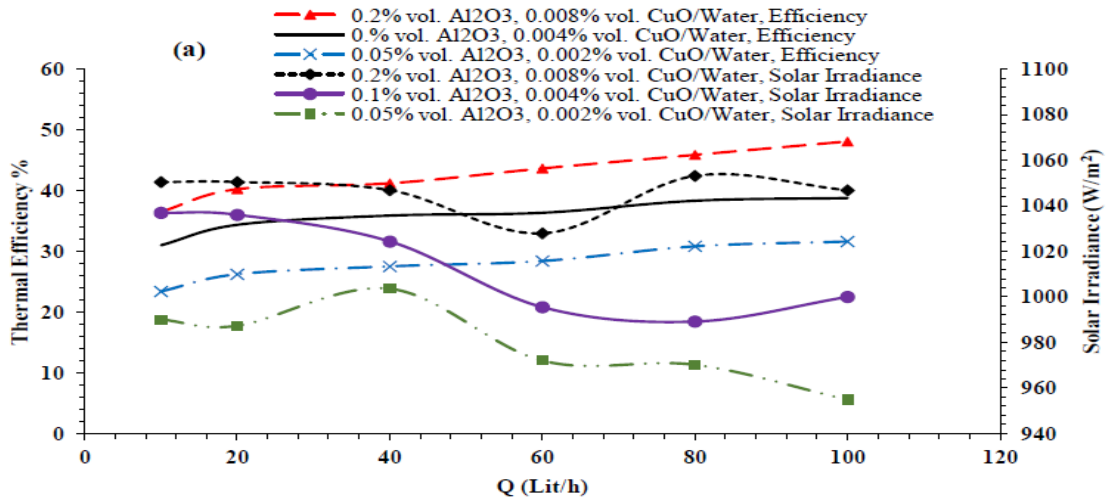
**Figure 2.5**: Efficiencies at different volume fraction and various flow rate.

Ladjevardi et al. [37] investigated the direct solar absorption in a volumetric compound, where the efficiency and distribution of the radio spectrum were measured against nanofluid depth. The study was conducted with two variables: the concentration of Graphite nanoparticles and the change in the diameter of the tube. The results showed that adding a very small amount of Graphite nanoparticles to the water by 0.000025% increased the absorption value of incident irradiation by 50% and increased the cost of 0.0045 $/L.

Khullar and Tyagi [38] examined the possibility of using the direct absorption method in heating applications (NCSWHS) as an alternative to the use of fossil fuels where the results showed the possibility of reducing the emission of gas to the amount of 2200 kg of /household/year and thus the possibility of reducing the consumption of fossil fuels and reduce the percentage of pollution if the NCSWHS are adopted.

**2.2.2.2 Indirect Absorption Solar Collector.**

Sharma and Kundan [39] experimentally investigated the performance of parabolic concentrating solar collector by using copper oxide (CuO) and alumina (Al2O3) nanoparticles in water, as base fluids. Three cases were studied with various volume flow rate (20, 40, 60) L/hr. The thermal efficiency improved when using (CuO) nanofluid with volume fraction 0.01% from 0.95 to 3.05%, 0.66 to 3.36%, and 1.7 to 4.87% for 20, 40 and 60 L/hr respectively. And the thermal efficiency improved when using (Al2O3) nanofluid with volume fraction 0.01% from 1 to 2.55%, 0.05 to 1.86%, and 0.01 to 3.67% for 20, 40 and 60 L/hr respectively. The results showed when used (CuO) nanofluid the maximum instantaneous and thermal efficiency improved.

Bellos et al. [40] designed and simulated parabolic trough collectors to study the enhancement of thermal efficiency of the parabolic collector by increasing the convective heat transfer coefficient between the working fluid and the absorber. The working fluid type and the receiver tube geometry are two main factors which influence on this parameter, pressurized water, thermal oil, thermal oil with nanoparticles and was chosen as working fluids to study the effect. The results showed those two methods improve the heat transfer coefficient and the thermal efficiency of the collector. specifically, when used nanofluids increases the collector efficiency by 4.25% while the geometry improvement increases the efficiency by 4.55%.

Ghasemi and Ahangar [41] A numerical study was conducted to add Cu nanoparticles with water and nanofluid was used as a heat transfer fluid in parabolic trough solar collector. A comparison was made between the conventional compound and the nanofluid compound in the field of temperature, thermal efficiency and mean outlet temperatures. In addition to studying the effect of the velocity of the fluid and the volume fraction of the nanoparticle and the length of the solar collector. The results showed that the solar collector containing nano-fluid was more efficient and performance than the conventional compound, and it has been shown that increasing the concentration of nanofluid has improved the performance of the solar collector.

Sokhansefat et al. [42] A three-dimensional numerical study of the heat receiver tube in the parabolic trough solar collector was carried out in the solar collector under the conditions of the fully developed turbulent mixed convection heat transfer of Al2O3-synthetic oil. The effect of nanofluid concentration was examined on the rate of heat transfer in the absorbent tube. The results showed that the use of nanoparticles improved the heat transfer coefficient in the fluid by increasing the concentration of nanoparticles.

Sunil et al. [43] Investigated the performance of parabolic trough solar collector using SiO2-H2O nanofluid with two concentrations of nanofluids are 0.01% and 0.05% and various volume flow rate (20, 40 and 60 l/h) At these flows, the thermal efficiency of the solar collector was calculated and calculated at a variable time (9:30 am to 3:00 pm). It was observed that the highest efficiency was in 60l/h at 11:30 am. It has been found that SiO2-H2O based nanofluid has comparatively higher efficiency at higher volume flow rates.

Wang et al. [44] numerically investigated the performance of parabolic trough solar collector and an optic-thermal-stress by using nanofluid as Al2O3/synthetic oil under non-uniform solar flux. The results display the bending of receiver tube decrease from 2.11 mm till 0.54 mm when the weight concentrating of nanofluid increase from 0 till 0.055. The results were compared with experimental data, it was very close and satisfactory results.

## Chapter 3: Simulation And Experimental set up

Direct Solar Absorption (DASC) is one of the novel technologies used recently for the new generation of solar energy collectors. Rather than the traditional technique of using metallic tube painted with a spectral selective coating to absorb the solar irradiation, DASC uses flowing nanofluid in a glass tube to the same effect. Since the development of DASC's, many researchers studied the performance of these collectors numerically and experimentally and compared it with the conventional solar collectors. The main parts of the conventional direct absorption parabolic solar collector are the receiver, reflector and heat exchanger. The important part is the receiver, made of glass such as Pyrex (borosilicate) or quartz. Figure 3.1 shows the conventional system of DASC with indirect heat exchange. When the nanofluid flows into the glass tube, the solar irradiation passes the glass wall and is absorbed by nanoparticles which raises the temperature rapidly see (Figure 3.2).
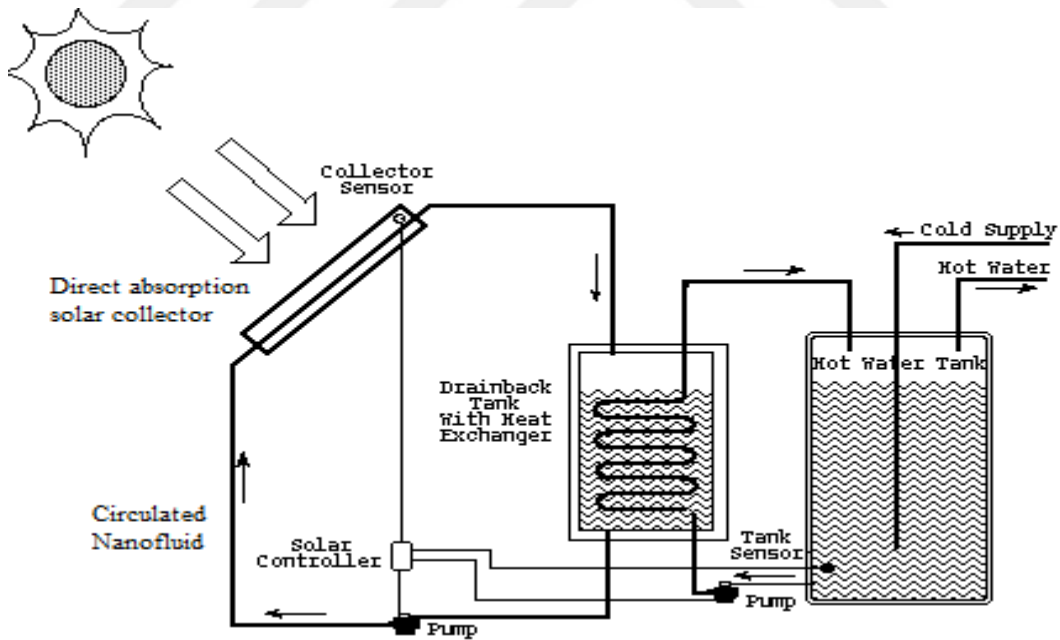


**Figure 3.1**: Outlines of traditional system of DASC with indirect heat exchange [45].
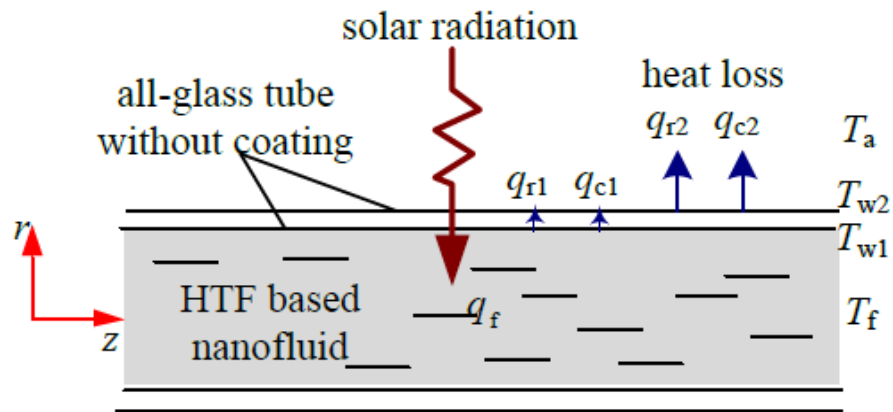
**Figure 3.2**: Receiver tube direct absorption solar collector.

Nanofluid conveys the absorbed heat to a cold water through a heat exchanger. The losses in the traditional DASC results due to reflecting off glass surface in addition to emittance of hot surfaces and losses by convection. Moreover, the output heat of the system depends on the thermal efficiency of the heat exchanger. The existence of heat exchanger reduces the overall efficiency of the system due to the additional thermal resistance with in it. To reduced this thermal resistance we propose changed the design of solar collector. The new design will reduce the total thermal resistance of the system by combining the two actions in one place. The heat absorption and heat exchang will occur at the solar collector to reduce the total thermal resistance (see Figure 3.3). As a result of the decrease of total thermal resistance, the overall efficeincy of the system will increase. In addition, one circulating pump is used instead of two. The outlines of the system for direct heat exchange is shown in Figure 3.4. The present collector uses a statianary glass envelop of nanofluid to collect and trep solar irradiation. This energy, as heat, is transfored through a copper tube to the cirulated water.
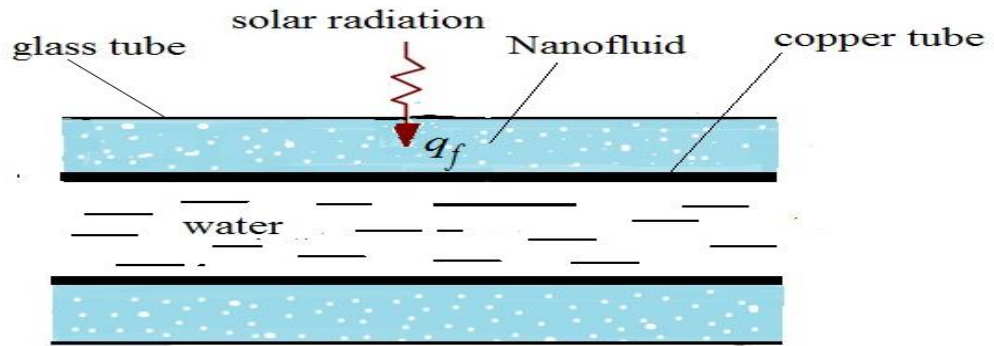
**Figure 3.3**: Receiver tube of new model.
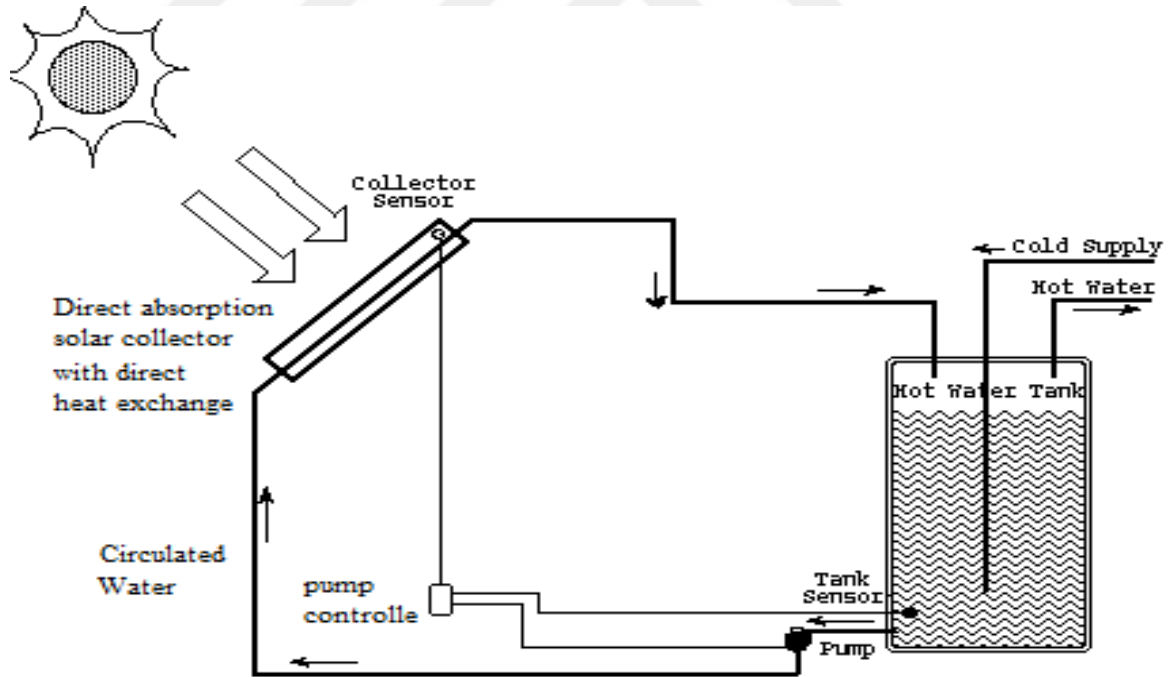


**Figure 3.4**: Outlines of new system of DASC with direct heat exchange.

The feasibility of this new technique to parabolic solar collector is investigated. Three different models were chosen, with glass-to-copper tube size ratio of ¼, ½, ¾ to know the best one of them. The above three cases on a parabolic trough solar collector were simulated in ANSYS FLUENT. In the following section, modeling equations and correlations used to calculate the new thermal properties of fluid after adding nanoparticles are explained. Furthermore, equations are presented to calculate heat generated inside nanofluid due solar energy absorption, as well as modeling equations of a parabolic solar collector.

### 3.1 Parabolic Trough Solar Collector modeling.

The parabolic solar collector consists of Reflector and an receiver tube. The receiver tube is located along the focal line of the reflector and is made of glass, compound with a copper tube for direct heat exchange. The new technique uses the nanofluid instead of the spectrally selective coating and making the receiver tube as heat exchanger to reduce the thermal resistance as shows Figure (3.3). In this, section we will focus on the receiver tube because it is considered the main part of the solar collector, and all thermal processes are carried out inside it. The assumptions and constants adopted in simulation are:

1- The Model works at steady state conditions.

2- Thermal and chemical balance at all phases.

3- The fluid is in one phase.

4- The density inside tube (water) is constant.

5- Symmetry about the vertical axis.

The model of the PTSC is done by performing numerical simulation of solar collector tube subjected to concentrated solar radiation via ANSYS FLUENT. Figure 3.5 shows the schematically diagram of a parabolic solar collector and how the beam radiation are reflected by the reflector onto the receiver tube.
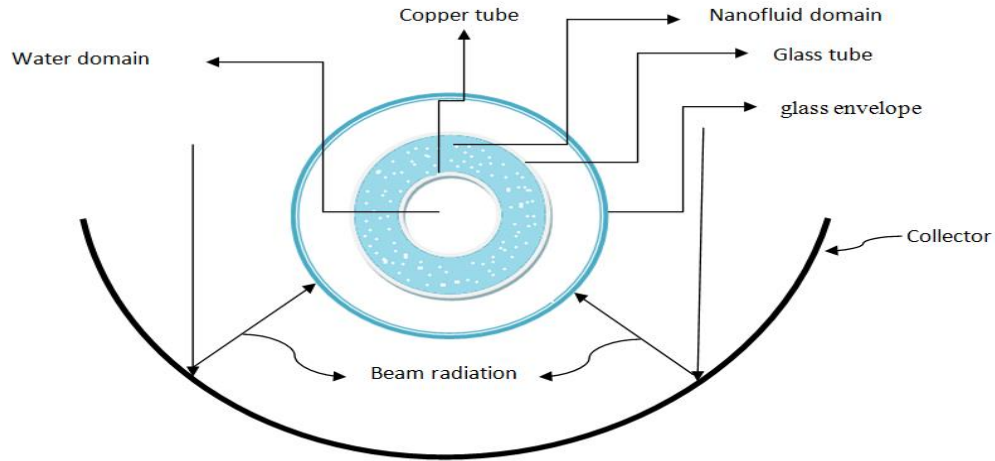
**Figure 3.5**: Parabolic trough solar collector.

### 3.1.1 Reflector.

This part is one of the main parts of parabolic trough solar collector which the other main parts influences it during sun tracing. It's usually made by bending highly reflective metallic sheet with the lowest absorptivity into a parabolic shape. To determine the shape of the curve of the parabolic trough collector and the possibility of determining the curve of the section with high precision suitable to be executed geometrically, especially that any deviation in the arc section will lead to the deviation of the sun's falling and reflected in the direction of the receiver tube to avoid the dispersion and ensure the concentration of radiation towards the receiver tube, the parabolic equation was programmed with the Excel program as shown in Figure (3.6). It is a sample of the program where the coordinates of the section and the desired shape are calculated by reference to the design variables where the arc section of the parabola has been determined the focal length and angle. Figure (3.7) shows the final shape for the parabolic solar collector with dimensions. The specifications of the parabolic trough solar collector used in the simulation shown in Table 3.1.

**Graphical Design of a Parabolic Trough Concentrator**

Please enter the width : _1.050_ m
Please enter the depth : _0.263_ m

Arc length = _1.21_ m
Focus = _0.262_ m
Equation : Y = _0.95_ X²
Rim Angle = _90.0_ °

| X | Y | Angle | R from focus in m |
|-------|-------|-------|-------|
| 0.000 | 0.000 | | |
| 0.105 | 0.011 | 11.3 | 0.27 |
| 0.210 | 0.042 | 21.8 | 0.30 |
| 0.315 | 0.095 | 31.0 | 0.36 |
| 0.420 | 0.168 | 38.7 | 0.43 |
| 0.525 | 0.263 | 45.0 | 0.53 |
| 0.630 | 0.379 | | |

In order to get depth to be equal to focus :
Width = 1.050 m
Focus = 0.263 m
Depth = _0.263_ m

**Figure 3.6:** The main interface of program to design of PCTS use Excel.
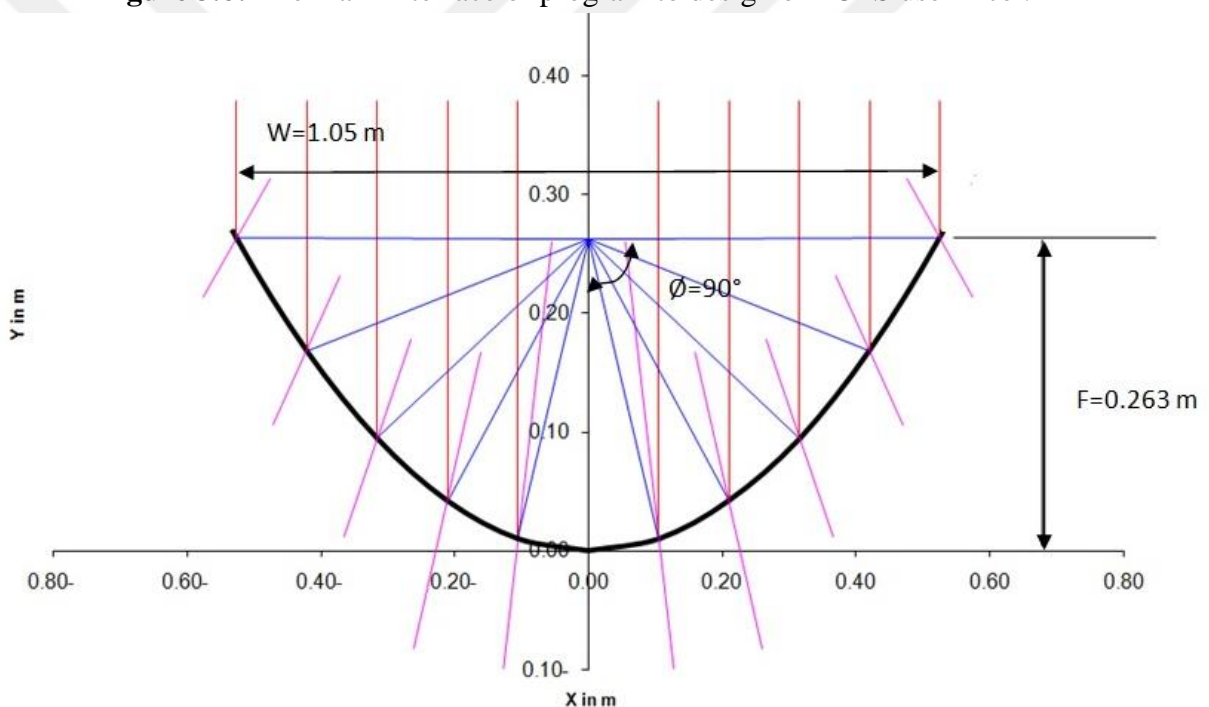


**Figure 3.7:** The final shape of the parabolic trough solar collector.

### 3.1.2 Receiver (receiver tube).

The receiver of the conventional parabolic trough solar collector contains the receiver tube where the rays are focused, this tube usually is coated in black with a view to absorb more heat. In this study, the design of the receiver is changed, by replacing the spectral selective coating with a glass envelop filled with nanofluid. This was done by making the receiver consist of glass tube compound with a copper tube and filling nanofluid in gap between them (see Figure 3.3). As the water is circulated in the copper

tube, the nanofluid remains stationary inside the gap. The incident solar radiation passes through the glass wall, absorbed by nanoparticles, and converted into heat rapidly. The heat generated inside nanofluid will be transferred to the circulated water through the copper wall. In this chapter, the heat generated, convective heat transfer and thermal losses in receiver tube will be studied. Table 3.1 shows the specifications of parabolic solar collector used in simulation and experiment.

**Table 3.1:** Receiver and Collector specifications.

| Receiver- glass tube | | | |
|---|---|---|---|
| Parameters | Symbol | Unit | Value |
| Inner diameter | $D_{gi}$ | mm | 51 |
| Outer diameter | $D_{go}$ | mm | 56 |
| Emissivity of glass | $\varepsilon_g$ | - | 0.89 |
| Transmittance of glass | $\tau_g$ | - | 0.93 |
| Material type | - | - | Pyrex glass |
| Receiver- copper tube | | | |
| Inner diameter | $D_{ci}$ | mm | 22 |
| Outer diameter | $D_{co}$ | mm | 25 |
| Emissivity of copper | $\varepsilon_c$ | - | 0.07 |
| Material type | - | - | copper |
| Collector | | | |
| width | w | m | 1.05 |
| length | L | m | 1.0 |
| Rim angle | Ø | deg | 90° |
| Optical efficiency | $f$ | - | 0.73 |
| Focal length | F | m | 0.263 |
| Concentrating ratio | $C_R$ | - | 6.55 |
| Material type | - | - | Stainless steel 430L |

### 3.1.2.1 Heat generated.

The receiver tube is simulated using ANSYS FLUENT steady state condition are assumed the derivations of the boundary condition source term are provided in this section clarified later. Figure 3.9 shows the solar irradiation transfer into the nanofluid. And within the nanofluid the transmitted radiation intensity ( $I_t$ ) changes only in two dimensions – (r,θ) direction in the cylindrical coordinate. Thus, no change of It with z-

direction. With reference to the Beer-Lambert Law, one could get the radiation intensity distribution inside the receiver tube by using a radiative transfer equation as follows:

$$\frac{\partial I_t(r,\theta)}{\partial r} = -K_\varrho I_t(r,\theta) \tag{3.1}$$

Which $K_e$ is the extinction coefficient of nanofluid, $I_t$ $(r,\theta)$ the transmitted radiation intensity at coordinate $(r,\theta)$.

As the solar collector is a parabolic the incident intensity around the cylindrical surface of tube is non-uniform changing with $(\theta)$ angle, it is necessary to find a method to calculate $I_o(\theta)$. Xu et al [4] derived the following equation for the calculation of radiation around the surface of the tube. The equation is applied to the model and the results are compared with the results obtained from the Soltrace software [46] (see Figure 3.8).

$$I_o(\theta) = 4\, fG\, \frac{p}{D_{go}}\, \frac{1-\cos\theta}{sin^2\theta} \tag{3.2}$$

Where $p$ is the focal length of parabolic trough. G is the incident global solar radiation. F is the optical efficiency. $D_{go}$ is the diameter of receiver tube.

When the rim angle$(\emptyset)$ is $(90°)$ the angle $(\theta)$ is in the range of $(-75°$ to $75°)$.

The incident global solar radiation. The transmitted radiation intensity at radius $r$ is calculated by equation 3.3 :

$$I_t(r,\theta) = e^{-K_e r} I_0(\theta) \tag{3.3}$$

There is some radiation scattering outside from the nanofluid as scatter radiation $I_s(r,\theta)$ as shown in Figure 3.9. To simplify the equation, the coefficient of absorption $(K_a)$ can be defined in terms of $I_t$ $(r,\theta)$ , $I_s(r,\theta)$ and $I_o(\theta)$ as follows [4]

$$\frac{I_t(r,\theta)+I_s(r,\theta)}{I_o(\theta)} = e^{-K_a r} \tag{3.4}$$
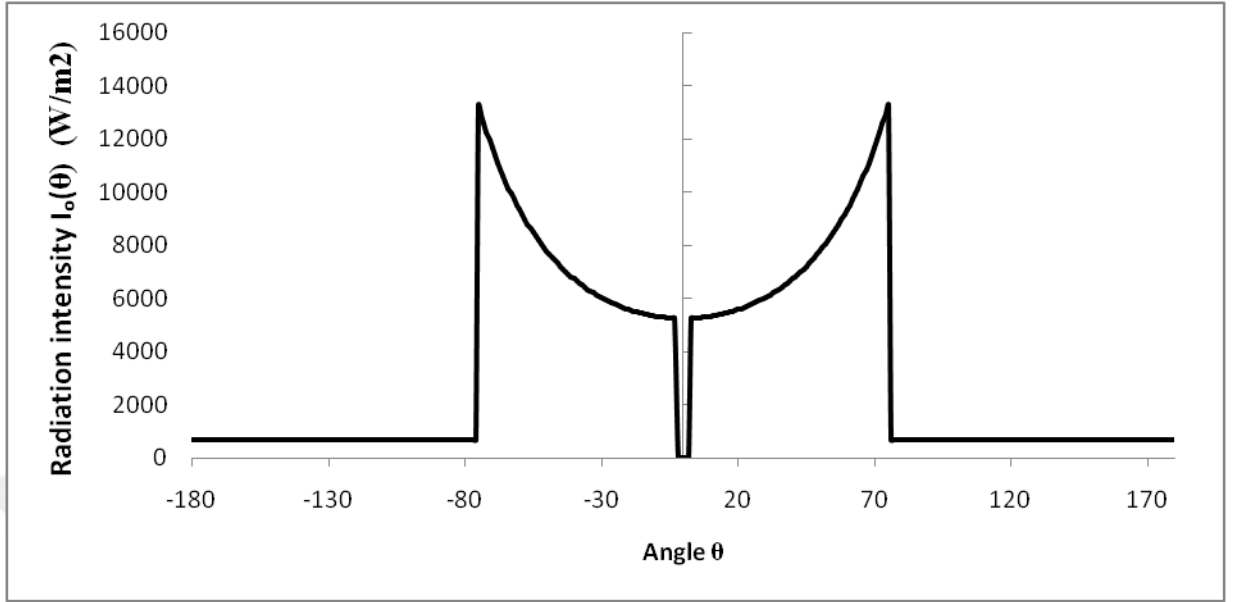
**Figure 3.8**: Solar radiation intensity around of receiver tube.

To calculated the absorbed heat flux of nanofluid qf(r,θ) from the surface to the radius, could by using absorption coefficient of nanofluid,

$$q_f(r,\theta) = I_0(\theta) - [I_t(r,\theta) + I_s(r,\theta)] = I_0(\theta)(1 - e^{-K_a r}) \tag{3.5}$$

The important part of the mentioned previously is how to calculate the heat generated inside the nanofluid, by using the equations (from 3.1 till 3.5). The heat generated is assigned as an internal heat source, the relationship shows that the change occurs with optical depth. In this case, the optical depth is the changed in radius, so the relationship is

$$\Phi = -\frac{\partial q_f}{\partial r} \tag{3.6}$$

For the purpose of deriving the equation (3.6) for the generated energy inside nanofluid, the control volume was used. The derived equation will be used, in the ANSYS software by creating UDF File (user-Defined function) as thermal solar energy source, to calculate the energy generated in the nanofluid zone. The UDFs used in this study found in Appendix A. Figure (3.5) shows the control volume.

28

$$\Phi = -\frac{\partial q_f}{\partial r} = \frac{q_f(r_{i+1},\theta j)r_{i+1} - q_f(r_i,\theta j)r_i}{r_i - r_{i+1}} \tag{3.7}$$

The mathematical form of energy equation including source term ($\Phi$) can express heat transfer in nanofluid region. The steady state form of energy equation has been solved as follows;

$$\frac{\partial(\rho u_x T_f)}{\partial x} + \frac{\partial(\rho u_y T_f)}{\partial y} + \frac{\partial(\rho u_z T_f)}{\partial y} = \frac{\partial}{\partial x}[\frac{k}{C}\frac{\partial T_f}{\partial x}] + \frac{\partial}{\partial y}[\frac{k}{C}\frac{\partial T_f}{\partial y}] + \frac{\partial}{\partial z}[\frac{k}{C}\frac{\partial T_f}{\partial z}] + \Phi \tag{3.8}$$
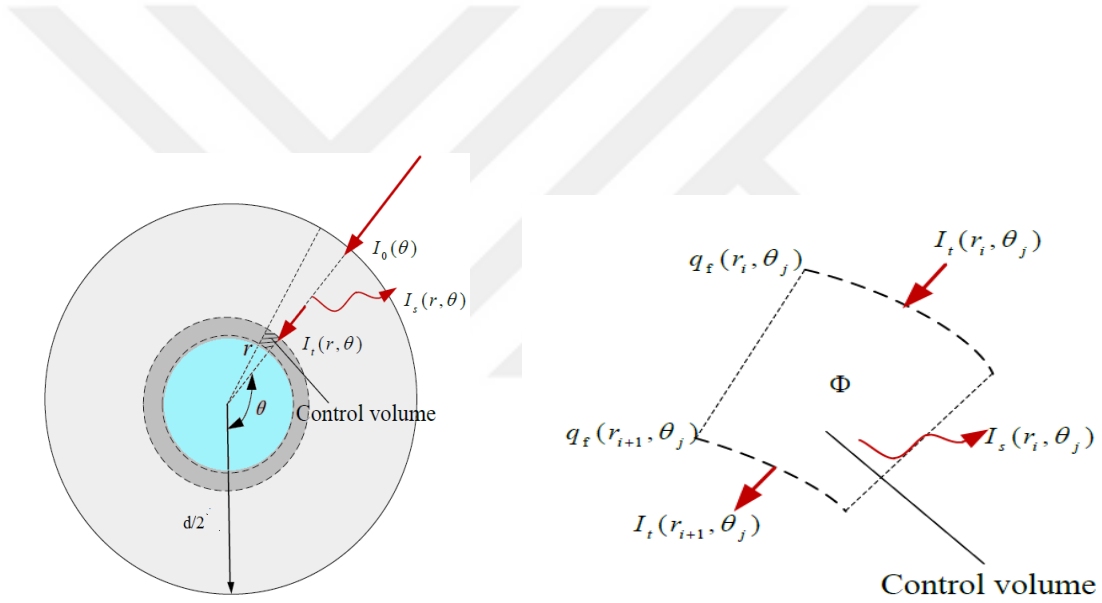


**Figure 3.9**: solar radiation transfer inside nanofluid tube and Characteristics control volume.

### 3.1.2.2 Convective heat transfer.

As explained previously, that the generation of heat in the nanofluid is due to the solar radiation absorbed by the nanoparticles and the oil. This heat induces a buoyancy driven flow field in the nanofluid. The heat is then transferred to the copper tube via convective heat transfer. The Rayleigh number is the parameter associated with the buoyancy-driven flow which cause the natural convection. The Boussinesq approximation is selected for the CFD model

### 3.1.2.2.1 Rayleigh number.

The Rayleigh number, Ra, is a dimensionless number associated with buoyancy driven flows. When the Rayleigh number is below some critical value specific for the fluid, the heat transfer process is primarily conductive. When the Rayleigh number exceeds that critical value there is an onset of convective heat transfer. The Rayleigh number is given in the equation (3.9) below.

$$R_{aL} = \frac{g\beta(T_o - T_i)L^3}{\alpha v} \tag{3.9}$$

Where $R_{aL}$ the Rayleigh number, $\beta$, $v$ $and$ $\alpha$ are the thermal expansion coefficient, the kinematic viscosity and the thermal diffusive coefficient respectively.

The heat convective is calculated by using the equation 3.10.

$$\bar{q} = \frac{2\pi \, k_{eff}}{\ln(r_0/r_i)} \, (T_0 - T_i) \tag{3.10}$$

where $k_{eff}$ is the effective conductivity of the stationary fluid, $k_{eff}$ can calculate by equation (3.11)

$$k_{eff} = 0.386 \, k \, [\frac{pr}{0.861 + pr}]^{0.25} \quad (R_{ac})^{0.25} \tag{3.11}$$

The three cases are studied and as mentioned in appendix B.

### 3.1.2.2.2 Boussinesq approximation.

The Boussinesq approximation is a method to solve nonisothermal flow, such as natural convection problem, without having to solve for the full compressible formulation of the Navier-stokes equations. The rule of this approximation is that there is flow within which the temperature variation is very little, and so the density variation is also very little, nevertheless within which the buoyancy drives the motion. so the variation in density is neglected all over except within the buoyancy term.

In Boussinesq approximation, the change in fluid properties is assume to be negligible except for the density ($\rho$). The mass conservation equation of Navier-stokes system is:

$$\frac{\partial \rho}{\partial t} + \nabla.(\rho u) = 0. \tag{3.12}$$

When the change in density is ignored:

$$\nabla.u = 0 \tag{3.13}$$

The Navier–Stokes momentum equation for incompressible flow is:

$$\frac{\partial u}{\partial t} + u.\nabla u = -\frac{1}{\rho}\nabla p + v\nabla^2 u + \frac{1}{\rho}F \tag{3.14}$$

$\nabla^2 u$ is the kinematic viscosity, and F is the bulk forces.

The density variation, from mean value of $\rho o$, due to

$$\rho = \rho o - \beta \rho o \Delta T \tag{3.15}$$

The above bulk force term in a constant gravitational field is written as F=$\rho$g.

The buoyancy force due to the temperature induced density variation can be written as F=$-g\beta\Delta T$ where $\beta$ is the coefficient of volumetric expansion and $\Delta T$ is the temperature difference from the state where the density is $\rho o$. The negative sign takes care of the direction of the buoyancy force which always acts on the opposite direction of acceleration g.

The momentum of the Navier–Stokes system, with the Boussinesq equation, can be written as:

$$\frac{\partial u}{\partial t} + u.\nabla u = -\frac{1}{\rho_0}\nabla p + v\nabla^2 u - g\beta\Delta T \tag{3.16}$$

### 3.1.2.3 Thermal losses

Thermal losses are one of the problems researchers are trying to reduce, to get the more energy. The thermal losses in parabolic trough solar collector is calculated by the equation (3.17) [15].

$$\frac{Q\ loss}{Ar} = h_w(T_r - T_a) + \varepsilon\sigma\ (T_r^4 - T_{sky}^4) + U_{cond}\ (T_r - T_a)$$
$$= (\hslash_w + h_r + U_{cond})\ (T_r - T_a)$$

$$U_L = \frac{Q_{loss}}{Ar\ (Tr - Ta)} \tag{3.17}$$

Where $T_r$ receiver temperature , $T_a$ ambient temperature ,$A_r$ receiver Area

Because of the temperatures variation on the outer surface of the receiver tube, the losses will be different on the different locations. A FLUENT user defined function (UDF) is constructed to model the losses from the wall accurately. See appendix A2 of the details

The radiation coefficient is calculated from

$$h_r = \frac{\varepsilon\sigma\ (Tr^4 - T^4 sky)}{(Tr - Ta)} \tag{3.18}$$

If an evacuated tube inclosing the nanofluid tube is used then convective heat losses can be ignored. Heat losses can be computed from:

$$Q_{loss} = \frac{2\pi k_{eff} L}{\ln(D_{eni}/D_r)}\ (T_r - T_{eni}) + \frac{\pi D_r L\sigma(T_r^4 - T_{sky}^4)}{\frac{1}{\varepsilon_r} + \frac{1-\varepsilon_{en}}{\varepsilon_{en}}(\frac{D_r}{D_{eni}})} \tag{3.19}$$

When an evacuated tube is not used both radiative and convective heat losses should be computed. The present work implements the following equation (3.20) as FLUENT UDF file to computed the wall heat losses.

$$Q_{loss} = \pi D_{eno} L h_w(T_{eno} - T_a) + \varepsilon_{en}\pi\ D_{eno} L\sigma\ (T_{eno}^4 - T_{sky}^4) \tag{3.20}$$

### 3.2 Types of fluids.

Tap water, flowing inside the copper tube, is used as working fluid. The nanofluid, contained within the volume between the copper tube and the glass tube, is made by 5W30 engine oil mixed with copper oxide nanoparticles of 200 nm. Two volume fraction of nanofluid are studied: 0.055% and 0.1%.

### 3.2.1 Nanofluid modeling.

This section present a formula to calculate the thermal properties of nanofluids. CuO nanoparticles mixed with engine oil 5W30 is the base fluid. The Nanofluid properties (density, dynamic viscosity, heat capacity in a constant pressure and thermal conductivity) are estimated by the formulae presented in the following section.

### 3.2.1.1 Base fluid Synthetic oil (5W30).

The high price of industrial oil used in the solar collectors, motivates us to use synthetic oil (5W30) due to low price and availability in the markets. At operating temperature of 250 °C, water used as working fluid can be in two phases.

### 3.2.1.2 Nanoparticles.

For the purpose of improving the physical and thermal properties of the heat transfer fluid, nanoparticles are added as these particles increase the value of the thermal conductivity coefficient, which in turn increases the fluid efficiency of heat transfer. This is in addition to the change in density and specific heat capacity. CuO nanoparticles was select in this study with (200nm) particle size and spherical shape.

### 3.2.1.2.1 CuO.

The copper oxide (CuO) particles were chosen for two main reasons: first is the oxygen facilitates the mixing of the nanoparticles with the base fluid. The second reason is that it has a high thermal conductivity, which increases the thermal conductivity of the compound fluid. The particles having 200 nm and spherical shape has been selected in the simulation before [31]. The thermophysical properties of nanoparticles and the base fluid at 27 °C are shown in Table 3.2.

**Table 3.2:** Thermophysical properties of nanoparticles and base fluid.

| parameter | temperature | $\rho$ | $C_p$ | k | $\mu$ | $\beta$ |
|---|---|---|---|---|---|---|
| Unit | °C | $Kg.m^{-3}$ | $J.(kg.K)^{-1}$ | $W.(m.K)^{-1}$ | Pa.s | $K^{-1}$ |
| Oil (5w30) | 27 | 840 | 1900 | 0.14 | 0.063 | 0.00070 |
| CuO | 27 | 6300 | 475 | 33 | - | $1.8*10^{-5}$ |

### 3.2.1.3 Density of Nano-fluid.

To calculate the density of the nanofluids the homogeneity of nanoparticles and the base fluid is assumed. Also, the base fluid is assumed to be in liquid phase only. The formula for the density of the nanofluid (see equation(3.21)) assumes a mass balance between the nanoparticles and the base fluid [42]:

$$\rho_{nf} = \rho_f(1 - \varphi) + \rho_p \varphi \qquad (3.21)$$

$\rho_{nf}$ is the density of the nanofluid, $\rho_f$ is the density of the base fluid, $\rho_p$ is the density of the nanoparticles, all quantities in kg/m$^3$.

### 3.2.1.4 Specific heat capacity of Nano-fluid.

Specific heat capacity have been estimated by supposing thermal equilibrium between the nanofluid and the copper particles. The formula for the specific heat capacity of the nanofluid mixture [42] is as follows:

$$C_{p\,nf} = C_{pf}(1 - \varphi) + C_{p\,p}\varphi \qquad (3.22)$$

Where $C_{pnf}$ is the specific heat of the nanofluid, $C_{pp}$ is the specific heat of the nanopartical, $C_{pf}$ is the specific heat of the bace fluid, all quantities in J•(kg•K) −1

### 3.2.1.5 Dynamic Viscosity of Nano-fluid.

Many models to calculate the dynamic viscosity of the nano-fluids are found in the literature, but in this study, the Einstien model [16] is used due to is validity for spheric particles with minimal concentration of 2%. Also the model is the oldest used to determine the viscosity of nano-fluids. The model for the viscosity of the nanofluid is represented below.

$$\mu_{nf} = \mu_f(1 + 2.5\,\varphi) \qquad (3.23)$$

Where $\mu_{nf}$ is the dynamic viscosity of the nanofluid, $\mu_f$ is the dynamic viscosity of the base fluid in Pa•s, $\varphi$ is the volume fraction on nanoparticles to base fluid.

### 3.2.1.6 Thermal conductivity of nanofluids.

In this study Maxwell model [21] is selected as spheric particles of minimal 1% concentration is used. Also, the Maxwell model is the oldest model used to calculate the thermal conductivity of solid-liquid mixtures. The model is as follows:

$$k_{nf} = k_f \frac{k_p + 2k_f + 2\varphi(k_p - k_f)}{k_p + 2k_f - \varphi(k_p - k_f)} \qquad (3.24)$$

Where $K_p$ is the thermal conductivity of nanoparticles, $k_f$ is the thermal conductivity of the base fluid, $k_{nf}$ is the thermal conductivity of nanofluid, all quantities in $W\bullet(m\bullet K)^{-1}$

### 3.2.1.7 Thermal expansion coefficient.

The thermal expansion characteristic is one such physical property, which plays an important role in many heat removal systems involving natural convection. The volumetric thermal expansion coefficient ($\beta$) of a nanofluid can be calculated by the following formula [47] :

$$\beta_{nf} = \varphi\,(\beta)_p + (1 - \varphi\,)\,(\beta)_f \qquad (3.25)$$

Where $\beta_{nf}$ is the thermal expansion the nanofluid, $\beta_p$ is the thermal expansion the nanoparticles, $\beta_f$ is the thermal expansion the base fluid, all quantities in $K^{-1}$.

### 3.2.1.8 Volume fraction

One of the important parameters in preparing nanofluids is its volume fraction. It is the ratio of the total volume of the nanoparticles to the total volume of the nanoparticles and base fluid. The formula to calculate the volume fraction is given by [48]:

$$\varphi = \left[ \frac{(\frac{W_{CuO}}{\rho_{CuO}})}{\left(\frac{W_{CuO}}{\rho_{CuO}} + \frac{W_{bf}}{\rho_{bf}}\right)} \right] \times 100 \qquad (3.26)$$

### 3.2.1.9 Optical Absorption properties of nanofluid.

Solar absorption is a key factor in the direct absorption solar collector. The addition of nanoparticles to water caused an increase in absorption of solar radiation 9 times compared to the pure water [2]. The absorption coefficient ($K_a$) is an important factor because it used in the calculation of the energy generated inside the nanofluid. The above energy generation is caused by the conversion of solar radiation into thermal energy by the nanofluid.

Present work uses two concentration of nanoparticales for both CFD simulation and experiments. The nanoparticales used are 200nm copper oxide particles with concentration 0.055% and 0.1%. the physical parameters, using the above formulae are computed (see table 3.33 and 3.4).

**Table 3.3. physical properties of nanofluid at concentrating 0.055%.**

| Parameters | Unit | CuO nanoparticles | Synthetic oil 5w30 | 0.055wt% CuO/oil nanofluid |
|---|---|---|---|---|
| $C_p$ | $J.(kg.K)^{-1}$ | 475 | 1900 | 1899.2 |
| $\rho$ | $Kg.m^{-3}$ | 6300 | 840 | 843.003 |
| $k$ | $W.(m.K)^{-1}$ | 33 | 0.14 | 0.14022 |
| $\mu$ | Pa.s | - | 0.063 | 0.06308 |
| $\beta$ | $K^{-1}$ | $1.8x10^{-5}$ | $7x10^{-4}$ | $6.9962x10^{-4}$ |
| $K_a$ | $m^{-1}$ | - | 2 | 103 |

**Table 3.4. physical properties of nanofluid at concentrating 0.1%**

| Parameters | Unit | CuO nanoparticles | Synthetic oil 5w30 | 0.1wt% CuO/oil nanofluid |
|---|---|---|---|---|
| $C_p$ | $J.(kg.K)^{-1}$ | 475 | 1900 | 1898.57 |
| $\rho$ | $Kg.m^{-3}$ | 6300 | 840 | 845.46 |
| $k$ | $W.(m.K)^{-1}$ | 33 | 0.14 | 0.1404 |
| $\mu$ | Pa.s | - | 0.063 | 0.06315 |
| $\beta$ | $K^{-1}$ | $1.8x10^{-5}$ | $7x10^{-4}$ | $6.9931x10^{-4}$ |
| $K_a$ | $m^{-1}$ | - | 2 | 345.49 |

### 3.2.2 Water modeling.

Many solar applications are used to heat water to use it in domestic applications and heating, or convert water into steam for use in power plants. The parabolic trough solar collectors either heat water directly or heat another liquid, such as oil, and using a heat exchanger, heat water. In this study, water is used as working fluid inside the copper tube, with various volumetric flow rates (20, 40, 60, 80 and 100 l/h) and different

inlet temperatures (300,325 and 350 K). Due to water flow inside the tube, temperature gradients are crated resulting in differential heat transfer coefficient. the convective heat transfer coefficient, for each location on the tube,  must be calculated. The physical properties of water used in the simulations is shown in table 3.5.

**Table 3.5. The physical properties of  water at different temperatures.**

| parameters | temperature | $\rho$ | Cp | k | $\mu$ |
|---|---|---|---|---|---|
| Unit | K | Kg.m$^{-3}$ | J.(kg.K)$^{-1}$ | W.(m.K)$^{-1}$ | Pa.s |
| | 300 | 997 | 4179 | 0.613 | 8.55x10$^{-4}$ |
| Water | 325 | 987 | 4182 | 0.645 | 5.28x10$^{-4}$ |
| | 350 | 973 | 4195 | 0.668 | 3.65x10$^{-4}$ |

### 3.2.2.1 Reynolds Number.

The Reynolds number is a dimensionless number that indicates the flow type of a fluid, whether it is laminar or turbulent; Reynolds number above 4000 for a pipe flow usually shows a turbulent flow. The equation of the Reynolds number is provided as follows:  $Re = \frac{\rho.v.Dci}{\mu}$ $\qquad\qquad$ (3.27)

### 3.2.2.2 Prandtl Number.

The Prandtl number is a dimensionless number that measures the ratio of the momentum diffusivity to the thermal diffusivity. The Prandtl number is given by:

$$Pr = \frac{\mu.Cp}{k} \qquad\qquad (3.28)$$

### 3.2.2.3 Nusselt Number.

The Nusselt number is a dimensionless number that measures the ratio of convective to conductive heat transfer in the fluid domain. It depends on the flow type, boundary and geometry of the surface, Reynolds number and Prandtl number. Since the flow has been imposed laminar, Nusselt number as shown below:

$$Nu= 4.36 \qquad\qquad (3.29)$$

### 3.2.2.4 Convective heat transfer coefficient.

The overall convective heat transfer coefficient of a fluid flow through the receiver tube of a PTSC can be calculated using the following equation:

$$h = \frac{Nu.k}{Dci} \qquad\qquad (3.30)$$

### 3.3 Computational Model

Computational fluid dynamics utilizes numerical methods and algorithms to solve equations governing fluid flow and heat and mass transfer. Commercial CFD package ANSYS FLUENT is used in this study. FLUENT is capable of analyzing a wide range of fluid flow problems including incompressible and compressible flows, laminar and turbulent flows, viscous and inviscid flows, Newtonian and non-Newtonian flows, single-phase and multi-phase flows, etc. In addition, both steady-state and transient analyses can be performed. Also, FLUENT provides a solution to heat and mass transfer problems. Conduction and convection can be easily implemented by adding one extra energy equation. Simulation can be done in 3D for the model. This section shows the drawing of the model by design modeler and the generated mesh by mesh manager. In addition, it explains the Governing equations used in Ansys fluent to solve the model numerically.

### 3.3.1 Governing equations.

Ansys Fluent solves fluid flow problems numerically by solving the governing equations. The equations of mass and momentum conservation can be solved for all types of flow, including flow involving heat transfer.

### 3.3.1.1 The Mass Conservation Equation.

The mass conservation equation in Ansys Fluent is:

$$\frac{\partial \rho}{\partial t} + \nabla \cdot \left( \rho \vec{\upsilon} \right) = S_m$$

(3.31)

Where $S_m$ is the source term added to the continuous phase from dispersed second phase or user-defined function sources.

### 3.3.1.2 Momentum Conservation Equation.

The equation for conservation of momentum solved in Fluent is:

$$\frac{\partial}{\partial t}(\rho \vec{v}) + \nabla.(\rho \vec{v} \vec{v}) = -\nabla p + \nabla.(\bar{\bar{\tau}}) + \rho \vec{g} + \vec{F} \qquad (3.32)$$

Where p is the static pressure, $\bar{\bar{\tau}}$ is the stress tensor, $\rho \vec{g}$ is the gravitational body force, and $\vec{F}$ is external forces including user-defined source terms.

### 3.3.1.3 Energy conservation equation.

The energy conservation equation, use by FLUENT,

$$\frac{\partial}{\partial t}(\rho E) + \nabla \cdot (\vec{\upsilon}(\rho E + p)) = \nabla \cdot \left( k_{eff} \nabla T - \sum_j h_j \vec{J}_j + (\bar{\bar{\tau}}_{eff} \cdot \vec{\upsilon}) \right) + S_h \qquad (3.33)$$

Where $k_{eff}$ is the effective conductivity. The first three terms on the right-hand side are the expressions of energy transfer due to conduction, species diffusion, and viscous dissipation, respectively. And $\vec{J}_j$ is the diffusion flux of species j.

$S_h$ is the volumetric heat sources we have derived and programming as a user-defined function to calculate internal heat generated inside the nanofluid zone.

### 3.3.2 Finite volume method.

The finite volume method (FVM) is a method to represent and evaluate partial differential equations in the form of algebraic equations. In Finite volume method the model is divided into a number of cells and elements as control volumes. The physical parameters of interest, such as temperature or pressure, is evaluated in the centroid of the control volume. Volume integral is performed to convert the divergence terms in the partial differential equations (Equation 3.34) into a surface integral (Equation 3.35) by using divergence theorem. The surface integral is then evaluated as the flow parameter at the surface of each control volume. The flow entering a certain volume is equal to that

leaving the neighboring volumes. Therefore, FVM is inherently conservative by construction.

$$\frac{\partial u}{\partial t} + \nabla \cdot f(u) = 0 \tag{3.34}$$

$$\frac{\partial}{\partial t} \int_v u \, dx + \oint_{\partial v} f_i n_i \, ds = 0 \tag{3.35}$$

### 3.3.3 Buoyancy-driven.

When the model is predominated by buoyancy force, for example, natural convection, it can be modeled in ANSYS FLUENT by various methods that approximate the density variation with respect to the temperature. For nanofluid, the Boussinesq approximation is frequently used by virtue of the relatively fast convergence rate. The model regards density as a constant quantity in all governing equations to be solved, except for the body force term in the momentum equation.

$$(\rho - \rho_\circ)g \approx -\rho_\circ \beta (T - T_\circ)g \tag{3.36}$$

Where $\rho_\circ$ is the constant density of the flow, $T_\circ$ is the operation temperature, and $\beta$ is the thermal expansion coefficient.

$$\beta = -\frac{1}{\rho}\left(\frac{\partial \rho}{\partial T}\right)_p \tag{3.37}$$

This approximation is valid when the density is small change $\beta(T-T_o)<<1$.

### 3.3.4 Solution methods.

The solver used in the simulation is pressure-Based. When solving the pressure-velocity coupling there are four schemes available for calculations: SIMPLE, SIMPLEC, PISO, and Coupled. This study uses coupled method due to its high precision in solution.

### 3.3.5 Numerical details.

The details of the Numerical used in the simulation as shown in Table 6.

**Table 3.6. Numerical details use in simulation.**

| Code | ANSYS FLUENT R15.0 |
|---|---|
| Flow | Laminar |
| Solver | Pressure-Based |
| Time | Steady |
| Velocity – Pressure Coupling | Coupled |
| Gradient | Least Squares Cell Based |
| Pressure | Second Order |
| Momentum | Second Order Upwind |
| Energy | Second Order Upwind |

### 3.4 Design Modeler

The ANSYS Design Modeler is the application used as a geometry editor of existing CAD models. Also, it is a parametric feature-based solid modeler designed so that one could intuitively and quickly begin drawing 2D sketches, modeling 3D parts, or uploading 3D CAD models for engineering analysis preprocessing. This property was used to draw the three models, the XY plane is selected to draw the model, using sketch tool and the Boolean tool for drawing 4 zones. Zone 1 is the water area, Zone 2 is the Copper tube area, Zone 3 is shows the nanofluid area, the last zone 4 is the glass tube. Then it is extruded to make the drawing 3D by using the symmetric option in both direction. This processes is used in drawing the three models required with different glass-to-copper tube size ratios (1/4, 1/2, 3/4). Table 7 shows the measurements that are used in the design of the three models. 3-D model is necessary because axial variation of the physical parameters. However, the geometry and the boundary condition are symmetric along the perpendicular plane that bisects the parabola and the tube along the axial direction. Figure 3.10 shows the Schematic diagram for receiver model geometry.

**Table 3.7: The tubes sizes used in the design.**

| Model ¼ | Copper tube | Glass tube |
|---|---|---|
| Inner diameter (mm) | 11.75 | 51 |
| Outer diameter (mm) | 12.75 | 56 |
| | | |
| Model ½ | Copper tube | Glass tube |
| Inner diameter (mm) | 22 | 51 |
| Outer diameter (mm) | 25 | 56 |
| | | |
| Model ¾ | Copper tube | Glass tube |
| Inner diameter (mm) | 35 | 51 |
| Outer diameter (mm) | 38 | 56 |
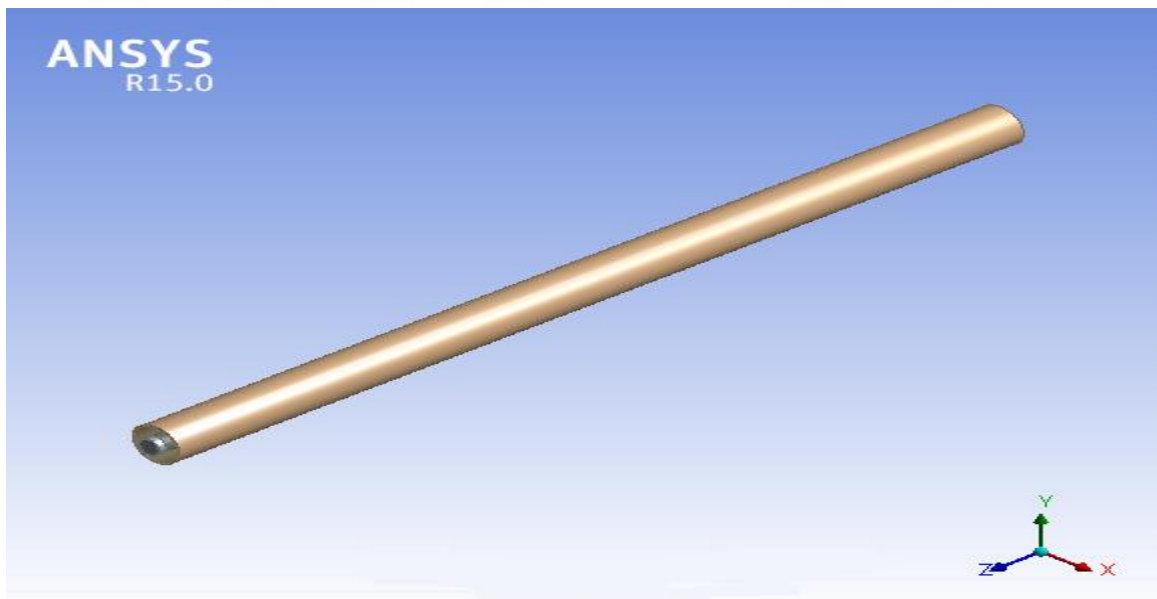


**Figure 3.10**: Schematic diagram for receiver model geometry.

### 3.5 Mesh Generation

Mesh is generated in a 3-dimensional model using mesh manager in ANSYS FLUENT. Hexahedral meshes are used in this study. The Z-axis which represents the length of the tube is divided into 500 divisions (see Figure 3.11). The zone 4, the volume of the glass tube, is segmented into 180 divisions in the axial direction with 6 nodes along the thickness of the tube. Zone 3 the nanofluid area is also segmented into 180 divisions and is 26 nodes in the depth. Zone 2 is the volume of the copper tube is segmented into 180 division with 7 nodes on the thickness of the tube. Zone 1 is the water area which is also segmented into 180 divisions and the cell size is selected to be 0.3 mm. The above fine mesh size is selected to capture the rapidly changing phenomena such as the temperature and momentum boundary layers. The mesh convergence study, discussed in chapter four provide a mesh of 4.6 million as the suitable mesh for the present study. Figure 3.12 shows all details of mesh.
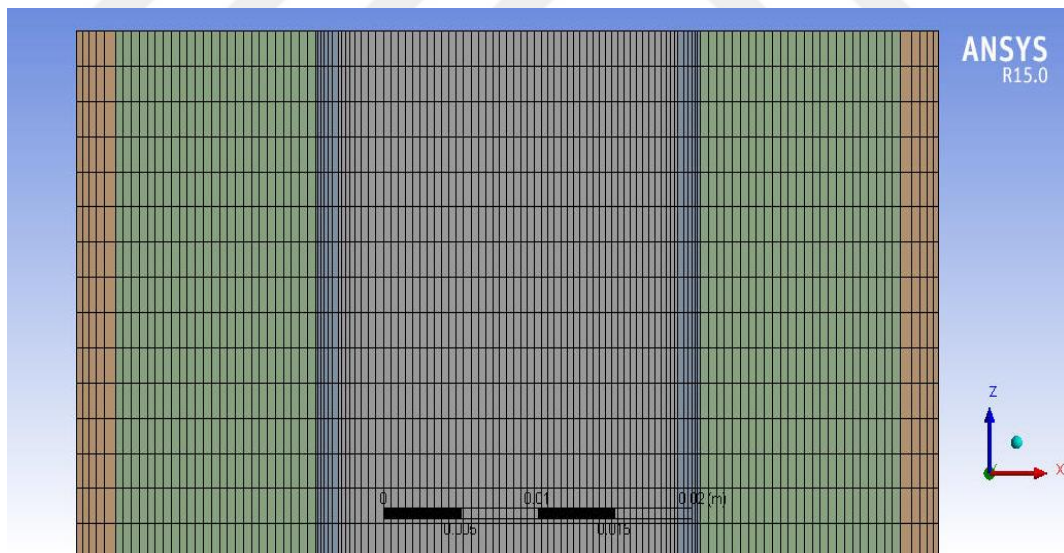


**Figure 3.11**: Mesh of the receiver tube in Z-axis.
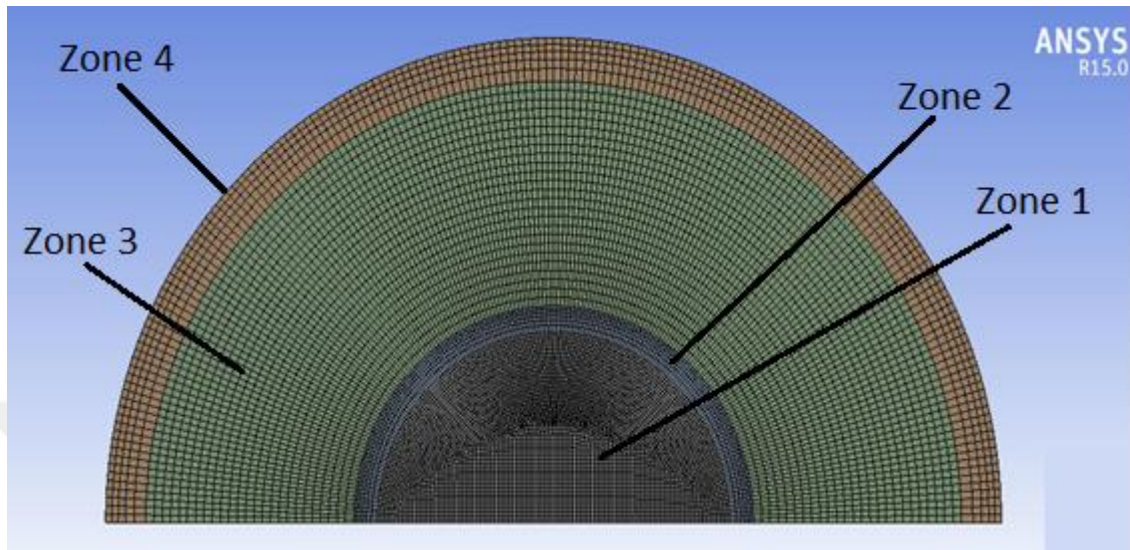
**Figure 3.12**: Mesh of the receiver tube.

### 3.6 Boundary condition.

In order to executed the simulation, certain boundary conditions must be provided to the model, including mass flow rate, temperature, heat generated into nanofluid etc. The inlet of water into the copper tube is defined as a mass flow rate and the outlet defined as outflow, with different flow rates (20,40,60,80,100 l/hr) and with varied inlet temperature (300, 325, 350 K) as shown in table 8. The heat generated in nanofluid is defined as UDF file as explained before in the section 3.1.2.1. The heat losses from the glass wall is also defined as UDF (see section 3.1.2.3). The receiver tube is model with the symmetry boundary condition as the geometry and the boundary conditions are symmetric along an axial vertical plane that bisects it.

**Table 3.8: The Boundary condition used in simulation.**

| | | |
|---|---|---|
| Inlet | Mass flow rate | 0.0055, 0.011, 0.0166, 0.022, 0.0277 kg/s |
| | Temperature | 300,325,350 K |
| Outlet | Outflow | 0.0055, 0.011, 0.0166, 0.022, 0.0277 kg/s |
| Heat generated | Source term | UDF file |
| Wall | Heat losses | UDF file |

## 3.7 Experimental work.

A parabolic trough solar collector is designed, manufactured, and tested. The collector design is the ½ ratio geometry. This geometry is selected for the experimentation as it outperformed the other two geometries studied with CFD. The measurements were made at University of Turkish Aeronautical Association campus in Ankara-Turkey.
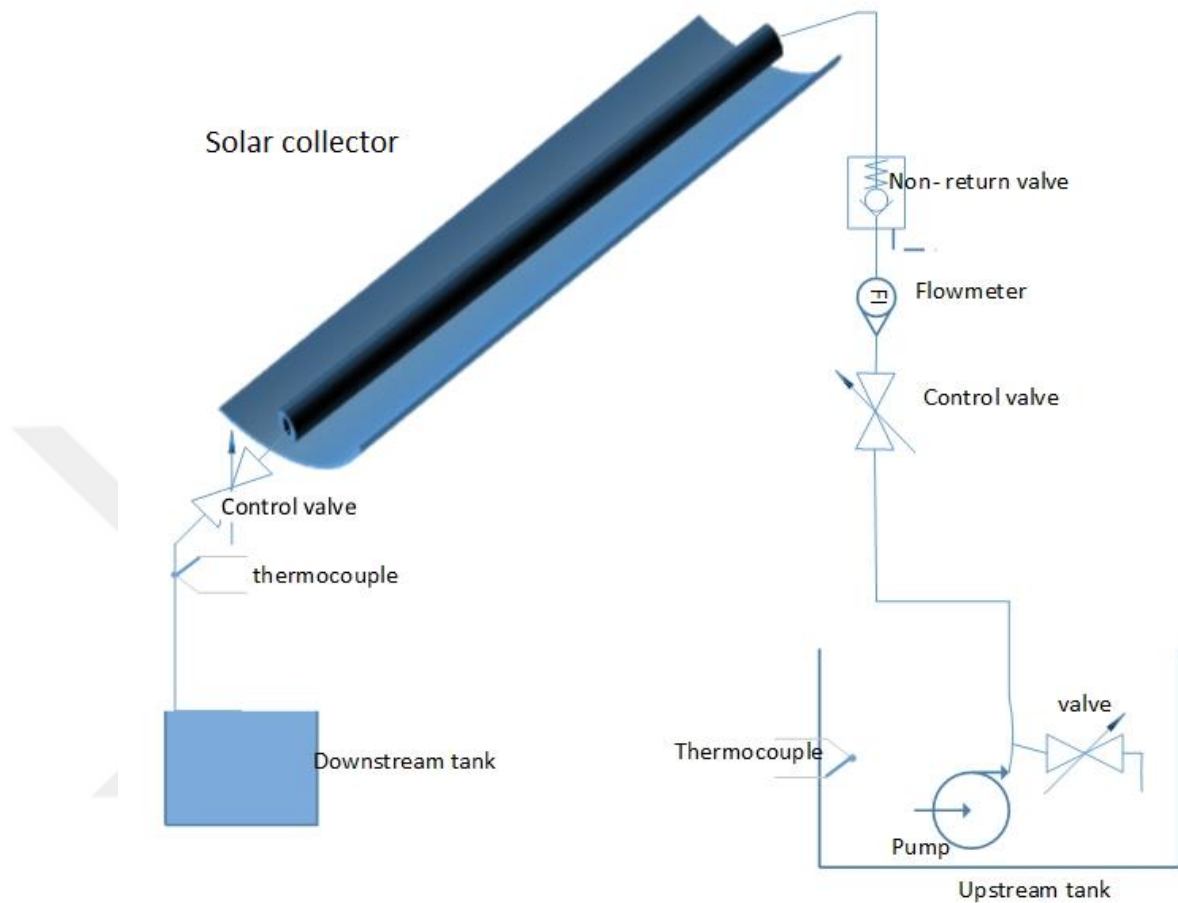
**Figure 3.13:** schematic diagram for experimental test

### 3.7.1 Design and manufacture of parabolic trough solar collector.

After obtaining the theoretical design of the solar collector as previously shown in Figure 3.6, the model was design and manufactured. The manufactured model consists of eight main parts, the Iron Frame, the reflector, the collector tube,  the Control Valves, the tank, the Flow Meter, the pump, Thermocouple and thermal control system in which temperatures are recorded.

### 3.7.1.1 Iron frame.

Framework with dimensions 1.05 m width with 1.02 m length is made of square steel strips. It is fitted with screw joints and columns that allows changing the angle as shown in Figure3.14. The control mechanism is a serrated rod fixed on the bolts to give the user the freedom to choose an angle.
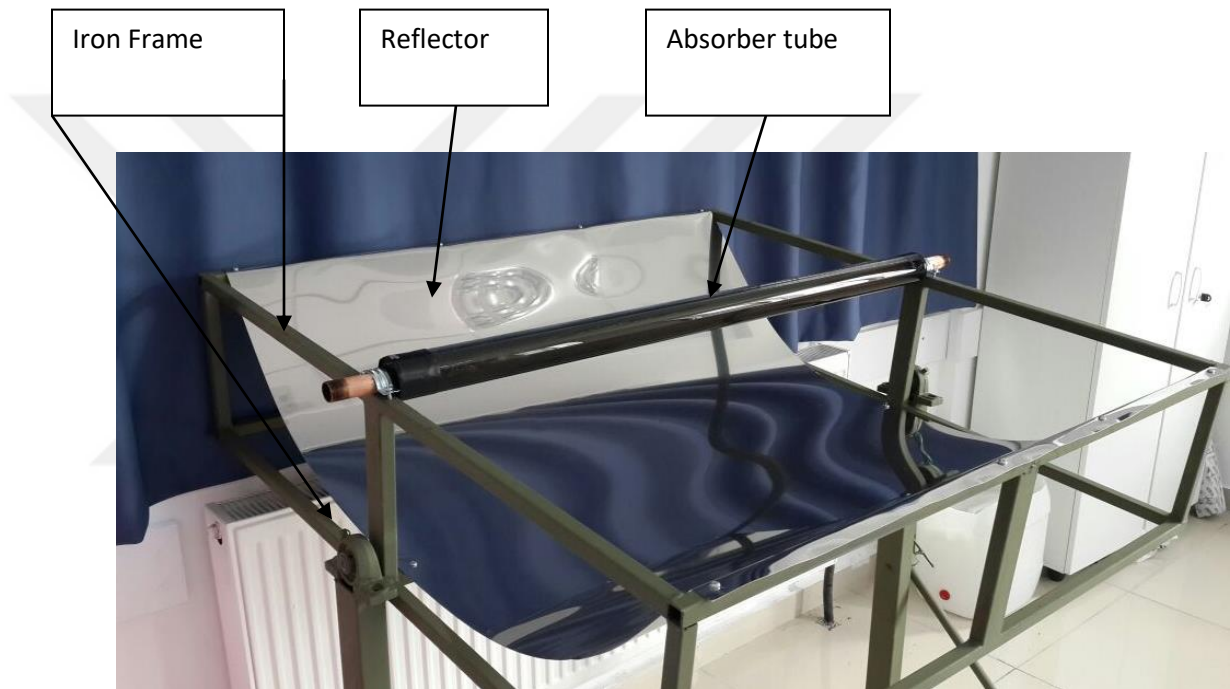


**Figure 3.14**: Photo of solar collector system.

### 3.7.1.2 Solar reflector.

The solar reflector is a polished sheet of stainless steel designed to give a suitable focal distance as shown in Figure 3.14. The coordinates for the desired parabola is computed using a spreadsheet software. The metal mirror is formed by a special rolling device. The plate is fixed on the iron structure. The manual tracking mechanism is a serrated rod. This mechanism is used to track the movement of the sun to keep the incident energy on the collector tube constant.

### 3.7.1.3 Receiver tube.

The receiver tube is made with an outer glass tube and an inner copper tube sharing the same axis. The copper tube extends horizontally 1.16 meters and its diameter is 25 mm. The common axis spans the length of the focus of the mirror. The gap between the glass tube and the copper tube is closed at both ends by a rubber seal and silicon. The gap is 1 m in length and is filled with nanofluid. The copper tube is open at both ends. The receiver tube is fixed onto the iron frame by screw and nuts to facilitate adjustment the ease of installation.

### 3.7.1.4 Control valve.

To control the fluid flow a 12 mm diameter valve is installed before the upstream of the receiver tube. Also a check valve in the entry area is installed to avoid a fluid return. Another 12 mm diameter control valve also installed, in outlet area, to obtain complete and accurate control over the amount of fluid flowing and as a result, obtain accurate readings. Figure (3.15) shown the type of valve and check valve.



**Figure 3.15**: check valve and Valve type ball valve.

### 3.7.1.5 Flow meter.

A rotameter of range 10 to 100 l/h (see figure 3.16) is installed upstream of the receiver tube. The experiment has flow rates larger than 20 l/h. The rotameter is calibrated before the experiments.

**Figure 3.16**: Flow meter used in the study.

### 3.7.1.6 pump.

A submersible water pump (see figure 3.17) with a volume flow rate of 30 liters per minute is used. The highest flow rate request for the experiments is 100 l/h which is considerable lower than the capacity of the pump. The water reservoir temperature is not appreciably increased due to the operation of the pump.



**Figure 3.17**: Submersible pump used in the study

### 3.7.1.7 Thermocouples.

The type K of the thermocouple is used in this study (see Figure 3.18) for measuring the temperatures at upstream and downstream of the receiver tube. The Arduino microcontroller is programmed to log the temperature data. Due to the high thermal conductivity of copper, inserting thermocouples through a hole in the water tube is not practice as the temperature of the tube interfere with the thermocouple through conduction. The water coming out of the receiver tube is immediately directed into a plastic tube where the thermocouple is inserted through a hole. The inlet water temperature is measured at the reservoir (see figure 3.13). The figure 3.19 shows the procedure diagram of installing Arduino.
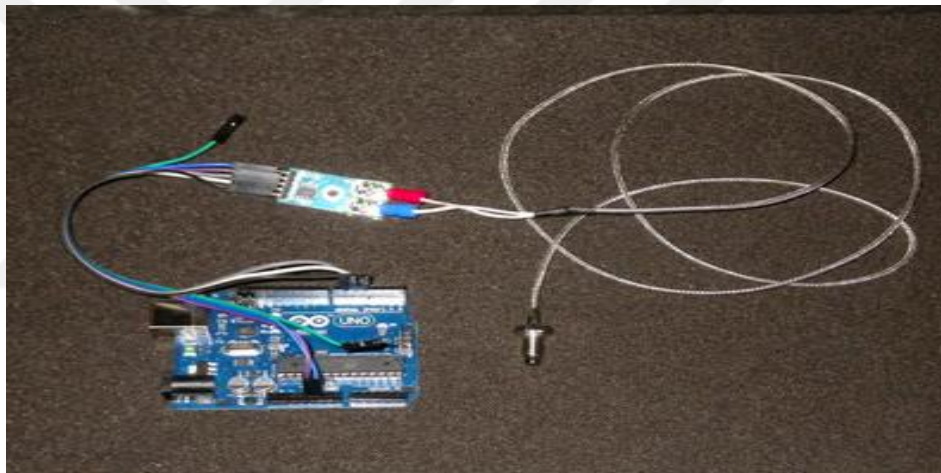


**Figure 3.18**: Thermocouple type k with Arduino used in the study.
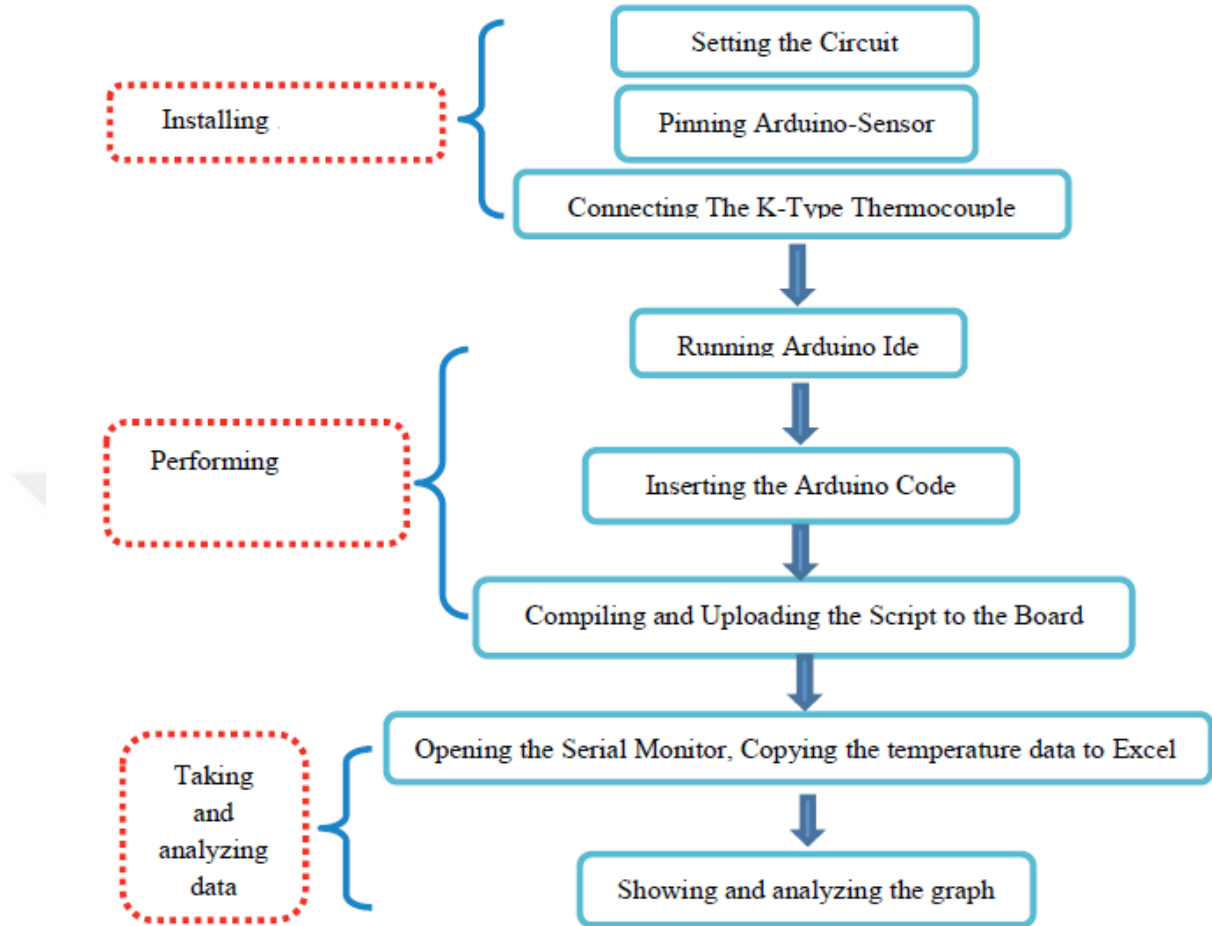
**Figure 3.19**: The procedure diagram of installing Arduino.

### 3.7.2 Preparing nanofluid.

There are two methods for preparing the nanofluid: The first method is the one-step method and the second is the two-step method. The two-step method is used widely for preparing nanofluid. In this study two-step method is used due to its economy.

Firstly, the nanoparticles of CuO is weighed in grams for preparing two volume concentrations, 0.055% and 0.1%, using the formula (3.26). The mass of nanoparticles for 0.055% concentration is 4.12 grams and for 0.1% is 7.50 grams, for one liter of nanofluid. Then the nanoparticles are mixed with the base fluid (5W30 oil) and mixing for one hour in mixer. The process is repeated twice to make 2 liters.

### 3.7.3 Measured solar irradiance.

The application of a Smartphone Okapi solar calculator is used to measure the radiation intensity. After calibrating the Smartphone, the measured solar irradiance is shown in Figure 3.20.
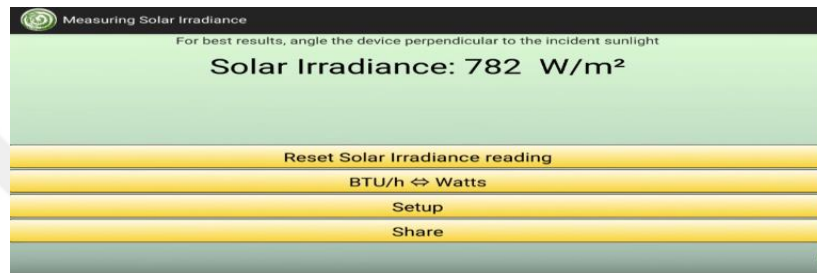


**Figure 3.20**: Interface of measuring solar irradiance application.

### 3.7.4 Calculated thermal efficiency

The thermal efficiency depends on the increase of the water temperature and the total solar irradiance collected by the mirror (G. $A_a$). The test are conducted for ten minutes and the measurement are taken every 6 seconds resulting in 600 readings per test. From these readings, thermal efficiency is calculated as follows[49].

$$\eta_{th} = \frac{\dot{m}\,C_p\left(T_{wo} - T_{wi}\right)}{G.A_a} \qquad (3.38)$$

Where $T_{wo}$, $T_{wi}$ is outlet and inlet temperature of water respectively..

In this study, the temperature of inlet and outlet in equation (3.38) is measured by thermocouple of type K as shown in Figure 3.18, which is calibrated. The mass flow rate is calculated by multiplying the measured flow rate of the fluid (L/h) by the temperature corrected of fluid density.

### 3.7.5 ASHRAE Standard 93-1986 (RA91).

ASHRAE standards are used as a general guide to design the experiments in this thesis. ASHRAE (93-1986), which applies to a working fluid in a single phase, is followed [49]. Testing the performance of the parabolic trough solar collector is also done according to the above standard. The ASHRAE (93-1986) defines permissible change of system variable to ensure the stability of the tests depending on fluid type, climate and solar irradiation parameters. These determinants are also intrinsically linked to the design variables of the system.

### 3.7.4.1 Fluid limit test.

The following guide lines from ASHRAE (93-1986) [49] is followed in this work.

1- The fluid temperature and flow rate of the fluid at the inlet of the tube must be constant within the permissible limit of change of one temperature and $315 \times 10^{-4}$ liters / second for 15 minutes from the start of the test.

2- Change in the fluid temperature at the inlet to the tube should not exceed (5%) $^\circ$ C during the test period.

3- Change in fluid temperature at the inlet of the tube. The change must not exceed 1 $^\circ$ C during the test period for the test case of the acceptance angle of the collector only.

### 3.7.4.2 Ambient limit test.

1- The temperature of the air during the test period should not exceed 30 $^\circ$ C.

2- The air temperature should not change more than 1.5 $^\circ$ C within 15 minutes before the process of taking readings and recording.

3- For test, the thermal efficiency, the air velocity should be within the permissible limits (2.2 to 4.5) meters / second during the test period and for ten minutes before the test results are recorded.

### 3.7.4.3 Measuring solar irradiance limit test.

1- During the test process, and before the test in 10 minutes, the solar radiation intensity rate does not exceed (1000 W/m$^2$) and does not change more than (32 W/m$^2$).

2- The amount of intensity of solar radiation must not be greater than (800 W/m$^2$) when testing the acceptance angle of the collector and preferably to be constant throughout the test period.

## Chapter Four: RESULTS AND DISCUSSION

### 4.1 Introduction

In this study, the experimental and numerical study is conducted to evaluate the performance and efficiency of a new model of direct absorption parabolic trough solar collector. This chapter presents the results obtained in both numerical and experimental terms. Firstly ANSYS FLUENT software is used for modeling the solar collector for choosing the highest performing model. The above model is experimentally investigated and simulation data is compared to measured data.

### 4.2 Optimum model

In order to obtain the best perfomling model, simulations are performed for three geometries with three different sizes of glass to copper tube ratios: 1/4, 1/2, 3/4. Numerical simulation are performed for the three different geometries with different mass flow rate of the water to compared the efficiency (see figure 4.1).

The size ratio of ¼ shows lesser efficiency because of reduced area of heat transfer between the nano-fluid and the water. Despite the large redaction in the area, the efficiency drop is lower due to the increase in Reynolds number and the heat transfer coefficient on water side.

The efficiency of the collector with (3/4) size ratio drops because of the reduced depth of absorption and reduced Reynolds number of water flow.

The optimum geometry, within the three considered, is the one with copper-to-glass size ratio of 1/2. The ANSYS FLUENT simulations are performed under the following conditions: solar radiation intensity at 650 W/m$^2$, ambient air temperature at 27 °C, ambient wind velocity at 2 m/s and various volumetric flow rate (20 to 100 l/h).

Figure 4.2 shows the streamline in the cross section at z = 0.95 m of the ratio ¼ model. The scaler coloring used is vorticity. The vorticity near the copper tube is observed to be higher than that of near the glass tube.

Figure 4.4 shows the streamlines and vorticity for the model with ratio ¾. This model has the least amount of the nanofluid as well as the lowest vorticity of the three

cases studied. The lower nanofluid volume results in lower heat generation as the solar heat is mainly converted into heat by the nanoparticles. What is more, the lower vorticity indicate to lower convective heat transfer.

The figure 4.3 shows the streamlines and vorticity for the model with ratio ½. The velocity of streamline near copper tube wall is much higher than velocity near glass wall. The above indicates that the convective heat transfer from the nanofluid to the copper tube is higher than that of between the nanofluid and the glass tube. This reduces the heat losses to the environment while improving heat transfer to the water thus increasing the overall efficiency of the solar collector.

.
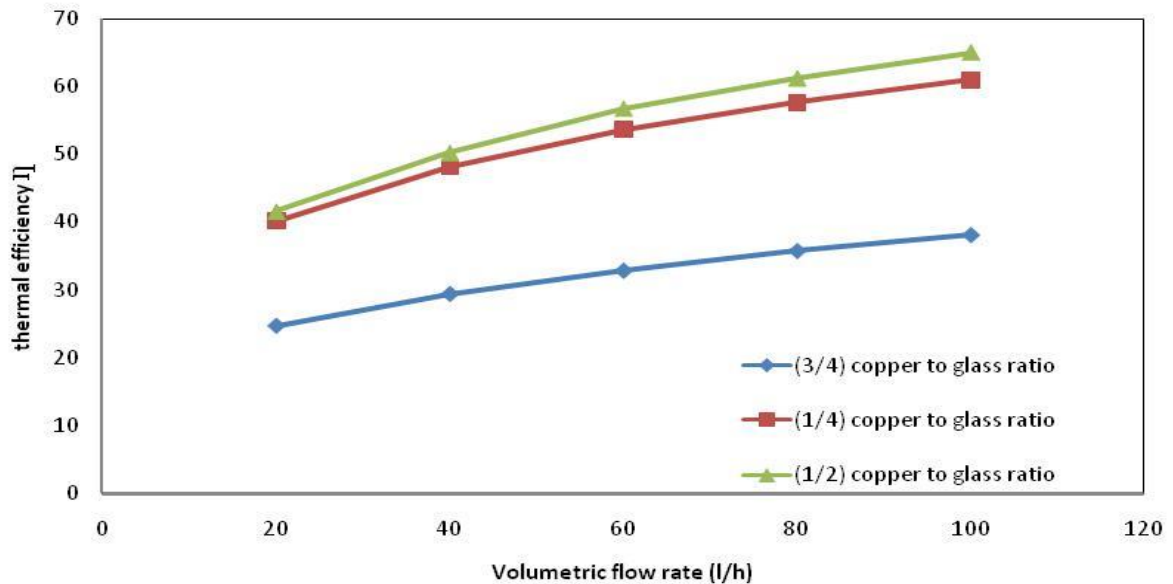


**Figure 4.1**: The effect of using different copper-to-glass size ratios on the on the efficiency of absorption.
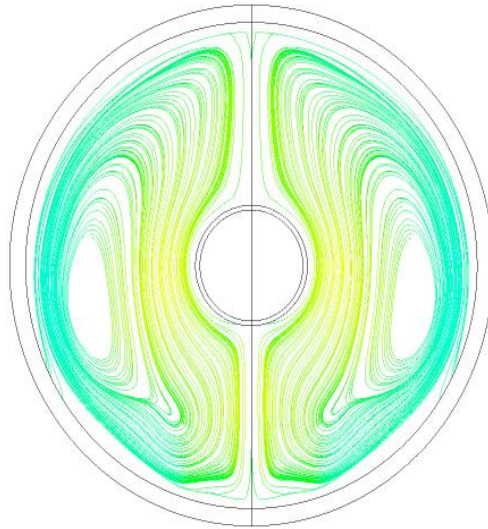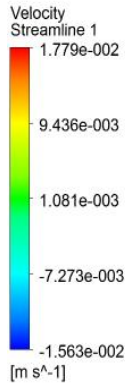
**Figure 4.2:** Streamlines in the cross-section at z = 0.95 m showing the vortices due to natural convection at model (1/4).
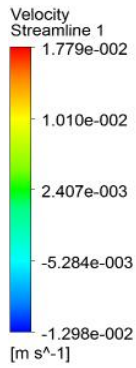


**Figure 4.3:** Streamlines in the cross-section at z = 0.95 m showing the vortices due to natural convection at model (1/2).

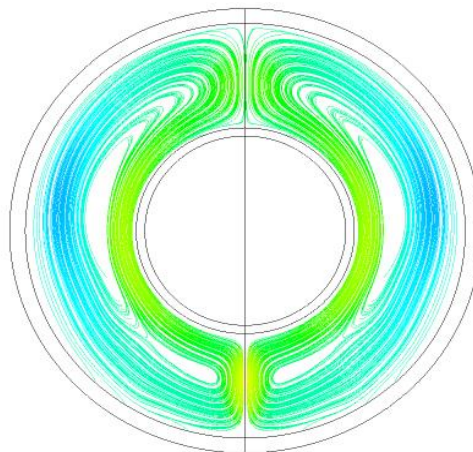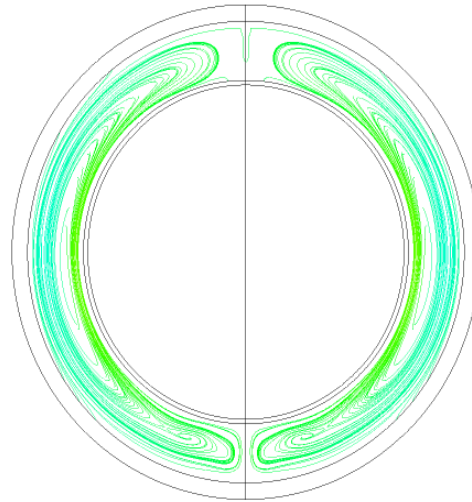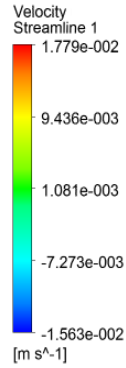**Figure 4.4**:  Streamlines in the cross-section at z = 0.95 m showing the vortices due to natural convection at model (3/4).

### 4.3 Simulation

As part of this study, ANSYS FLUENT software is used for the simulations to determine the performance of the solar collector. ANSYS UDF (User-Defined Function), written in C language, is used to calculate the heat generated in the nanofluid (see appendix A and chapter 3). The heat generated is modeled as a source term in the nanofluid zone. A second UDF is also developed for calculating the heat losses to the environment from the surface of the glass tube (see appendix A and chapter 3).

The application of both UDF codes in the ANSYS FLUENT calculations are made at the specified conditions, limits and according to the proposed design requirements. The results obtained shows a performance efficiencies of 39.63% to 61.23% at a volumetric flow rates of water from 20 to 100 liters/hour. The simulation are conducted to study 30 cases in which the difference in the inlet fluid temperature and the flow rate, as well as the concentration of nanofluid is changed.

### 4.3.1 Mesh refinement study.

CFD simulation results needs to be independent of the computational mesh used. The flow fields obtained should not contain any numerical artifacts. A coarse mesh can lead to a less accurate solution as the flow field can contain features in the same order or smaller than the size of a mesh element. As the mesh is refined, or in other words its elements made smaller, the solution would become more accurate. This idea is called spatial convergence.

This study preforms a mesh refinement while observing the temperature difference between the inlet and the outlet of the water as well as observing the maximum velocity in the nanofluid domain. The starting mesh is of 600000 cells and is increased five times each refinement while obtaining the above two flow parameters (see figure 4.5). After 4.6 million cells, both the temperature difference and the maximum velocity is observed to have reached their converged values. The mesh with 4.6 million cells, which is the smallest converged mesh, is selected for further investigation.

CFD solution process in this study uses iterative solvers. Each iteration an intermediate solution closer to the final solution is generated. The residual is a measure of how much the solution is changing per iteration. The iterative convergence is achieved when the residual does not change. All computations in this thesis are iteratively converged. Approximately 70 iterations with flat residual values are made for each simulation.

The mesh refinement study is conducted on the ratio ½ model. The modeled concentration of nanoparticles is 0.055%. The mesh of 1m length half cylinders using symmetry boundary conditions is used.
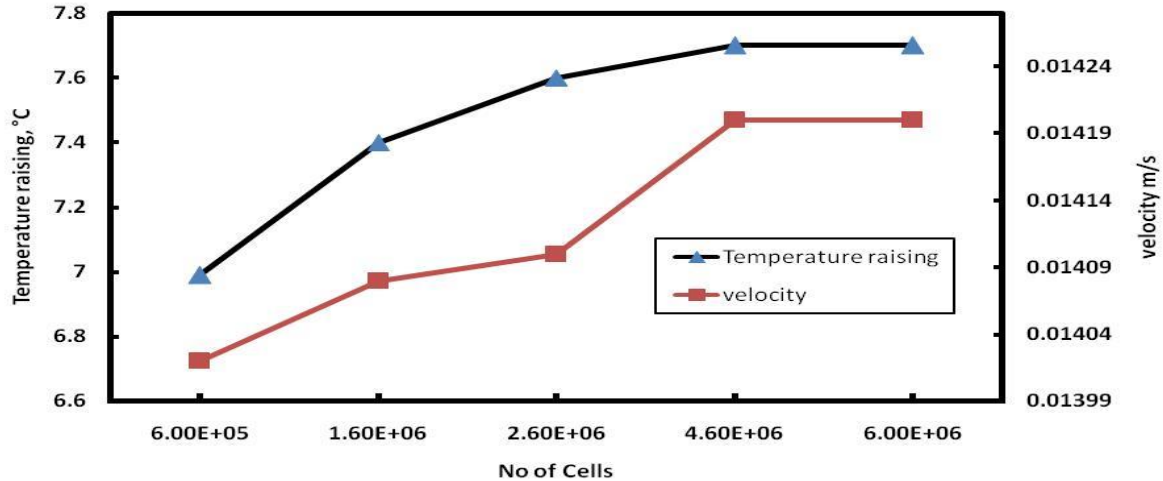
**Figure 4.5**: Mesh refinement study. The parameters consider are the temperature difference in the water flow and the maximum velocity in the nanofluid domain

### 4.4 Experimental results

In the experimental part, the thermal efficiency of the solar collector is calculated by the reading the temperatures that is recorded by the K-type thermocouple and the Arduino based data logger mentioned in Chapter 3. The readings are taken at different volumetric flow rates of 20, 40, 60, 80, 100 l/h. The solar collector is tested when the solar radiation is 650 W/m$^2$ and ambient temperature is 27°C.

### 4.5 Discussing and comparing numerical and experimental results

Tables (4.1) shows the numerical and experimental results obtained. The percentage error of the water temperature difference ranged from 3% to 3.84% at various volumetric flow rates. Figure 4.6 compares the change in rising temperature of the water with various flow rates in numerical and experimental results. The Figure (4.7) shows the thermal efficiency of the collector at a various volumetric flow rate in numerical and experimental part. The CFD results show increasing thermal efficiency when increasing the flow rate of the water in the solar collector. This is consistent with the experimental results as shown in Figure (4.7).

**Table 4.1 Numerical and Experimental results**

| | Numerical results | Experimental results | |
|---|---|---|---|
| Flow rate (l/h) | $\Delta T$ (°C) | $\Delta T$ (°C) | Error% |
| 20 | 11.65 | 11.21 | 3.77 |
| 40 | 7.02 | 6.75 | 3.84 |
| 60 | 5.31 | 5.12 | 3.57 |
| 80 | 4.32 | 4.19 | 3.0 |
| 100 | 3.6 | 3.48 | 3.33 |
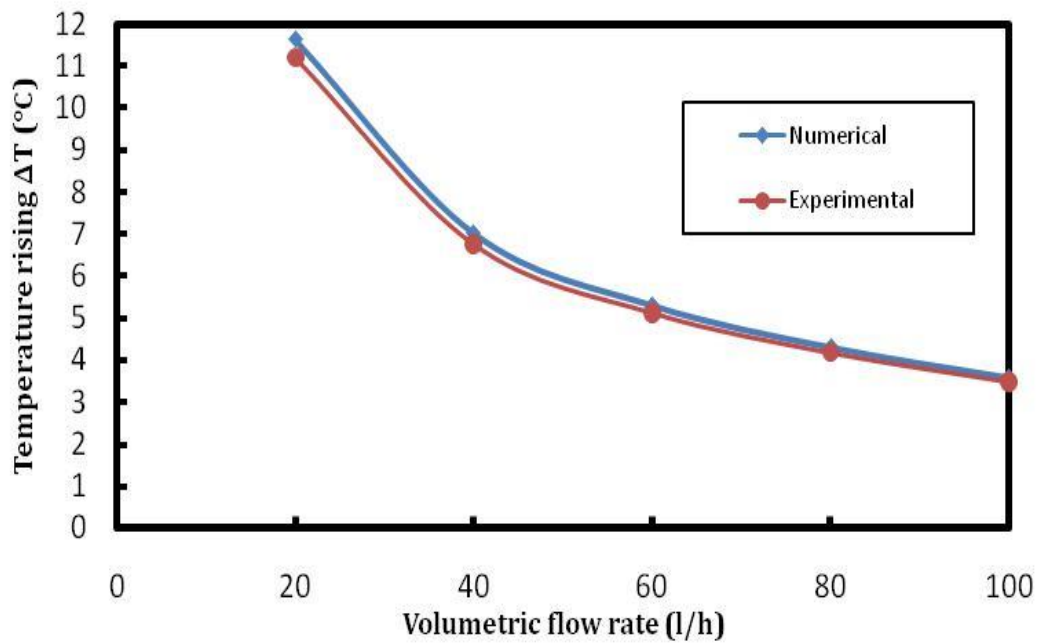


**Figure 4.6**: The rising temperature with various flow rate in numerical and experimental results.
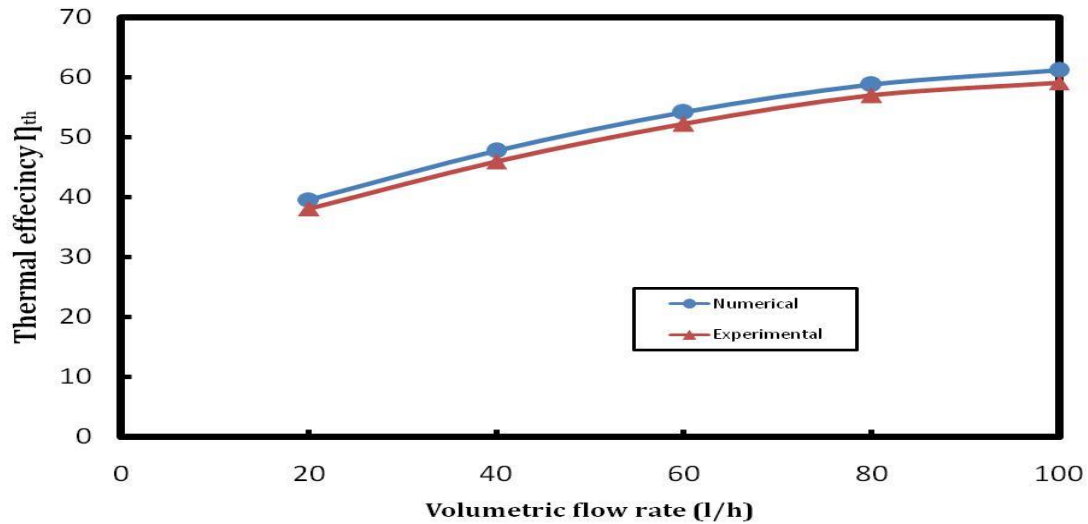
**Figure 4.7**: Thermal efficiency with various volume flow rate for numerical and experimental results.

## 4.6 Differences in the temperature of the inlet fluid

### 4.6.1 Effect of inlet fluid temperature on outlet temperature

After the validation of the numerical results with the experimental data simulations are carried out to investigate the effect of inlet water temperature. Simulations are performed at the following temperature levels: 300, 325 and 350 K. Different water flow rates for each temperature is simulated (see Figure 4.8). CFD data shows that the increasing temperature of inlet water lead to lower temperatures differences.

The above simulation data can be understudied on the basis of heat transfer between the nanofluid and the water domains. Higher water temperature would result in lower temperature gradient between the two domains. This lower temperature gradient would result in less heat transferred from the nanofluid to the water resulting in reduced temperature increment within water.
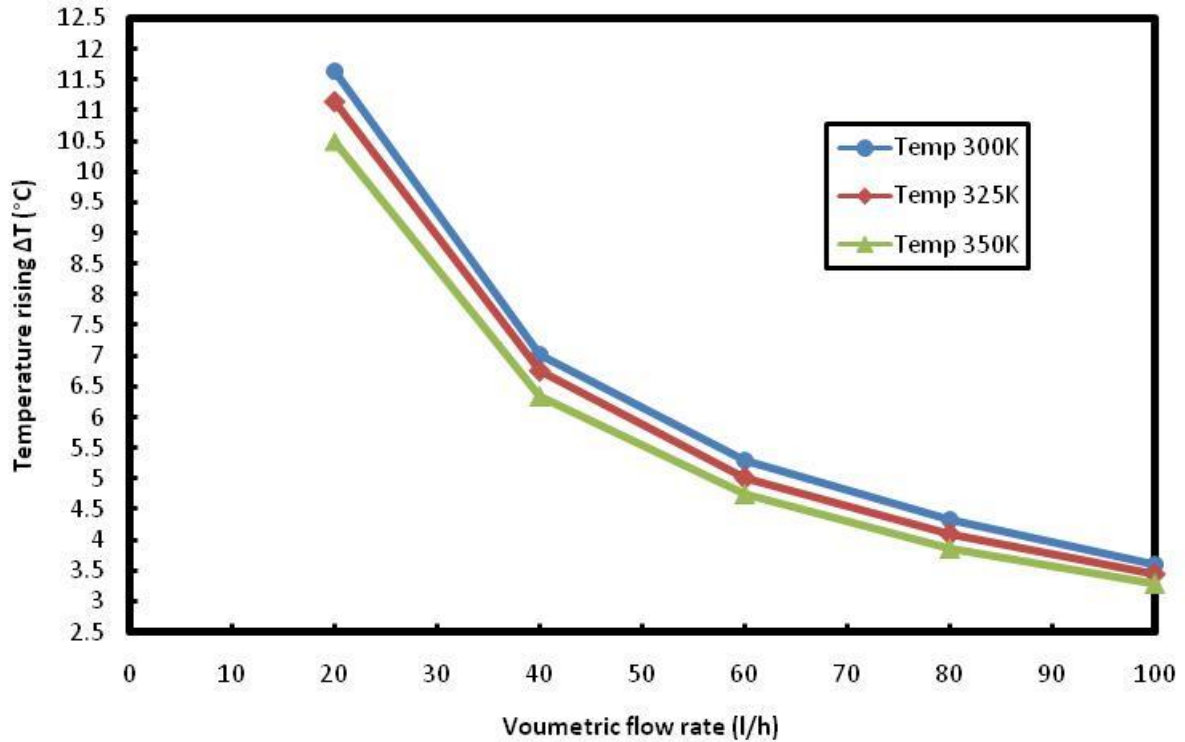
**Figure 4.8**: Different temperature inlet with various volumetric flow rate.

### 4.6.2 Effect of inlet fluid temperature on thermal efficiency

The thermal efficiency of the collector is simulated for five different volumetric flow rates of water (see Figure 4.9). The thermal efficiency increased with increasing flow rate of the water. The increase inlet temperature of the water resulted in decrease of thermal efficiency.

Increasing the volumetric flow rate would increase the removal of the thermal energy from the collector resulting in lower water temperatures. The above situation would increase the thermal gradient between the nanofluid domain and the water domain thus increasing the heat transfer rate and the thermal efficiency. As in the previous case, increasing the inlet temperature of the water would result in reduced thermal gradient between the two domains. With the lower thermal gradient less energy will be transferred to the water reducing the collector efficiency.
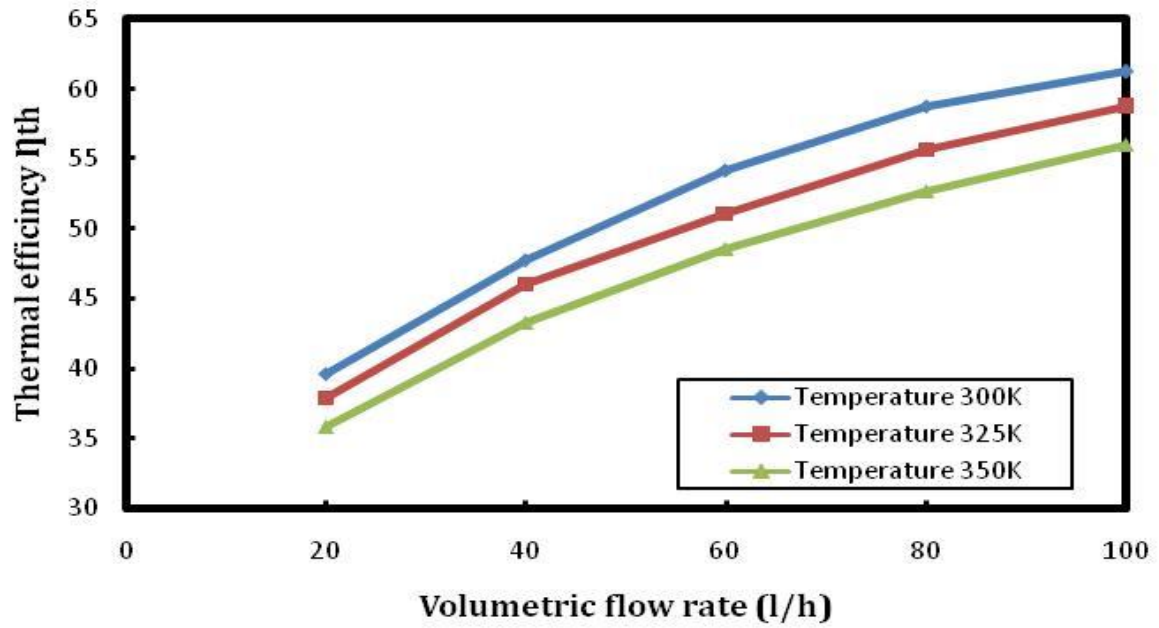
**Figure 4.9**: CFD simulation of the Thermal efficiency with respect to volumetric flow rate of water at three different temperature.

### 4.6.3 Effect of inlet water temperature on nanofluid temperature

Nanofluid temperature field when for three different mass flow rates is investigated. First we consider inlet water temperature of 300K (see Figure 4.10, 4.11, 4.12).

The CFD simulation show as the water flow rate is increased its temperature stays lower. The nanofluid temperature is also lowered as the water flow rate is increased
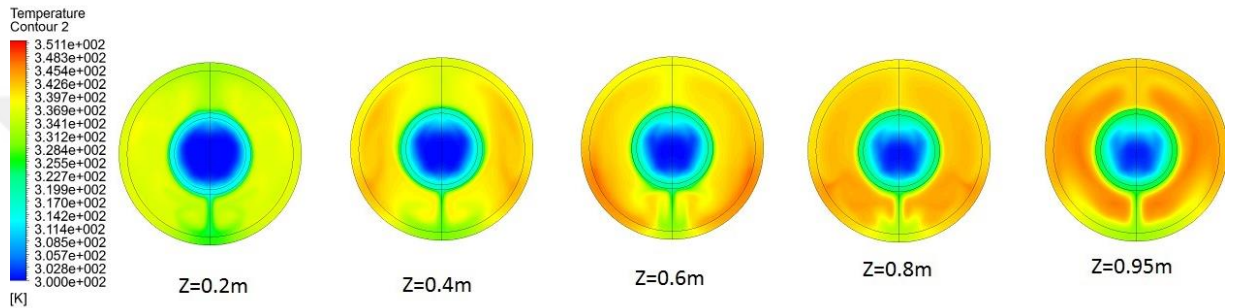


**Figure 4.10** : Heat distribution at different cross-sections at 300K  and flow rate 20 l/h
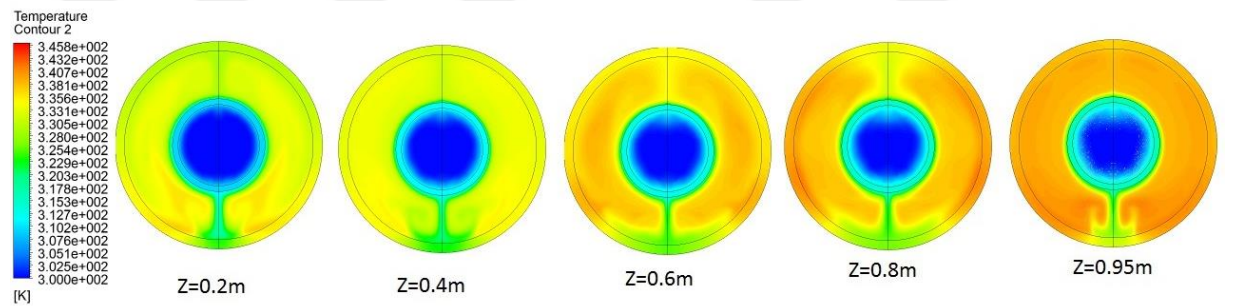


**Figure 4.11**: Heat distribution at different cross-sections at 300K  and flow rate 60 l/h
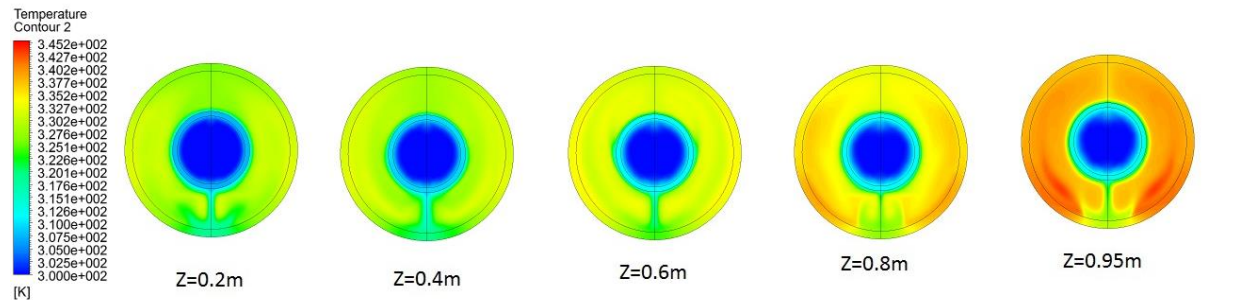


**Figure 4.12**: Heat distribution at different cross-sections at 300K and flow rate 100 l/h

The same trend observed in the previous section is observed when the water temperature is 325K. Both the nanofluid temperature and the water temperature is lower as the water flow rate is increased (see Figure 4.13, 4.14, 4.15).
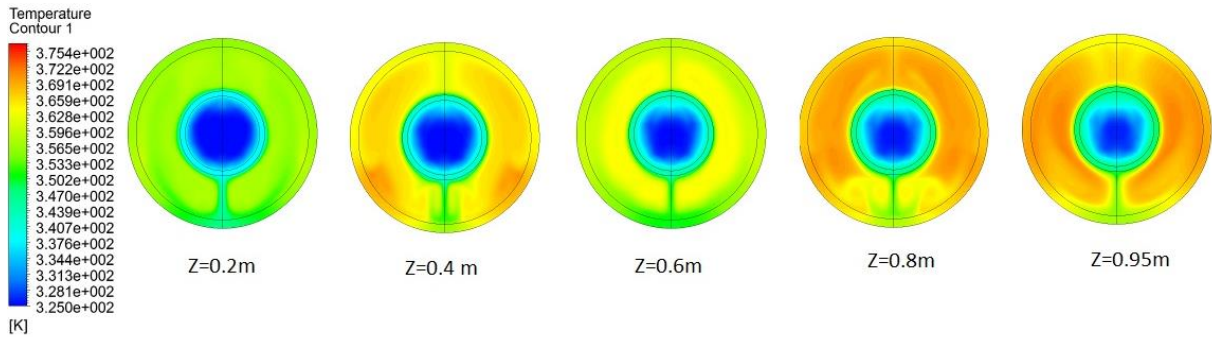


**Figure 4.13**: Heat distribution at different cross-sections at 325K and flow rate 20 l/h.
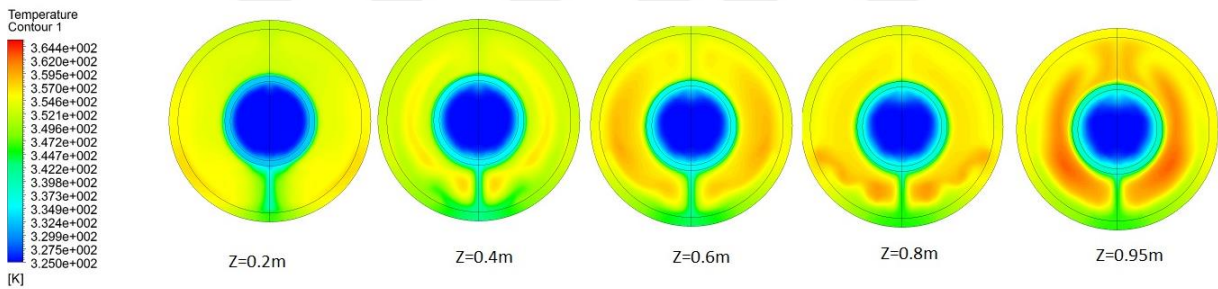


**Figure 4.14**: Heat distribution at different cross-sections at 325K and flow rate 60 l/h.
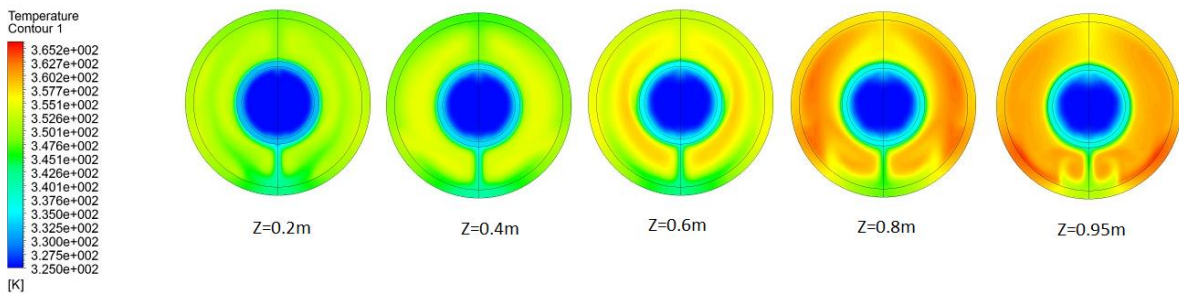


**Figure 4.15:** Heat distribution at different cross-sections at 325K and flow rate 100 l/h.

The same trend observed in the previous two cases is observed when the inlet water temperature is 350K.

As the inlet water temperature is increased the temperature of the nanofluid domain also
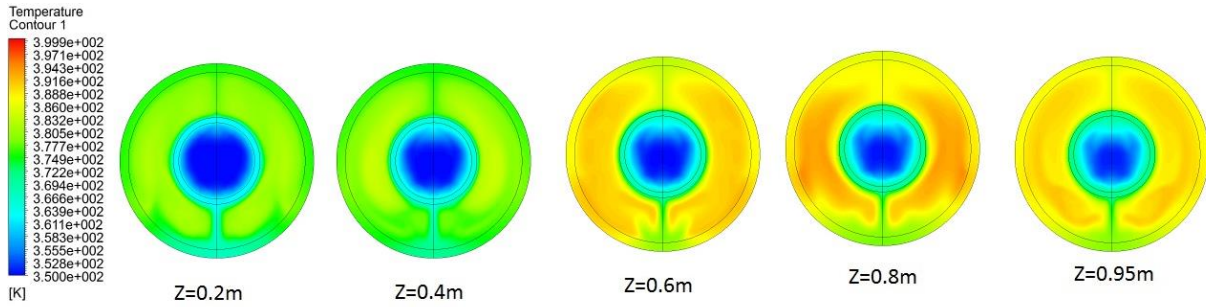


**Figure 4.16:** Heat distribution at different cross-sections at 350K and flow rate 20 l/h.
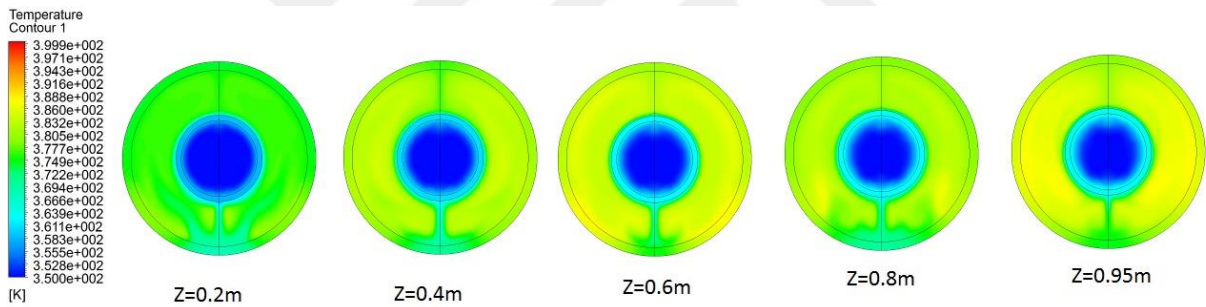


**Figure 4.17**: Heat distribution at different cross-sections at 350K and flow rate 60 l/h.
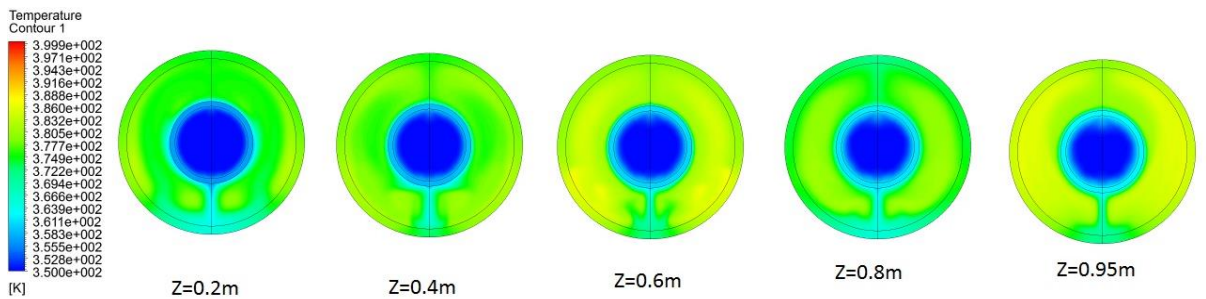


**Figure 4.18:** Heat distribution at different cross-sections at 350K and flow rate 100 l/h.

## 4.7 Effect volume flow rate on thermal efficiency

The effect of the volumetric flow rate on the thermal efficiency is investigated both experimentally and numerically. Both data sets show the same trend of increasing thermal efficiency with respect to increasing volumetric flow rate.

The thermal efficiency is improved when the volumetric flow rate is increased (see Figure 4.22). The increase in the volumetric flow rate will increase Reynolds' number leading to increase in the heat exchange between nanofluid and the flowing water in the copper tube. The increase in efficiency is observed with increasing Reynolds. This study only considers laminar flow.
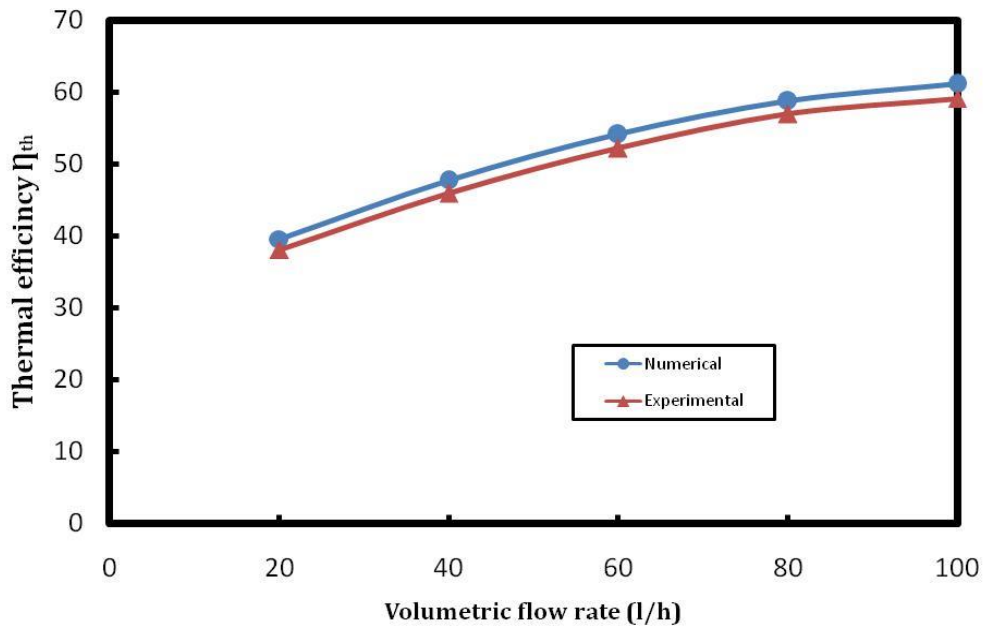


**Figure 4.22**: Thermal efficiency at various volumetric flow rate.

### 4.8 Temperature and velocity profiles along the receiver tube

#### 4.8.1 Temperatures profiles at nanofluid zone

The temperature field of the nanofluid at the boundary of the glass tube shows several hot and cold region (see Figure 4.19). The temperature profile indicates that heat flux within the nanofluid is not uniform the above non uniformity is created by the buoyancy driven convective flow.
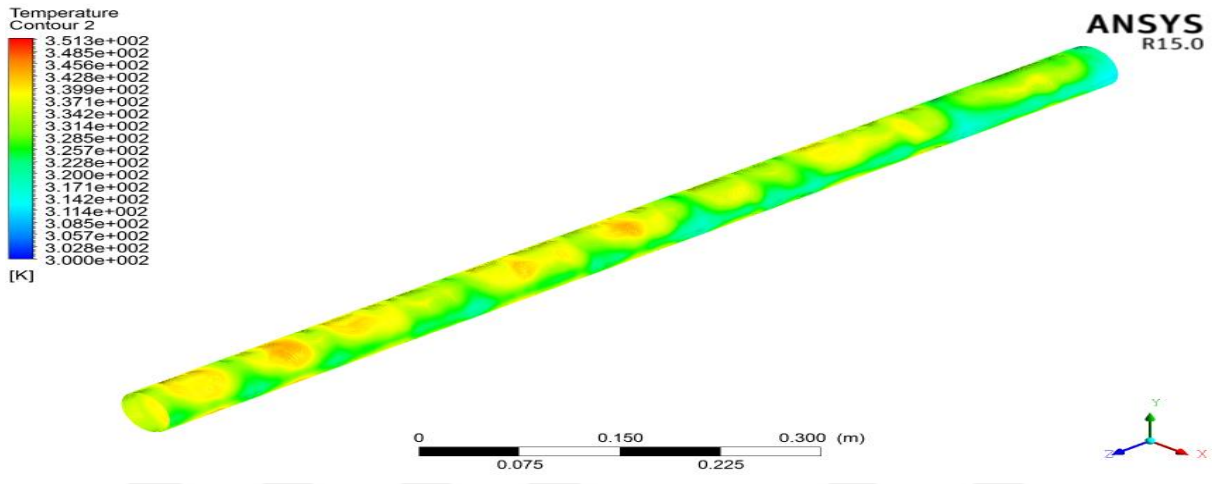


**Figure 4.19:** Temperature profiles of nanofluid at the glass tube boundary along receiver tube.

#### 4.8.2 Temperatures profiles at water zone

The temperature profile of the water next to the copper tube is much smoother than that of nanofluid (see Figure 4.20). This can be understood by the facts that copper has a high thermal conductivity diffusing any thermal gradients and water is forced along the tube.
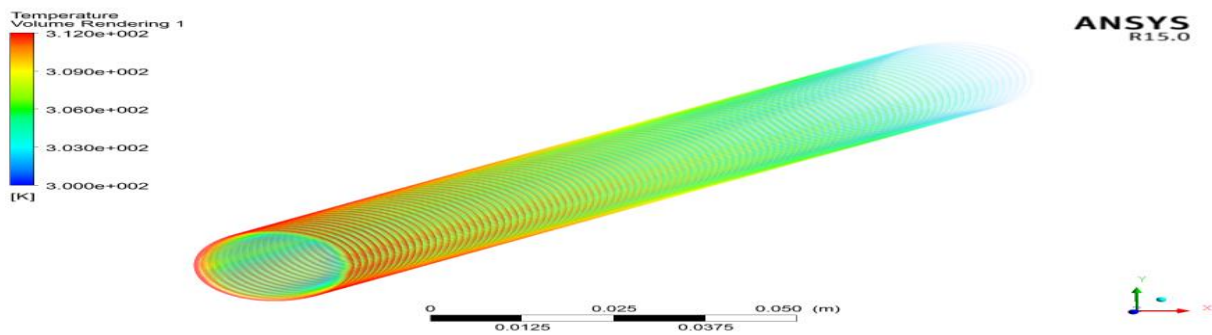


**Figure 4.20:** Water temperature at the boundary of copper tube.

### 4.8.3 Velocity streamline profiles at nanofluid zone

The thermal expansion of the nanofluid due to differential temperatures cause buoyancy driven flow. This flow will further convect the heat increasing inhomogeneity in the temperature field. CFD flow field show buoyancy driven flow pattern (see Figure 4.21) with differential temperature field. It appears that there is a characteristic length scale, along the axis, for the buoyancy driven flow.
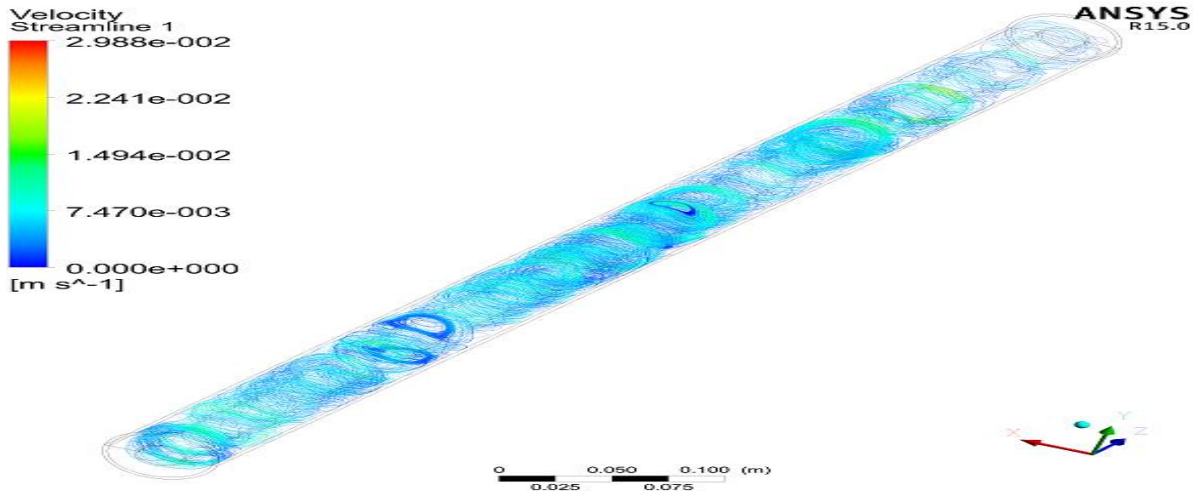


**Figure 4.21:** Velocity streamline along receiver tube in nanofluid zone.

### 4.9 Nanofluid volume fraction

### 4.9.1 Effect of nanofluid volume fraction on absorption solar irradiance

The nanofluid is considered to be homogeneous. The solar energy absorption by the nanofluid is modeled as an internal heat source. The incident solar irradiance on the receiver tube is not homogeneous (see chapter 3). The above fact results in different amount of heat generated in the nanofluid depending on the position.

Two concentration of nanofluid is numerically investigated. The heat generation within the nanofluid is observed to be dependent on the nanofluid concentration (see Figure 4.23). The simulation results show that for concentration of 0.100% the heat generation is significantly higher than for the concentration 0.055%. At the higher nanofluid concentration more heat is generated near the glass tube. 95% of solar irradiance is absorbed within the depth of 9mm. The lower concentration permits more

penetration of solar irradiance. There is no solar radiation at the bottom of the tube because of the shadow of the tube.



$\varphi=0.1\%$

$\varphi=0.055\%$
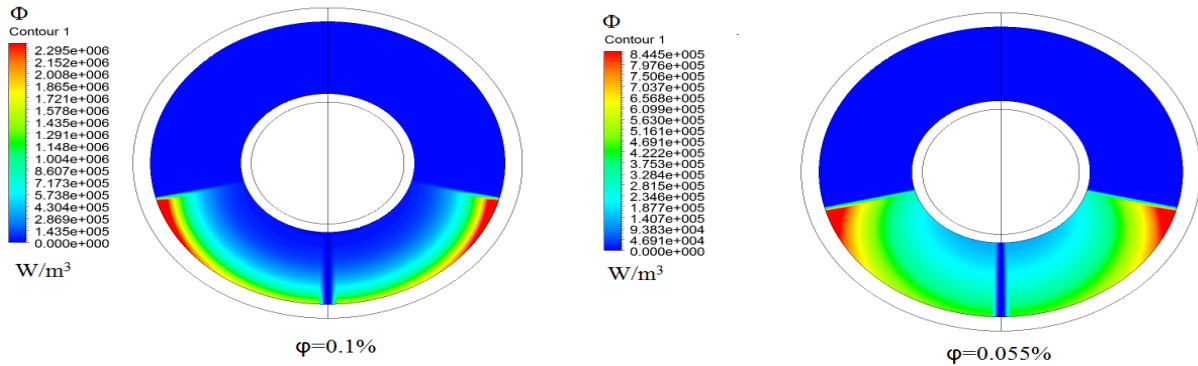
**Figure 4.23**: The difference of internal heat source with optical paths at different concentration of nanofluid.

### 4.9.2 Effect volume fraction of nanofluid on thermal efficiency

The effect of the nanofluid concentration on the collector thermal efficiency is investigated. Simulations show that the collector with the volume fraction with 0.100% has a thermal efficiency of 66.5% when the volumetric flow rate of the water is 100l/h the efficiency of the collector with concentration of nanofluid 0.055% in the same conditions is 61.23%. The performs of the collector with the higher nanofluid concentration is observed to be superior to that of the lower concentration at all water flow rates considered in this study (see Figure 4.24).
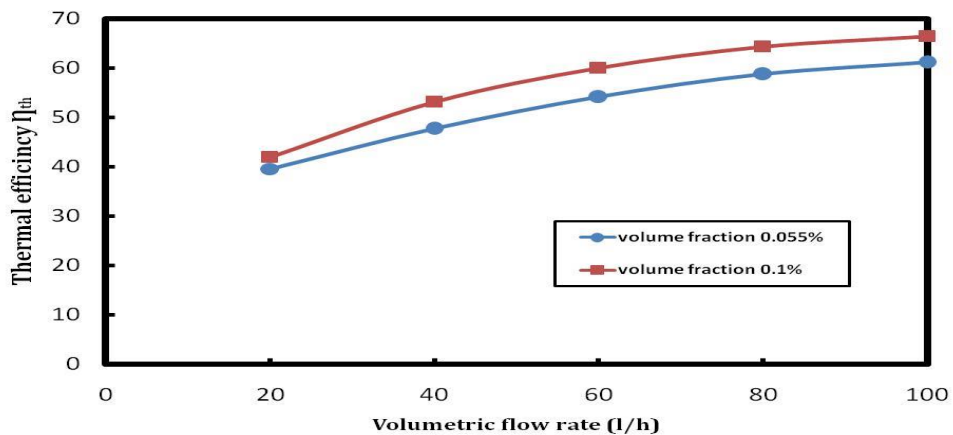


**Figure 4.24:** Effect volume fraction on thermal efficiency.

71

### 4.10 The cost of the model.

In this section we study the cost and performance of the new design proposed in this thesis with that of the conventional direct absorption solar collector based system. The cost of material for the present system is 400US$. The estimated cost of a comparable direct absorption system is 1000US$. The difference in the cost is partly due to the need of a heat exchanger and an additional pump for the conventional system. In addition to this, more nanofluid is needed in the conventional system contributing to the price difference.
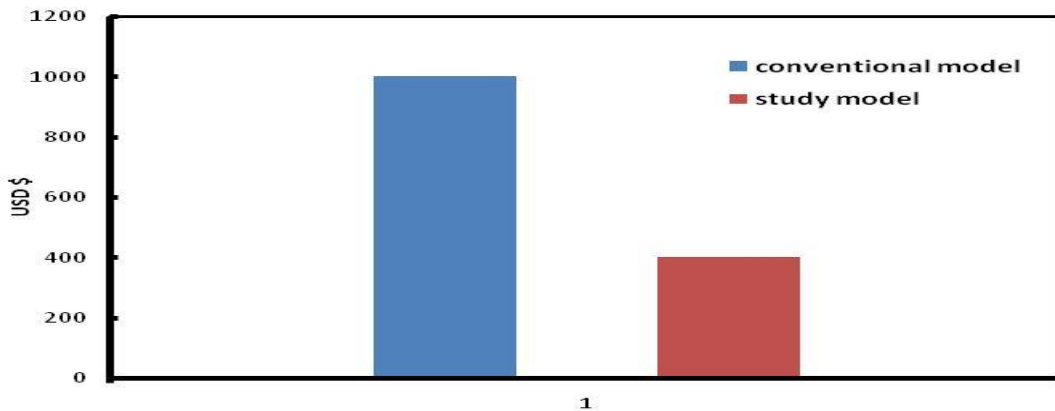


**Figure 4.25**: Comparison of cost between the study model and the traditional model.

The efficiencies of conventional direct absorption system reported in the literature are 62 to 65% depending on the inlet temperature of the fluid. These system are highly optimized for performance. The ratio ½ model of the present study with nanofluid concentration of 0.100% has a measured efficiency of 65% and CFD simulated efficiency of 66.5% at the same inlet temperature and mass flow rate. The present system, though the best of the three geometries considered, is not optimized. It is conservable that an optimized system would outperform the ratio ½ model as well as the conventional systems.

## Chapter Five:  CONCLUSION AND FUTURE WORK

Using Nano-fluid in direct absorption system with direct heat exchange improves the performance of solar collector. Direct heat exchange within the solar receiver will reduce the total thermal resistance of solar collector system by eliminating the need of a heat exchanger. In this study, none-circulating Nano-fluid absorbs solar radiation and conveys heat directly to circulating water passes through copper tube submerged in the Nano-fluid.

First, the simulations are carried out using the ANSYS FLUENT program on three different receiver tube geometries with the diameter ratios of the pipes 1/4, 1/2 and ¾. The simulation results showed that the best model is the ratio ½ in terms of efficiency. The ratio ½ model is manufactured and measurement are taken. The measurements and CFD simulations agreed within 3.84% of error.

The measurements are conducted at the solar irradiance of 650 W/m$^2$ and the ambient temperature of 27 C. further CFD simulations with above conditions are preformed and compared with measurements.

It is observed that increasing the volumetric flow rate of water increased the efficiency of the receiver. The thermal efficiency is 39.63% at the flow rate of 20 l/h and it is 61.23% when the flow rate is 100 l/h. increasing the fluid inlet temperature has a negative effect on thermal efficiency.

It has been shown that changing the concentration of nanofluid has a significant effect on increasing the thermal efficiency. When the nanofluid volume fraction is 0.055% the efficiency is 61.23% however, when the volume fraction is increased to 0.100% the efficiency becomes 66.5%.

Solar receiver with new configuration provides comparatively high efficiency up to 65%, which is similar to the best conventional collectors, however the present system is not optimized.

In order to achieve higher efficiency of the solar collector, we recommend the following future work:

1- Conducting a study to optimize the performance by changing the volume fraction of the nanofluid and the collector geometry (the ratio of inner tube and outer tube).

2- Conducting study on different types of nanoparticles and different sizes to determine the best chemical and physical composition suitable for the weather conditions of the area to be studied.

3- Using an evacuated tube to reduce the thermal losses resulting from convection.

4- Conduct a study on the use of other types of heat-transfer fluids as Therminol VP 1 and Syltherm at a different concentration of nanoparticles.

**Appendix A User Defined Functions**

In some cases where the simulation requires the insertion of the values of the boundary condition as a variable value with time or calculated value according to equation specific the case, for the purpose of conducting more flexibility in input the Boundary condition ANSYS FLUENT use of the method called UDF (User Defined Function). This method uses language C codes for the purpose of definition different types of macros and functions. The DEFINE macro is the most significant types of macro that using to define UDF. There is an assortment of DEFINE macros are supplied by ANSYS FLUENT.

In this Appendix, clarifying the user-defined functions that were created with a view to being able to apply to the model, all information used in this appendix were obtained from manual[50]. The equations were used in the section (3.1.2.1) for the purpose of creating the UDFs

Before going into the UDF details used in this study, some of the concepts of the grid (mesh) will be presented. The computational domain can be divided into several cells where data is read and stored in these cells to be used when programming UDFs to access data from the solver as shown in Figure A1:
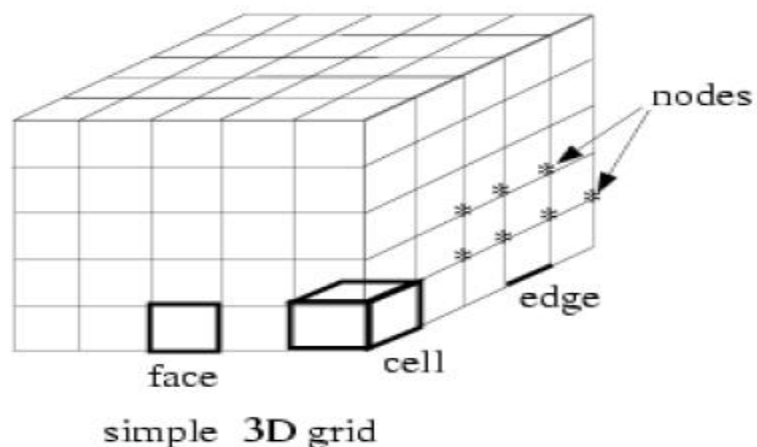


Figure A1: Mesh Components

- Node : A structure data type that stores data associated with a mesh point.
- face:  is an integer data type that identifies a particular face within a thread.
- cell:  is an integer data type that identifies a particular cell within a cell thread.
- Thread: structure data type that stores data that is common to the group of cells or faces that it represents. For multiphase applications, there is a thread structure for each phase, as well as for the mixture.

During the study, two different kinds of DEFINE macros were carried out. The macros using were DEFINE_SOURCE and DEFINE_PROFILE. For the heat generated UDF and Heat losses UDF. The heat generation rates free and heat losses, the system due changed with the angle (θ). The functions are written for achieved these changing

### A.1 UDF for Heat generated (DEFINE_SOURCE).

For the purpose of creating a UDF for calculating heat generated inside the nanofluid due to absorption of solar radiation, as the heat generated is the source of the heat, the Define_Source macro was used to defined the equation that shown in section (3.1.2.1) for calculated the source of energy, then put the UDF as the source term in nanofluid zone. The UDF as shown below.

```
#include "udf.h"  /*compiler directives for C library function header files */

real abs_coeff = 103.0; /* absorption coefficient */
DEFINE_SOURCE(energy_source, cell, thread, dS, eqn)
{

real x[ND_ND];  /* this will hold the position vector*/
real C;
real x1;
real y1;
real r;
real r000;
real source;
real rin = 0.0125;   /* radius inner tube*/

real rout = 0.0255;  /* radius outer tube*/

real n = 25;         /* number of division in annular */

real dr = (rout-rin)/n;
real PI=3.141592654;
real angle;
```

```
real Io; /* solar radiation intensity*/

C_CENTROID(x,cell, thread); /* centroid of cell*/
source = 0.0;
 x1=x[0];                      /* x position in matrix */
 y1=x[1];                      /* y position in matrix */
 r000 = sqrt(x1*x1+y1*y1);
 r = rout-r000 ;              /* optical depth */
angle = acos(x1/r000)*180/PI;
C= 18750/(1 + (x1/r000));
if (angle >= 2 && angle <= 75 )
{
Io = C*(1-(x1/r000))/(pow((y1/r000),2));
source = (Io*(1-exp(-103*(r+dr/2)))-Io*(1-exp(-103*(r-dr/2))))/dr;
dS[eqn] =0.0;
}
else
{
source = 700;
}
C_UDMI(cell,thread,0)=source; /* This is UD memory*/

return source;

}
```

**Table A-1 Description The UDF (Fluent UDF Manual)**

| Argument Type | Description |
|---|---|
| symbol energy_source | UDF name |
| cell | Index that identifies cell on which the source term is to be applied |
| thread | Pointer to cell thread |
| real dS[] | Array that contains the derivative of the source term with respect to the dependent variable of the transport equation. |
| int eqn | Equation number. |

The equations used in section(3.1.2.1) were used for the purpose of writing the UDF, and because the source is variable with the angle, it is necessary to calculated each cell separately depending on the location of the centroid of each cell and where the term source is conducting a looping on all the cells without having to make a looping in the UDF that make programming easy. [50].

### A.2 UDF for calculated Heat losses

To calculated the losses for the model with the free stream A DEFINE_PROFILE macro was used. The Heat losses of the model varies on every face of cell due the solar radiation non uniform around the receiver tube. The equation used in the UDF was dissection in section (3.1.2.3). The UDF for the losses is shown below.

The UDF File for calculated the Heat losses necessary to be able computed the value of the losses in each face, and loop over all of the faces. For completed this task, the pre-defined face looping macro begin_f_loop(f,t) is used. The equation for the heat losses is assigning to the corresponding face by using; F_PROFILE. The macro F_PROFILE is put within the face loop (begin_f_loop(f,t)). The loop will continue to iterate until it has gone through; all the faces in the given cell thread.

```
#include "udf.h"

DEFINE_PROFILE(losses, thread, position)
{
real PI=3.14159263;
real L=1; /* Length of the tube */
real  ρ = 1.25; /* density of air */
real Do = 0.090; /* outer diameter */
real Dci =0.082; /* inner diameter cover */
real v = 5 ; /* velocity of air */
real hw ; /*Heat transfer coefficient of air */
real Ka = 0.0263; /*thermal conductivity of air */
real u = 0.0000179; /* viscosity of air */
real Ɛ = 5.67E-08 ; /* The Stefan-Boltzmann Constant */
real T1=310;
real Ta = 300; /*ambient temperature of air */
real Tw; /* wall temperature */
real Tsky =295; /* temperature of sky */
real Tci ; /* temperature of cover inside*/
real Re; /* Reynolds number of air */
real Q1; /* losses 1  */
real Q2; /* losses 2 */
real Nu; /* nusselt number of air */
real UL ; /* loss coefficient */

cell_t c;

real x[ND_ND]; /* this will hold the position vector */
```

```
Re=(ρ*v*Do/u);

Nu=0.3*pow(Re,(3/5));

hw= Nu *(Ka/Do);

begin_c_loop(c,thread)
{
C_CENTROID(x, c, thread);
Tw = C_T(c,thread);

Q1=PI*Do*L*(hw*(T1-Ta)+0.88*Ɛ*(Pow(T1,4)-pow(Tsky,4)));

Tci= T1 +(Q1*ln(Do/Dci)/(2*PI*1.4*1));

Q2= PI*0.051*Ɛ*(pow(Tw,4)-pow(Tci,4))/((1/0.88)+((1-
0.88)/0.88)*(0.051/Dci));

if (Q2 == Q1 )
{
UL = Q2/(PI*0.051*1*(Tw-Tsky));
C_PROFILE(c, thread, position) = UL;
}
else
{
end_c_loop(c, thread)
}
```

**Appendix B : Calculated Heat Convective.**

In this section, the convective heat value was calculated for the three models that were simulated. For nanofluid temperatures were obtained from the results of the ANSYS FLUENT.

The best model in terms of efficiency and performance for the three models was determined by calculating the efficiency of each model. Model (1/2) was the best and for the purpose of checking the heat transfer in the three models, the heat convective was calculated as shown below.

**B.1 Model (1/4).**

Properties : from table (3.3)   $\mu$=0.06308 pa.s  , k=0.14022 W.(m.K)$^{-1}$ ,

$C_p$=1899.2 J.(kg.K)$^{-1}$, $\rho$= 843.003 Kg.m$^{-3}$, $\beta$=6.9962x10$^{-4}$ K$^{-1}$

*thermal diffusivity*   $\alpha = \dfrac{k}{\rho.C_p}$   $= 0.14022/843.003*1899.2 = 8.758*10^{-8}$ m$^2$/s

*momentum diffusivity* $\nu = \dfrac{\mu}{\rho}$   $= 0.06308/843.003 = 7.4827*10^{-5}$ m$^2$/s

*Prandtl's number*   $P_r= \nu/\alpha$     $= 7.4827*10^{-5} / 8.758*10^{-8} = 854.38$

$$L_c = \frac{2\left[\ln\left(r_o / r_i\right)\right]^{4/3}}{\left(r_i^{-3/5} + r_o^{-3/5}\right)^{5/3}}$$

$T_n$ =352 K  ,  $T_w$ =300 K

$r_o$= 0.0255 m        $r_i$= 0.006375 m

$L_c$= 2[ln(0.0255/0.006375)]$^{4/3}$ / (0.006375$^{-3/5}$ + 0.0255$^{-3/5}$)$^{5/3}$

$L_c$= 0.01079 m

$$R_{ac} = \frac{g.\beta\left(T_n - T_w\right)L_c^3}{\nu\alpha}$$   Rayleigh Number

$R_{ac}$= 9.81*6.9962x10$^{-4}$ *(352-300)*(0.01079)$^3$/7.4827*10$^{-5}$ *8.758*10$^{-8}$

$R_{ac}$= 68412

The effective conductivity of a fictitious stationary fluid

$$\frac{k_{eff}}{k} = 0.386 \left( \frac{P_r}{0.861 + p_r} \right)^{1/4} Rc_a^{1/4}$$

$k_{eff}$ = 0.386(0.14022)(854.38/0.861+854.38)$^{1/4}$ *(68412)$^{1/4}$

$k_{eff}$ = 0.877 W/m.K

$$q^- = \frac{2\pi . k_{eff}}{\ln(r_o / r_i)} (T_n - T_w)$$

$q^-$ = 2* $\pi$ *(0.877)*(352-300)/(ln(0.0255/0.006375))

$q^-$ = 206.694  W/m

**B.2 Model (1/2).**

$T_n$= 344 K   , $T_w$ = 300 K

$r_o$= 0.0255 m  ,  $r_i$ = 0.0125  m

$$L_c = \frac{2 \left[ \ln \left( r_o / r_i \right) \right]^{4/3}}{\left( r_i^{-3/5} + r_o^{-3/5} \right)^{5/3}}$$

$L_c$= 2[ln(0.0255/0.0125)]$^{4/3}$ / (0.0125$^{-3/5}$ + 0.0255$^{-3/5}$)$^{5/3}$

$L_c$ = 6.8973*10$^{-3}$ m

$$R_{ac} = \frac{g.\beta(T_n - T_w)L_c^3}{\upsilon\alpha}$$

$R_{ac}$= 9.81*6.9962x10$^{-4}$ *(344-300)*(6.8973*10$^{-3}$)$^3$/7.4827*10$^{-5}$ *8.758*10$^{-8}$

$R_{ac}$ = 15120

$$\frac{k_{eff}}{k} = 0.386 \left( \frac{P_r}{0.861 + p_r} \right)^{1/4} Rc_a^{1/4}$$

$k_{eff}$ = 0.386(0.14022)(854.38/0.861+854.38)$^{1/4}$ *(15120)$^{1/4}$

$k_{eff}$ = 0.6   W/m.K

$$q^- = \frac{2\pi.k_{eff}}{\ln(r_o/r_i)}(T_n - T_w)$$

$q^-$ = 2* $\pi$ *(0.6)*(344-300)/(ln(0.0255/0.0125))

$q^-$ = 232.66  W/m

## B.3 Model (3/4).

$T_n$ = 332 K   ,  $T_w$ = 300 K

$r_o$ = 0.0255 m   ,  $r_i$ = 0.019125 m

$$L_c = \frac{2[\ln(r_o/r_i)]^{4/3}}{\left(r_i^{-3/5} + r_o^{-3/5}\right)^{5/3}}$$

$L_c$= 2[ln(0.0255/0.019125)]$^{4/3}$ / (0.019125$^{-3/5}$ + 0.0255$^{-3/5}$)$^{5/3}$

$L_c$ = 2.6258*10$^{-3}$ m

$$R_{ac} = \frac{g.\beta(T_n - T_w)L_c^3}{\upsilon\alpha}$$

$R_{ac}$= 9.81*6.9962x10$^{-4}$ *(332-300)*(2.6258*10$^{-3}$)$^3$/7.4827*10$^{-5}$ *8.758*10$^{-8}$

$R_{ac}$ = 606.74

$$\frac{k_{eff}}{k} = 0.386\left(\frac{P_r}{0.861 + p_r}\right)^{1/4} Rc_a^{1/4}$$

$k_{eff}$ = 0.386(0.14022)(854.38/0.861+854.38)$^{1/4}$ *(606.74)$^{1/4}$

$k_{eff}$ = 0.26855  W/m.K

$$q^- = \frac{2\pi.k_{eff}}{\ln(r_o/r_i)}(T_n - T_w)$$

$q^- = 2* \pi *(0.26855)*(332\text{-}300)/(\ln(0.0255/0.019125))$

$q^- = 187.69$ W/m

Note : observed from the calculations that the best model in terms of heat transfer is the model glass-to-copper tube size ratio of (½) and thus the model is better in terms of efficiency and heat transfer.

# References

[1]  T. P. Otanicar, P. E. Phelan, and J. S. Golden, "Optical properties of liquids for direct absorption solar thermal energy systems," *Solar Energy,* vol. 83, pp. 969-977, 2009.

[2]  H. Tyagi, P. Phelan, and R. Prasher, "Predicted efficiency of a low-temperature nanofluid-based direct absorption solar collector," *Journal of solar energy engineering,* vol. 131, p. 041004, 2009.

[3]  Z. Luo, C. Wang, W. Wei, G. Xiao, and M. Ni, "Performance improvement of a nanofluid solar collector based on direct absorption collection (DAC) concepts," *International Journal of Heat and Mass Transfer,* vol. 75, pp. 262-271, 2014.

[4]  G. Xu, W. Chen, S. Deng, X. Zhang, and S. Zhao, "Performance evaluation of a nanofluid-based direct absorption solar collector with parabolic trough concentrator," *Nanomaterials,* vol. 5, pp. 2131-2147, 2015.

[5]  S. A. Kalogirou, "A detailed thermal model of a parabolic trough collector receiver," *Energy,* vol. 48, pp. 298-306, 2012.

[6]  H. Al-Ansary and O. Zeitoun, "Numerical study of conduction and convection heat losses from a half-insulated air-filled annulus of the receiver of a parabolic trough collector," *Solar Energy,* vol. 85, pp. 3036-3045, 2011.

[7]  M. Öztürk, N. Ç. Bezir, and N. Özek, "Optical, energetic and exergetic analyses of parabolic trough collectors," *Chinese Physics Letters,* vol. 24, p. 1787, 2007.

[8]  M. Li and L. Wang, "Investigation of evacuated tube heated by solar trough concentrating system," *Energy Conversion and Management,* vol. 47, pp. 3591-3601, 2006.

[9]  R. V. Padilla, G. Demirkaya, D. Y. Goswami, E. Stefanakos, and M. M. Rahman, "Heat transfer analysis of parabolic trough solar receiver," *Applied Energy,* vol. 88, pp. 5097-5110, 2011.

[10]  D. H. Lobón, L. Valenzuela, and E. Baglietto, "Modeling the dynamics of the multiphase fluid in the parabolic-trough solar steam generating systems," *Energy Conversion and Management,* vol. 78, pp. 393-404, 2014.

[11]  Y.-L. He, J. Xiao, Z.-D. Cheng, and Y.-B. Tao, "A MCRT and FVM coupled simulation method for energy conversion process in parabolic trough solar collector," *Renewable Energy,* vol. 36, pp. 976-985, 2011.

[12]  Z. Cheng, Y. He, F. Cui, R. Xu, and Y. Tao, "Numerical simulation of a parabolic trough solar collector with nonuniform solar flux conditions by coupling FVM and MCRT method," *Solar Energy,* vol. 86, pp. 1770-1784, 2012.

[13]  K. Reddy, K. R. Kumar, and G. Satyanarayana, "Numerical investigation of energy-efficient receiver for solar parabolic trough concentrator," *Heat Transfer Engineering,* vol. 29, pp. 961-972, 2008.

[14]  Y. Tao and Y. He, "Numerical study on coupled fluid flow and heat transfer process in parabolic trough solar collector tube," *Solar Energy,* vol. 84, pp. 1863-1872, 2010.

[15]  P. Daniel, Y. Joshi, and A. K. Das, "Numerical investigation of parabolic trough receiver performance with outer vacuum shell," *Solar Energy,* vol. 85, pp. 1910-1914, 2011.

[16]  A. Einstein, "Eine neue bestimmung der moleküldimensionen," *Annalen der Physik,* vol. 324, pp. 289-306, 1906.

[17] H. Brinkman, "The viscosity of concentrated suspensions and solutions," *The Journal of Chemical Physics,* vol. 20, pp. 571-571, 1952.

[18] N. Frankel and A. Acrivos, "On the viscosity of a concentrated suspension of solid spheres," *Chemical Engineering Science,* vol. 22, pp. 847-853, 1967.

[19] T. S. Lundgren, "Slow flow through stationary random beds and suspensions of spheres," *Journal of Fluid Mechanics,* vol. 51, pp. 273-299, 1972.

[20] C. Nguyen, F. Desgranges, G. Roy, N. Galanis, T. Maré, S. Boucher*, et al.*, "Temperature and particle-size dependent viscosity data for water-based nanofluids– hysteresis phenomenon," *International Journal of Heat and Fluid Flow,* vol. 28, pp. 1492-1506, 2007.

[21] J. C. Maxwell, *A treatise on electricity and magnetism* vol. 1: Clarendon press, 1881.

[22] P. Bhattacharya, S. Saha, A. Yadav, P. Phelan, and R. Prasher, "Brownian dynamics simulation to determine the effective thermal conductivity of nanofluids," *Journal of Applied Physics,* vol. 95, pp. 6492-6494, 2004.

[23] S. Mehta, K. P. Chauhan, and S. Kanagaraj, "Modeling of thermal conductivity of nanofluids by modifying Maxwell's equation using cell model approach," *Journal of Nanoparticle Research,* vol. 13, pp. 2791-2798, 2011.

[24] W. Yu and S. Choi, "The role of interfacial layers in the enhanced thermal conductivity of nanofluids: a renovated Maxwell model," *Journal of Nanoparticle Research,* vol. 5, pp. 167-171, 2003.

[25] B. Xiao, Y. Yang, and L. Chen, "Developing a novel form of thermal conductivity of nanofluids with Brownian motion effect by means of fractal geometry," *Powder Technology,* vol. 239, pp. 409-414, 2013.

[26] M. Chandrasekar, S. Suresh, and A. C. Bose, "Experimental investigations and theoretical determination of thermal conductivity and viscosity of Al 2 O 3/water nanofluid," *Experimental Thermal and Fluid Science,* vol. 34, pp. 210-216, 2010.

[27] P. Namburu, D. Kulkarni, A. Dandekar, and D. Das, "Experimental investigation of viscosity and specific heat of silicon dioxide nanofluids," *Micro & Nano Letters,* vol. 2, pp. 67-71, 2007.

[28] Y. H. Shokrlu and T. Babadagli, "Viscosity reduction of heavy oil/bitumen using micro-and nano-metal particles during aqueous and non-aqueous thermal applications," *Journal of Petroleum Science and Engineering,* vol. 119, pp. 210-220, 2014.

[29] J. Eastman, U. Choi, S. Li, L. Thompson, and S. Lee, "Enhanced thermal conductivity through the development of nanofluids," in *MRS proceedings*, 1996, p. 3.

[30] H. Xie, J. Wang, T. Xi, Y. Liu, F. Ai, and Q. Wu, "Thermal conductivity enhancement of suspensions containing nanosized alumina particles," *Journal of Applied Physics,* vol. 91, pp. 4568-4572, 2002.

[31] C. H. Li and G. Peterson, "Experimental investigation of temperature and volume fraction variations on the effective thermal conductivity of nanoparticle suspensions (nanofluids)," *Journal of Applied Physics,* vol. 99, p. 084314, 2006.

[32] G. Colangelo, E. Favale, A. de Risi, and D. Laforgia, "Results of experimental investigations on the heat conductivity of nanofluids based on diathermic oil for high temperature applications," *Applied Energy,* vol. 97, pp. 828-833, 2012.

[33] M.-S. Liu, M. C.-C. Lin, C. Tsai, and C.-C. Wang, "Enhancement of thermal conductivity with Cu for nanofluids using chemical reduction method," *International Journal of Heat and Mass Transfer,* vol. 49, pp. 3028-3033, 2006.

[34]    V. Khullar, H. Tyagi, P. E. Phelan, T. P. Otanicar, H. Singh, and R. A. Taylor, "Solar energy harvesting using nanofluids-based concentrating solar collector," *Journal of Nanotechnology in Engineering and Medicine,* vol. 3, p. 031003, 2012.

[35]    W. Chen, G. Xu, S. Zhao, and X. Zhang, "Numerical Simulation on the Performance of Nanofluid-Based Direct Absorption Solar Collector With Parabolic Trough Concentrator," in *ASME 2016 5th International Conference on Micro/Nanoscale Heat and Mass Transfer*, 2016, pp. V001T05A012-V001T05A012.

[36]    A. Menbari, A. A. Alemrajabi, and A. Rezaei, "Experimental investigation of thermal performance for direct absorption solar parabolic trough collector (DASPTC) based on binary nanofluids," *Experimental Thermal and Fluid Science,* vol. 80, pp. 218-227, 2017.

[37]    S. Ladjevardi, A. Asnaghi, P. Izadkhast, and A. Kashani, "Applicability of graphite nanofluids in direct solar energy absorption," *Solar Energy,* vol. 94, pp. 327-334, 2013.

[38]    V. Khullar and H. Tyagi, "A study on environmental impact of nanofluid-based concentrating solar water heating system," *International Journal of Environmental Studies,* vol. 69, pp. 220-232, 2012.

[39]    Kapil Sharma and L. Kundan, "Nanofluid Based Concentrating Parabolic Solar Collector (NBCPSC): A New Alternative," *International Journal of Research in Mechanical Engineering and Technology (IJRMET),* vol. 4, 2014.

[40]    E. Bellos, C. Tzivanidis, K. Antonopoulos, and G. Gkinis, "Thermal enhancement of solar parabolic trough collectors by using nanofluids and converging-diverging receiver tube," *Renewable Energy,* vol. 94, pp. 213-222, 2016.

[41]    S. E. Ghasemi and G. R. M. Ahangar, "Numerical analysis of performance of solar parabolic trough collector with Cu-Water nanofluid," *International Journal of Nano Dimension,* vol. 5, p. 233, 2014.

[42]    T. Sokhansefat, A. Kasaeian, and F. Kowsary, "Heat transfer enhancement in parabolic trough collector tube using Al 2 O 3/synthetic oil nanofluid," *Renewable and Sustainable Energy Reviews,* vol. 33, pp. 636-644, 2014.

[43]    K. Sunil, L. Kundan, and S. Sumeet, "Performance evaluation of a nanofluid based parabolic solar collector—An experimental study," *International Journal of Mechanical and Production Engineering Research and Development (IJMPERD),* vol. 10, pp. 2320-2400, 2014.

[44]    Y. Wang, J. Xu, Q. Liu, Y. Chen, and H. Liu, "Performance analysis of a parabolic trough solar collector using Al 2 O 3/synthetic oil nanofluid," *Applied Thermal Engineering,* vol. 107, pp. 469-478, 2016.

[45]    Amar Hasan Hameed, Mohammed Yaseen Nawaf, and S. Balage, "NOVEL CONFIGURATION FOR DIRECT ABSORPTION SOLAR COLLECTOR WITH NONE-CIRCULATED NANOFLUID," *JOURNAL OF THERMAL ENGINEERING , INTERNATIONAL CONFERENCE ON ENERGY AND THERMAL ENGINEERING: ISTANBUL*

*25-28 April 2017, Yildiz Technical University, Istanbul, Turkey*

[46]    "SolTrace optical modelling software v2012.7.9

", ed.

[47]    T. Tayebi, A. J. Chamkha, M. Djezzar, and A. Bouzerzour, "Natural convective nanofluid flow in an annular space between confocal elliptic cylinders," *Journal of Thermal Science and Engineering Applications,* vol. 9, p. 011010, 2017.

[48]    S. Senthilraja, K. Vijayakumar, and R. Gangadevi, "A comparative study on thermal conductivity of Al2O3/water, CuO/water and Al2O3–CuO/water nanofluids," *Digest Journal of Nanomaterials and Biostructures,* vol. 10, pp. 1449-1458, 2015.

[49]    A. Handbook, "Fundamentals. 1993," *American Society of Heating, Refrigerating, and Air Conditioning Engineers, Atlanta,* 1993.

[50]    F. Manual, "Manual and User Guide of Fluent Software, FLUENT," ed: Inc, 2005.

# NOVEL CONFIGURATION FOR DIRECT ABSORPTION SOLAR COLLECTOR WITH NONE-CIRCULATED NANOFLUID

**\*Amar Hasan Hameed**
KTO Karatay University
Konya, Konya, Turkey

**Mohammed Yaseen Nawaf**
University of Turkish Aeronautical Association
Ankara, Turkey

**Sudantha Balage**
University of Turkish
Aeronautical Association
Ankara, Turkey

*Keywords: Solar collector, direct absorption, concentrated solar collector,   nano-fluid*
*\* Corresponding author:, +905060663653:, Fax: +903322020043*
*E-mail address: dr.eng.amar@gmail.com*

## ABSTRACT

Novel configuration for direct absorption  solar  collector  has been developed. In the new configuration none-circulated nano-fluid absorbs solar radiation through glass wall. The absorbed heat directly transfers to circulated water  flowing inside copper tube submerged  into  the  nano-fluid. Numerical model has been developed for flowing water, nano-fluid annular region and the copper  tube  which  separates  the  two  different fluids. Heat absorption of concentrated solar arrays reflected by parabolic trough is simulated as a heat source in the energy equation solved in nano-fluid region. The efficiency of  one  meter of solar receiver unit  with  glass-to-copper tube size ratio     of (½) increases significantly with flow rate up to  55%.  However the receiver wasn't covered by evacuated tube to reduce losses, circulating water restricts the raising of  nano- fluid temperature and in turn reduces  thermal  losses. Since,    water flow rate changes increasingly affect the efficiency, the depth of absorption in nano-fluid and characterized length of natural convection are not inconveniently selected. However, further investigations are planned to be done to optimize heat absorption and convection in nano-fluid region. Temperature rising per one meter decreases with flow rate despite of performance  enhancing.

## INTRODUCTION

Solar energy harvesting needs further development to  reduce the consumption of fossil fuel due to its cost and its environmental concerns of burning it. However, solar collectors  got  extended interest from researchers, but still the incident   heat of the sun faces multi stages of thermal resistances to flow of  heat to the hand of the user. Direct solar absorber collector (DSAC) is a novel technique used recently for the new  generation of solar collectors. Instead of using metallic tube painted with special spectral paint to  absorb  solar  irradiation and transfer heat to a fluid inside the tube, flowing nano-fluid in  a glass tube absorbs solar irradiation directly and transport the absorbed energy as heat to a heat exchanger for usage. However DSAC 's are newly developed, many researchers studied the performance of these collectors numerically and experimentally and compared it with the normal solar collectors. Water  was found as the best absorber for solar radiation  among  four liquids, namely; water; ethylene glycol; propylene glycol and therminol VP-1, which has been tested by (Otanicar, Phelan, & Golden, 2009). However it is still a weak absorber, only absorbing 13% of the energy. The presence of nanoparticles promises superior capability for solar irradiation absorption  since nanoparticles are generally opaque and may be black. (Tyagi, Phelan, & Prasher, 2009) observed that for non-concentrating flat-plate collector the presence of nanoparticles increases the absorption of incident radiation by more than 9 times over that of pure water. The efficiency of DAC by using nanofluid has been found to be up to 10% higher than that of flat-plate collector. Nanofluids, even of low-content, has good absorption in direct absorption collector (DAC) compared with the base fluid or compared with coating absorber as has been demonstrated by (Luo, Wang, Wei, Xiao, & Ni, 2014). The  model of (Xu, Chen, Deng, Zhang, & Zhao)

The purpose of this study is to enhance irradiance absorption capacity and efficiency of concentrating parabolic solar collectors by using nano-fluid for direct absorption in glass tube compound with copper tube for direct heat exchange. The thermal conductivity of the fluid conveying thermal heat was improved by using nano-fluid in the literature. But, still heat exchange needs more improvement by enhancing the fluid thermal conductivity or by improving the configuration to boost heat transfer. The main objective of this research is to increase solar energy harvesting by reduction of thermal resistance in medium fluid. New configuration will be discussed for heat transmitting from nano-fluid to heating system.

## Novel collector design

In direct absorption solar collector (DASC), nanofluid is circulated in a system. Nanofluid absorbs solar irradiation during flowing inside a glass tube. Nanofluid absorbs heat from irradiation, then it conveys the absorbed heat to a cold water through a heat exchanger. Nanofluid in traditional system circulates and transfers heat from solar collector to heat exchanger. In heat exchanger, heat is used for heating the domestic water or swimming pool water or any other required application of heating, as shown in **Figure 1**.

The losses in the traditional collector results due to reflecting of glass surface in addition to emittance of hot surfaces and losses by convection. Moreover, the output heat of the system depends on the thermal efficeincy of the heat exchanger exchanging heat from nanofluid to water. The existing of heat exchanger reduces the overall efficeincy of the system due to existing of additional thermal resistance. This work will reduce the total thermal resistance of the system by combining the two actions in one place. Heat absorbing and heat exchanging will occur at solar collector to reduce the total thermal resistance.

The new system will use the principle of direct heat exchange between uncirculated nanofluid and circulating water inside collector tube without using heat exchanger. As a result of total thermal resistance decreasing, the overall efficeincy of the system will increase. In addition, one circulating pump will be used instead of two. The outlines of the system for direct heat exchange is shown in **Figure 2**. The invented collector works for solar irradiation absorption and heat exchange between the absorber (nanofluid) and the transporter (circulated water). Solar irradiation passes through glass walls and it is absorbed by nanofluid, then nanofluid temperature raises. Circulated water passes through one/multi copper tube/tubes which submerged in nanofluid. Then heat exchange takeplaces between nanofluid and circulated water through the copper walls. The water flows on the inner surface of copper tube, whereas the outer surface of copper tube is in contact with none-circulated nanofluid, as has been explained in Figure 3. The two processes of heat absorbing in nanofluid and heat rejection to the water are combined in one device (collector). Heat exchange between nanofluid and circulated water depends on the area of heat transfer, copper tube thermal conductivity,

and heat transfer coefficeint at inner side and outer side of copper tube. So, the new solar collector has capacity to develop many designs to get the best required efficeincy for heat exchange. One or multi copper tube conveying water and submerged in nanofluid which put in a glass tube is the first design, as shown in Figure 3.
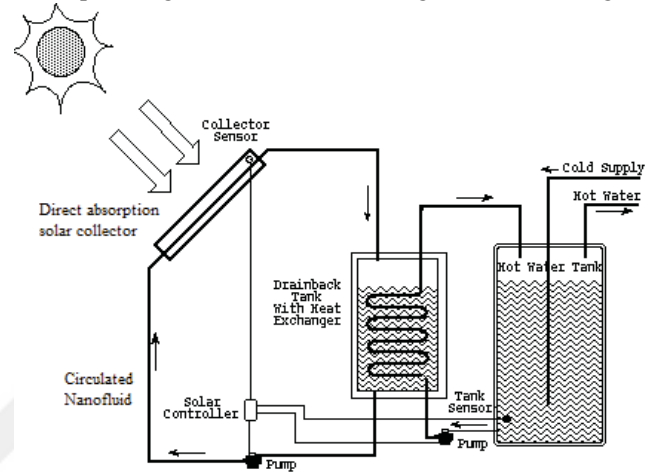


Figure 1. Outlines of traditional system of DASC with indirect heat exchange.
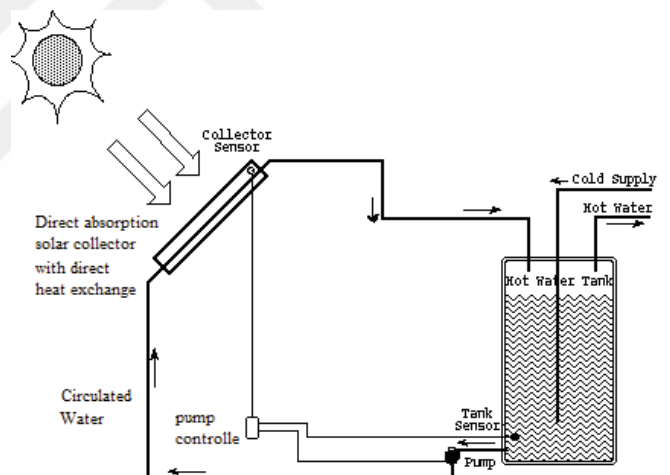


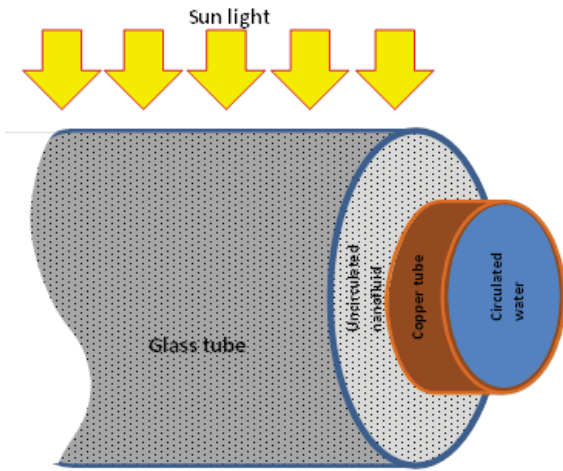Figure 2. Outlines of system of DASC with direct heat exchange.

**Figure 3. Collector tube with one copper tube inside.**

## Methodology

The mathematical form of energy equation including source term can express heat transfer in nanofluid region. The steady state form of energy equation has been solved as follows;

$$\frac{\partial(\rho u_x T_f)}{\partial x} + \frac{\partial(\rho u_y T_f)}{\partial y} + \frac{\partial(\rho u_z T_f)}{\partial z} = \frac{\partial}{\partial x}\left[\frac{k}{C}\frac{\partial T_f}{\partial x}\right] + \frac{\partial}{\partial y}\left[\frac{k}{C}\frac{\partial T_f}{\partial y}\right] + \frac{\partial}{\partial z}\left[\frac{k}{C}\frac{\partial T_f}{\partial z}\right] + \Phi$$

…(1)

Where $T_f$ is the fluid temperature, $\rho$ is the density of the fluid, $k$ is the thermal conductivity of the fluid, $C$ is the thermal capacity of the fluid, and $\Phi$ is the thermal solar energy source defined in nano-fluid region. Heat transfer analysis in circulating water in solar collector is solved by using same above energy equation with zero source term. The absorption of solar irradiance increases nano-fluid temperature by amount depends on solar intensity reaches to this point and the absorption capability of the fluid. The presence of nanoparticles in the fluid improves radiation absorption capability for the fluid (Tyagi et al., 2009). The thermal energy source is defined as the dissipation of radiative heat flux into the fluid from the surface of array entrance;

$$\Phi = -\frac{\partial q_r}{\partial x}$$     …(2)

ANSYS FLUENT simulator is used to perform numerical simulation of solar collector tube subjected to concentrated solar radiation.

## RESULTS AND DISCUSSION

### Mesh study

Mesh is generated in 3-dimensional model using mesh manager in ANSYS. The number of cells has been increased until the results got to stability. Temperature rising per one meter changes with mesh number until 4.6 million as shown in **Figure 4**. Critical changes of temperature and velocity near to walls need finer grid especially in water flow region. Buoyancy effect plays role of creating motion or even vorticities in different unknown places in nano-fluid region, so mesh distributes uniformly in this region as shown in **Figure 5**.
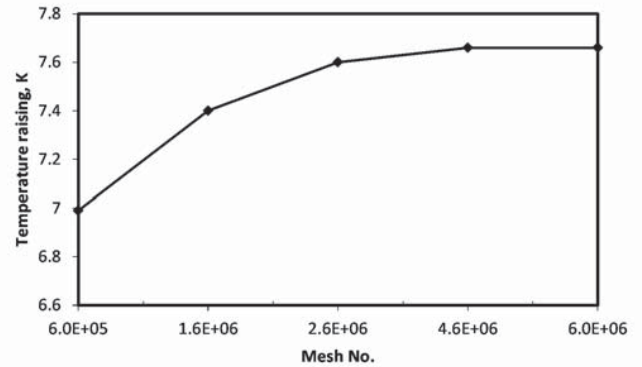


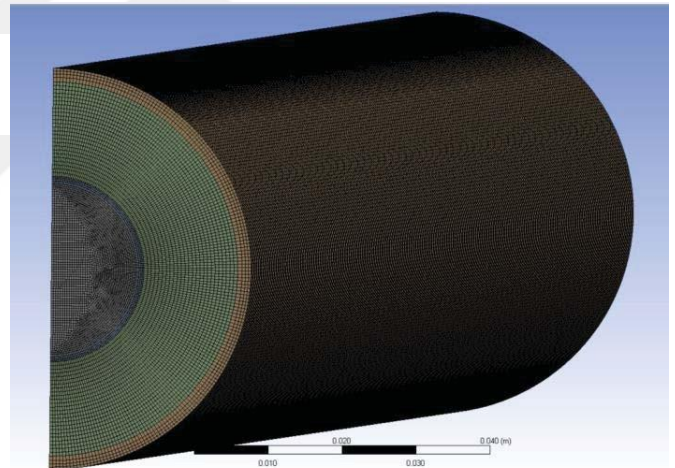Figure 4. Mesh study by increasing mesh number various temperature rising through 1 m of receiver.



Figure 5. The axisymmetric model with the final mesh.

### Efficiency

There are many thermal resistant's restrict the outcome of solar absorber and reduce the efficiency of the receiver. Energy gained by receiver and temperature rising per one meter play as most two important factors to evaluate the performance of solar collector. In **Figure 6**, the flow rate of water inside the receiver affects significantly the efficiency of solar receiver and temperature rising per one meter. Improving the efficiency by this substantial rate refers to the role of thermal resistance between water and copper tube. Since, the other side of copper tube contacts nano-fluid, and heat transfer in nano-fluid improves considerably due to the presence of nanoparticles as

has been concluded in many literatures like (Mwesigye, Huan, & Meyer, 2015). Heat transfer from copper tube to inside improves by increasing Reynolds number either by increasing velocity or changing the size of the tube or increasing contact area by using internal fins or by creating turbulence by turbulence stimulator at the entrance of the tube. Referring to that, the efficiency improving will not stop at 65%, since thermal resistance at the internal side of copper tube can be reduced in many traditional ways. Furthermore, thermal losses of solar receiver unit to the ambient relates strictly to the thermal resistance at the internal side. Since, as much as thermal resistance decreases, temperature of nano-fluid decreases and then thermal losses decreases. However, flow rate increasing plays important role in improving the performance of solar receiver, it faces an obstacle of limited temperature rising when the required output temperature has to be high enough for some applications.

In the outer side of the copper tube where nano-fluid is absorbing and conveying heat to the copper tube, both absorbing and transferring process affect the efficiency. Absorbing process depends on absorption factor and depth of solar arrays travelling. Absorption factor of nano-fluid depends on many factors like; volume fraction, spectral absorption properties for each of fluid and solid particles, size and shape of nanoparticles. The depth of solar arrays travelling determines the amount of solar energy absorption in addition to defining Rayleigh number in the annular region occupied by nano-fluid. Rayleigh number plays the most important role in heat transfer from nano-fluid to copper tube by natural convection. Therefore, the authors will conduct the simulation for different copper tube sizes, different glass-tube/copper-tube size ratio, and various volume fraction ratios.
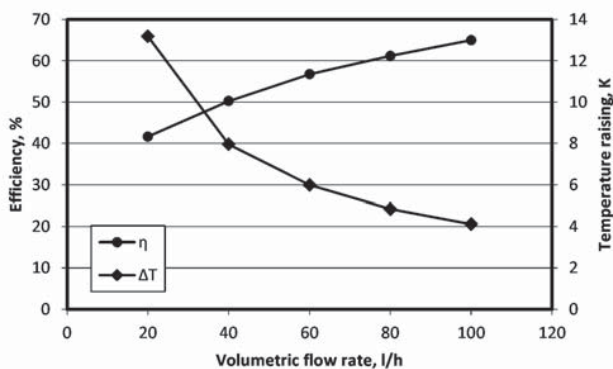


Figure 6. The effect of water flow rate on receiver efficiency and temperature raising per 1 m.

## CONCLUSION

Using nano-fluid in direct absorption system with direct heat exchange improves the performance of solar collector. Direct heat exchange within the solar receiver will reduce the total thermal resistance of solar collector system. In this innovative configuration, none-circulating nano-fluid absorbs solar radiation and conveys heat directly to circulating water

passes through copper tube submerged in the nano-fluid. The losses of exchanging heat in external separate heat exchanger will be omitted. Solar receiver with new configuration proves comparatively high efficiency up to 55%, however there was no consideration of vacuum tube in the simulation. The efficiency shows significant influencing by circulated water flow rate. At the inner side of copper tube (water-side), thermal resistance reduction plays an important role in improving the performance of the system. At the outer surface of copper tube (nanofluid- side), thermal resistance for the tested size and nano-fluid properties shows good convenience to get performance up to 60%. However, the research can be extended more for higher performance by increasing nano-fluid volume fraction, copper tube size, glass-tube/copper-tube sizes ratio, and by considering using vacuum tube to reduce thermal losses to ambient. Temperature rising per one meter of receiver decreases with flow rate, so thermal resistance of water-copper surface should be improved by using fins or turbulence stimulators if high temperature water required by the user.

## NOMENCLATURE

## REFERENCES

Luo, Z., Wang, C., Wei, W., Xiao, G., & Ni, M. (2014). Performance improvement of a nanofluid solar collector based on direct absorption collection (DAC) concepts. *International Journal of Heat and Mass Transfer, 75*, 262-271.

Mwesigye, A., Huan, Z., & Meyer, J. P. (2015). Thermodynamic optimisation of the performance of a parabolic trough receiver using synthetic oil–Al 2 O 3 nanofluid. *Applied Energy, 156*, 398-412.

Otanicar, T. P., Phelan, P. E., & Golden, J. S. (2009). Optical properties of liquids for direct absorption solar thermal energy systems. *Solar Energy, 83*(7), 969-977.

Tyagi, H., Phelan, P., & Prasher, R. (2009). Predicted efficiency of a low-temperature nanofluid-based direct absorption solar collector. *Journal of solar energy engineering, 131*(4), 041004.

Xu, G., Chen, W., Deng, S., Zhang, X., & Zhao, S. Performance evaluation of a nanofluid-based direct absorption solar collector with parabolic trough concentrator. *Nanomaterials, 5*(4), 2131-214